

GLACIAL EROSION IN ATLANTIC AND ARCTIC CANADA
DETERMINED BY TERRESTRIAL IN SITU
COSMOGENIC NUCLIDES AND
ICE SHEET MODELING

by

Jane K. Willenbring Staiger

Submitted in partial fulfillment of the requirements
for the degree of Doctor of Philosophy

Dalhousie University
Halifax, NS
September 2005

© Copyright by Jane K. Willenbring Staiger, 2005

Approved by

Supervisor

John C. Gosse, Ph. D.
Associate Professor of Earth Sciences

Supervisory Committee

Lawrence Plug, Ph. D.
Assistant Professor of Earth Sciences

Departmental Reader

Djordje Grujic, Ph. D.
Associate Professor of Earth Sciences

Department Chair

Martin Gibling, Ph. D.
Professor of Earth Sciences

External Examiner

Shawn J. Marshall, Ph. D.
Associate Professor of Geography

DALHOUSIE UNIVERSITY

DATE: September 23, 2005

AUTHOR: Jane K. Willenbring Staiger

TITLE: GLACIAL EROSION IN ATLANTIC AND ARCTIC CANADA
DETERMINED BY TERRESTRIAL IN SITU COSMOGENIC
NUCLIDES AND ICE SHEET MODELING

DEPARTMENT OR SCHOOL: Department of Earth Sciences

DEGREE: Ph.D. CONVOCATION: May YEAR: 2006

Permission is herewith granted to Dalhousie University to circulate and to have copied for non-commercial purposes, at its discretion, the above title upon the request of individuals or institutions.

Signature of Author

The author reserves other publication rights, and neither the thesis nor extensive extracts from it may be printed or otherwise reproduced without the author's written permission.

The author attests that permission has been obtained for the use of any copyrighted material appearing in the thesis (other than the brief excerpts requiring only proper acknowledgement in scholarly writing), and that all such use is clearly acknowledged.

Distribution License

DalSpace requires agreement to this non-exclusive distribution license before your item can appear on DalSpace.

NON-EXCLUSIVE DISTRIBUTION LICENSE

You (the author(s) or copyright owner) grant to Dalhousie University the non-exclusive right to reproduce and distribute your submission worldwide in any medium.

You agree that Dalhousie University may, without changing the content, reformat the submission for the purpose of preservation.

You also agree that Dalhousie University may keep more than one copy of this submission for purposes of security, back-up and preservation.

You agree that the submission is your original work, and that you have the right to grant the rights contained in this license. You also agree that your submission does not, to the best of your knowledge, infringe upon anyone's copyright.

If the submission contains material for which you do not hold copyright, you agree that you have obtained the unrestricted permission of the copyright owner to grant Dalhousie University the rights required by this license, and that such third-party owned material is clearly identified and acknowledged within the text or content of the submission.

If the submission is based upon work that has been sponsored or supported by an agency or organization other than Dalhousie University, you assert that you have fulfilled any right of review or other obligations required by such contract or agreement.

Dalhousie University will clearly identify your name(s) as the author(s) or owner(s) of the submission, and will not make any alteration to the content of the files that you have submitted.

If you have questions regarding this license please contact the repository manager at dalspace@dal.ca.

Grant the distribution license by signing and dating below.

Name of signatory

Date

dedication page

TABLE OF CONTENTS

TITLE PAGE	i
SIGNATURE PAGE.....	ii
COPYRIGHT AGREEMENT.....	iii
DEDICATION PAGE	iv
LIST OF TABLES	xi
LIST OF FIGURES	xii
ABSTRACT.....	xv
ACKNOWLEDGEMENTS	xvi
CHAPTER 1	1
INTRODUCTION.....	1
CHAPTER 2.....	8
ATMOSPHERIC SCALING OF COSMOGENIC NUCLIDE PRODUCTION: THE CLIMATE EFFECT	8
2.1 ABSTRACT.....	9
2.2 INTRODUCTION.....	10
2.3 METHODOLOGY	12
2.3.1 <i>UMISM</i>	13
2.3.2 <i>CCM3</i>	14
2.3.3 <i>PRODUCTION RATE CALCULATIONS</i>	16
2.4 RESULTS	17
2.5 DISCUSSION	18

2.6 CONCLUSIONS	21
2.7 ACKNOWLEDGEMENTS	21
2.8 REFERENCES	22
CHAPTER 3	37
QUATERNARY RELIEF GENERATION BY POLYTHERMAL GLACIER ICE	37
3.1 ABSTRACT	38
3.2 INTRODUCTION	39
3.3 GEOMORPHIC SETTING	41
3.4 TCN SURFACE EXPOSURE METHOD	45
3.5 RESULTS	47
3.6 DISCUSSION	48
3.6.1 INTERPRETING TCN DATA IN GLACIATED TERRAINS	48
3.6.2 ESTIMATING GLACIAL EROSION RATES	50
3.6.3 ICE SHEET MODEL TESTS	51
3.6.4 RELIEF GENERATION BY GLACIERS	54
3.7 SUMMARY	56
3.8 ACKNOWLEDGEMENTS	57
3.9 REFERENCES	58
CHAPTER 4	82
GLACIAL EROSION AND SEDIMENT DISPERSION FROM DETRITAL COSMOGENIC NUCLIDE ANALYSES	82
4.1 ABSTRACT	83
4.2 INTRODUCTION	84

4.3 PHYSIOGRAPHY OF THE STUDY AREA	87
4.4 GLACIAL HISTORY	88
4.5 METHODOLOGY	89
4.6 RESULTS	94
4.7 DISCUSSION	95
4.7.1 ICE SHEET MODEL TESTS	97
4.7.2 SHORT AND LONG TILL TRANSPORT DISTANCES.....	100
4.7.3 DEPTH OF GLACIAL EROSION	101
4.8 CONCLUSIONS	103
4.9 ACKNOWLEDGEMENTS.....	104
4.10 REFERENCES	105
CHAPTER 5.....	132
IMPLICATIONS AND CONCLUSIONS	132
5.1 IMPLICATIONS OF DIFFERENTIAL GLACIAL EROSION	132
5.1.1 ESTIMATE OF EROSION IN WARM-BASED GLACIAL ZONES	132
5.1.2 ESTIMATE OF EROSION IN COLD-BASED GLACIAL ZONES	136
5.1.3 INTERPRETATION SUMMARY	137
5.2 CONCLUSIONS	138
5.2.1 CLIMATE-INDUCED GLOBAL VARIABILITY OF TCN PRODUCTION RATES.....	138
5.2.2 RELIEF GENERATION IN THE TORNGAT MOUNTAINS.....	139
5.2.3 GLACIAL EROSION AND SEDIMENT DISPERSION FROM DETRITAL TCN	140
5.2.4 CONCLUSIONS SUMMARY	142
APPENDIX 1.....	145

ESPL COPYRIGHT RELEASE LETTER	146
APPENDIX 2.....	147
TERRESTRIAL IN SITU COSMOGENIC NUCLIDE (TCN) SYSTEMATICS	147
A2.1 HISTORY.....	147
A2.2 FUNDAMENTAL TECHNIQUE	147
APPENDIX 3.....	152
SUMMARY OF ASSUMPTIONS IN CHAPTER 3 CALCULATIONS.....	152
A3.1 FOR APPARENT AGE CALCULATIONS:.....	152
A3.2 FOR EROSION CALCULATIONS:.....	152
APPENDIX 4.....	155
TERRESTRIAL IN SITU COSMOGENIC NUCLIDE CHEMISTRY	155
A4.1 INTRODUCTION.....	155
A4.2 PHYSICAL PRE-TREATMENT	155
A4.3 CHEMICAL PRE-TREATMENT	156
<i>A4.3.1 QUARTZ DISSOLUTION</i>	<i>159</i>
<i>A4.3.2 ION CHROMATOGRAPHY.....</i>	<i>160</i>
A4.4 OXIDE PREPARATION	161
A4.5 AMS AND DATA REDUCTION.....	162
APPENDIX 5.....	175
ICE SHEET MODELING WITH UMISM	175
A5.1 INTRODUCTION.....	175
A5.2 BOUNDARY CONDITIONS.....	177
<i>A5.2.1 CLIMATE.....</i>	<i>177</i>

<i>A5.2.2 SEA LEVEL</i>	178
<i>A5.2.3 GEOTHERMAL HEAT FLUX</i>	179
<i>A5.2.4 TOPOGRAPHY</i>	180
A5.3 COMPUTATIONS	180
<i>A5.3.1 ISOSTASY</i>	180
<i>A5.3.2 TEMPERATURE CALCULATIONS</i>	181
<i>A5.3.3 SLIDING VELOCITY</i>	182
<i>A5.3.4 BASAL WATER</i>	183
A5.4 SENSITIVITY ANALYSES	184
<i>A5.4.1 INTRODUCTION</i>	184
<i>A5.4.2 EISMINT</i>	184
<i>A5.4.3 COMPARISON WITH REAL EXAMPLES</i>	185
A5.5 DIFFICULTIES	186
APPENDIX 6	194
USISM INSTRUCTIONS AND PARAMETER TABLES	194
A6.1 INTRODUCTION.....	194
A6.2 BED SELECTION.....	194
A6.3 ICE SHEET MODEL.....	195
A6.4 POST-PROCESSING.....	196
APPENDIX 7	200
DERIVATION OF DEPTH CALCULATIONS USED IN CHAPTER 4	200
APPENDIX 8	202

STUDENT CONTRIBUTION TO MANUSCRIPTS IN THESIS – FACULTY OF GRADUATE

STUDIES FORM..... 203

REFERENCES..... 205

LIST OF TABLES

Table 3.1 Sample location and exposure age data for Torngat Mountain samples.....	80
Table 3.1 Sample location and exposure age data for Torngat Mountain samples (continued)	81
Table 4.1 Sample location and TCN data for the Baffin Island till samples	131
Table 5.1 Erosion rates versus the average sliding speeds and their associated glacial erosion coefficients	144
Table A3.1 Site characteristics and sample correction data for cosmogenic data presented in Chapter 3	154
Table A4.1 Chemical data for Labrador samples	172
Table A4.2 Baffin Island till sample Be chemistry data	173
Table A4.3 Baffin Island till sample Al chemistry data	174
Table A6.1 Console.* file parameter selections for map5.e runs for the Labrador Peninsula.....	198
Table A6.2 Console.* file parameter selections for map5.e runs for Baffin Island.....	199

LIST OF FIGURES

Figure 2.1 Difference in 200-hPa height field between LGM and present-day CCM3-simulation	29
Figure 2.2 Longitudinal cross-section of average simulated pressure for present-day and LGM	30
Figure 2.3 Illustration of atmosphere density redistribution due to cooling	31
Figure 2.4 Percentage deviation of LGM production rates from present-day production rates.....	32
Figure 2.5 Surface elevations, production rate and time-averaged production rate of the Himalayas due to LGM conditions.....	34
Figure 2.6 Calibrated and measured production rates of ^{10}Be vs. altitude.....	36
Figure 3.1 The Torngat Mountains location map	71
Figure 3.2 Low angle photograph of the Korok River valley	72
Figure 3.3 Exposure age vs. altitude plot for bedrock samples in the Torngat Mountains, Labrador.....	73
Figure 3.4 Exposure ages of erratic boulders.....	74
Figure 3.5 Exposure-erosion diagram of $^{26}\text{Al}/^{10}\text{Be}$ vs. $\log ^{10}\text{Be}$	75
Figure 3.6 UMISM results over a 100-ka cycle for the Labrador Peninsula	77
Figure 3.7 Erosion rate vs. normalized sliding distance based on the 100 ka UMISM simulation	78
Figure 4.1 Study area in north-central region of Baffin Island, Nunavut	119
Figure 4.2 Paleo-ice margin positions adapted from Dyke et al. (2003)	121

Figure 4.3 Till sample site photographs.....	122
Figure 4.4 Map of 37G area showing surface till sites	123
Figure 4.5 Sedimentology of till samples	124
Figure 4.6 The exponential production profile for bedrock and till.....	125
Figure 4.7 Exposure-erosion diagram of $^{26}\text{Al}/^{10}\text{Be}$ vs. $\log^{10}\text{Be}$	126
Figure 4.8 ^{10}Be concentrations versus clast exotic lithology and sample altitude.....	127
Figure 4.9 Modeled ice cover, basal freezing and melt production in a 100-ka glacial cycle.	128
Figure 4.10 The effect of erosion on the secular equilibrium concentration using a ^{10}Be concentration.....	129
Figure 5.1 Warm-based portion of the LIS over a 100-ka glacial cycle.....	143
Figure A2.1 TCN spallation production with depth below the surface	151
Figure A4.1 Generic procedure for quartz dissolution	163
Figure A4.2 Generic procedure for anion column chemistry	164
Figure A4.3 Generic procedure for controlled precipitate chemistry	165
Figure A4.4 Generic procedure for cation column chemistry	166
Figure A4.5 Generic procedure for Be sample chemistry	167
Figure A4.6 Speciation with pH diagram (from Ochs and Ivy-Ochs, 1996)	168
Figure A4.7 Generic procedure for Be oxide preparation	169
Figure A4.8 Generic procedure for Al sample chemistry.....	170
Figure A4.9 Generic procedure for Al oxide preparation.....	171
Figure A5.1 The major components of the ice sheet model, UMISM.....	188

Figure A5.2 Temperatures used for the initial temperature input from Johnsen et al. (1995)	189
Figure A5.3 Net mass balance for climate.....	190
Figure A5.4 Sea level used for the sea level input derived from a model run for the Northern Hemisphere.....	191
Figure A5.5 Gridded GTOPO 30 dataset used for the North America ice simulation coarsely sampled by UMISM (1.8 deg. by 1.8 deg.)	192
Figure A5.6 Bed topography ETOPO2 gridded elevation dataset	193

ABSTRACT

Landscapes of northern Canada are often associated with subglacial erosion during the Quaternary glaciations; however, the rates and spatial pattern of subglacial erosion are unknown. Terrestrial in situ cosmogenic nuclides (TCN) extracted from glaciated bedrock and till provide a new method to identify paleo-glacier basal thermal conditions. Differential preservation of pre-glacially produced TCN reflects the degree of glacial erosion. In warm-based zones, subglacial erosion stripped the upper few meters of regolith and bedrock and effectively removed the pre-glacial TCN. In cold-based subglacial conditions, the ice was frozen to the bed and the inherited TCN concentration survived.

Measurements of TCN concentrations from bedrock indicate that the valleys were eroded > 2.5 meters during a glacial-interglacial cycle. On summit plateaus, however, the long-term erosion rate is < 1.4 m/Ma. The juxtaposition of erosive ice in valleys and non-erosive ice atop interfluvial plateaus has generated relief in arctic and sub-arctic regions.

Tills with monolithologic, angular clasts associated with cold-based ice contain 2-50 times the TCN concentration of silt-rich tills with polyolithologic, striated clasts associated with warm-based ice. Measurement of minimum ice burial durations of >3 Ma suggest that recently deglaciated surfaces near modern ice caps may have been covered by cold-based ice since Pliocene time. Identifying cold-based anomalies in basal sliding is an obstacle to interpreting glacial dispersal patterns for mineral exploration.

Glacial erosion and till production are inferred to be functions of the thermal regime at the base of glacier ice and are tested by linking the distribution of TCN in bedrock and till with modeled basal thermal conditions using the University of Maine Ice Sheet Model (UMISM). TCN-derived glacial erosion rates vary linearly with modeled average sliding velocity by a glacial erosion coefficient of 5×10^{-7} – three orders of magnitude lower than in other regions.

Quaternary ice sheets and the driving global cooling during glaciations cause synoptic atmospheric pressure fluctuations from katabatic winds and atmospheric compression. Modeled atmospheric pressure changes due to presence of global ice sheets produces up to a 10% difference in TCN production rates for samples exposed near ice sheets and at high elevations during glaciations when compared to present-day production rates.

ACKNOWLEDGEMENTS

CHAPTER 1

INTRODUCTION

My original motivations for addressing the magnitude, rate, and effect of glacial erosion over the Quaternary period were three separate themes of recent research in which glacial erosion could play a prominent role. These themes are: the influence of erosion on orogenic processes (e.g., Zeitler et al. 2001; Beaumont et al., 2001; Tomkin and Braun, 2003); increased sediment flux during the Quaternary reflecting or promoting climate variability (e.g., Molnar and England, 1990; Raymo and Ruddiman, 1992; Montgomery et al., 2001); and glacial erosion perturbing stable landscape hypsometries to create relief (e.g. Brozovic et al. 1997; Small and Anderson, 1998; Whipple et al., 1999; Tomkin and Braun, 2002).

The rationale behind these themes is that Quaternary erosion rates that include both glacial and fluvial components have been thought to exceed pre-Quaternary fluvial erosion rates by more efficiently removing larger clasts, by eroding in places where fluvial erosion is largely inept, and by switching from fluvial erosion to glacial erosion to fluvial erosion. This rationale relies on the premise that glaciers steadily incise and remove hillslope colluvium more effectively than streams (Hallet et al., 1996; Elverhoi et al., 1998; Montgomery, 2002). However, in a survey of global Quaternary marine sediment thicknesses, Peizhen et al. (2001) showed that some northern areas with great glacier expansion during continental scale glacial advances do not necessarily show increased sedimentation rates, i.e. greater erosion rates. Sedimentation rates from the

Labrador Sea also suggest relatively steady sedimentation rates from the Miocene to the Quaternary (Bell, 1989; Balkwill, 1990). If the inception, growth and recession of continental ice sheets such as the Laurentide Ice Sheet (LIS) are the most significant events of the Quaternary period in North America, one must ask why, if glaciers are able to erode so effectively, did they not produce a greater northern ocean basin sediment signal? As a corollary, what effect did Quaternary glaciation have on these northern landscapes?

Working in northern North America, Sugden (1978) observed scant but perceptible evidence of late Pleistocene glaciation on interfluvial summits between deep U-shaped valleys containing classic glacial depositional and erosional landforms, and labeled this fiord and plateau topography as “landscapes of selective linear erosion.” In these landscapes, differential erosion has juxtaposed weathered, un-eroded summits and unweathered, eroded valley bedrock surfaces.

The glaciological rationale for the differential erosion has followed the empirical evidence. Meter-scale bed relief causes fluctuations in hydraulic pressure at overdeepenings (Hooke, 1991) where plucking and frazil freeze-on of particles in basal ice may occur (Alley et al., 2003). At larger scales, ice flowing through valleys or fiords beneath an ice sheet or ice cap can achieve wet-based conditions because ice is thick and traps geothermal heat, converges at the confluence of tributary valleys, moves quickly due to bed lubrication, and reaches the pressure-melting point at lower temperatures (Cuffey et al., 2000). Sufficiently warm basal ice facilitates erosion mainly due to availability of water and enhanced abrasion (Hallet, 1979), glacial quarrying or plucking from higher ice velocities (Hallet, 1996; Alley et al., 2003). Cold-based ice inhibits

glacial erosion and may protect rock from periglacial processes (Tomkin and Braun, 2002). Relatively thin ice on interfluvial summits loses more geothermal heat to the cold atmosphere and moves by internal deformation above the frozen ice-substrate interface (Paterson, 1994).

Modern sediment yield from polar (entirely cold-based), polythermal (partly cold-based), and temperate (entirely warm-based) glacier basins show a clear dependence with thermal regime; the sediment yield-derived erosion rates differ by several orders of magnitude with the greatest amount of sediment derived from erosion by temperate glaciers (Elverhoi et al., 1998). These erosion rates were determined by dividing the volume of sediment delivered per unit time by the contributing basin areas. Limitations of using modern sediment to estimate erosion rates include: (1) non-uniform subglacial sediment storage; (2) the assumption that sliding velocity equals surface velocity; (3) systematic bias that makes contemporary sedimentation rates higher than longer term rates due to today's anomalously high glacier retreat velocities; (4) input of subaerial sediments into the sediment sinks; (5) flux variation resulting from a number of factors, including less precipitation in areas with polythermal or polar glaciers, lithological differences etc.; and finally, (6) the dearth of modern sediment fluxes' spanning the interesting glacial-interglacial transition. Ocean basin sediment records that do span the last glacial-interglacial transition often have limited chronological constraints and may have experienced post-depositional sediment winnowing.

Recent attempts to constrain rates of glacial erosion have mimicked the empirical method that fluvial geomorphologists have used for river systems (Summerfield and Hulton, 1994; Hay, 1998), where the physical system can be too complicated to model by

relying on first principles. These empirically-derived erosion rules for fluvial systems are sufficiently robust to reproduce landscape morphologies with spatially varying precipitation using state-of-the-art coupled surface process-geodynamic models (e. g., Willgoose et al., 1991a, 1991b; Tucker and Slingerland, 1997; Whipple and Tucker, 1999; Willette, 1999).

This paucity of reliable empirical data on basin-scale glacial erosion rates contrasts with the insight that has emerged from theoretical studies of the small-scale dynamics of glacial erosion (e.g., Röthlisberger, 1968; Boulton, 1974, 1979; Hallet 1976, 1996; Cuffey and Alley, 1996; Alley et al., 2003). Large-scale theoretical models using simple idealized bed geometries have suggested that glacial erosion rates scale with basal sliding velocity and can allow simulation of certain features of mountain ranges (Hallet, 1979; Oerlemans, 1985; Puranen, 1988; Hallet et al., 1996; Braun et al., 2001, MacGregor et al., 2000 and Tomkin and Braun, 2002). Few studies that attempt to validate these large-scale glacial erosion models on field sites with realistic glacier bed geometries have focused on polythermal or polar glaciers.

Working on polar outlet glaciers in Antarctica, Cuffey et al. (2000) supported the notion of limited erosion by cold-based ice and calculated rates of cold-based ice erosion ($3 \times 10^{-9} - 9 \times 10^{-9} \text{ cm} \cdot \text{a}^{-1}$) derived from subglacial debris measurements. To explain the erosion, they invoked the presence of interfacial water films even at extremely low temperatures as Gilpin (1979) originally reported. Boulton (1979) and Shreve (1984) also provided theoretical mechanisms whereby debris within cold-based ice may be entrained by plucking of subglacial asperities or by clast rotation initiated by differential creep of the zone directly above the frozen bed. In keeping with the use of fluvial classification

and terminology, one previous effort to determine the rate of glacial erosion beneath an Antarctic polythermal ice stream focused on “transport-limited” erosion systems. This erosion is thought to deform and transport thick subglacial till and marine sediments beneath Ice Stream C. The transport-limited erosion model also assumes that transport scales with basal ice velocity and produces reasonable glacial erosion estimates (Bougamont and Tulaczyk, 2003).

Of those studies that have focused on non-temperate glaciers, fewer yet have focused on sediment-limited systems similar to those that may be dictating the erosion of northern North America. To borrow terminology again, “sediment-limited” fluvial erosion systems where the streams incise into bedrock are limited by the availability of alluvial tools to erode the bedrock. In northern Atlantic and Arctic Canada, the absence of glacially-molded landforms such as flutes and drumlins (Dyke and Morris, 1988; Stokes and Clark, 2001) as well as the presence of bare bedrock may indicate that the mode of glacial erosion may have been sediment-limited.

This distinction is important when considering that there have been very few glacial erosion “rules” to be tested or calibrated for areas with significant portions once covered by cold-based ice. Still fewer empirical-tests span the glacial-interglacial transition and fewer still consider the basal conditions and bed properties, and the likelihood that they vary significantly with time and space. When determining glacial erosion rates, the transport of sediment also becomes important to parameterize because till protects the bedrock from further erosion and so the presence of this protective till film becomes crucial to understand.

The themes in this thesis are presented as three individual chapters prepared as manuscripts and focus on glacial erosion rates and processes derived from terrestrial in situ cosmogenic nuclide (TCN) techniques applied to bedrock and till. These themes are viewed in a context of cold-based and warm-based thermal regimes of ice protecting and eroding northern landscapes, respectively. A refinement of the TCN technique for samples that have been exposed near Earth's surface during a glaciation also strengthens the TCN method for these areas.

Chapter 2 addresses the change in TCN production rates during glaciation due to the compression of atmospheric mass from a colder atmosphere and redistribution of atmospheric mass from large-scale wind patterns moving around voluminous continental ice masses during the last glacial maximum (LGM). This chapter is a manuscript that was submitted for publication to *Journal of Geophysical Research, Solid Earth*. The manuscript has not been accepted or rejected as of the submission of this thesis. The co-authors, J. Fastook and J. Johnson provided the UMISM output of global LGM ice configuration to R. Toracinta and B. Oglesby. Co-authors, R. Toracinta and B. Oglesby provided output of surface pressures from the CCM3 general circulation model. Co-author, J. Gosse revised and clarified the text.

Chapter 3 presents TCN in bedrock as evidence for the extent of ice cover in the Torngat Mountains, as in previous studies (Marquette et al. 2004), but also extends the use of TCN to ascertain the dynamic state of the ice with the help of a thermo-mechanical ice sheet model. A new calibration of a glacial erosion rule using both model-derived basal velocities and TCN in bedrock is derived. Some of the data reported in Marquette et al. (2004) are reproduced in this chapter, but are updated to recent production rates. This

manuscript was accepted to Earth Surface Processes and Landforms and is in press as of the submission of this thesis. Co-authors, J. Fastook and J. Johnson provided the ice sheet model that was used to simulate ice cover over the Torngat Mountains. Co-authors, J. Gray and D. Stockli assisted sample collection in the field. Co-authors, L. Stockli and B. Finkel provided laboratory assistance and accelerator mass spectrometry (AMS) analyses, respectively. Co-author, J. Gosse, helped refine the goal of the work and revised the text.

Chapter 4 addresses the use of glacial till as an indicator of areally averaged basal thermal conditions, transport and the implications of this novel technique for drift prospecting in glaciated terrains, interpreting paleo-ice flow indicators, constraining landscape preservation, and assessing TCN exposure ages of boulders. This manuscript has not yet been submitted for publication. Co-authors, T. Little and D. Utting provided till samples and helped choose the subset of till samples to analyze. Co-authors, J. Johnson and J. Fastook provided the ice sheet model. Co-author, R. Finkel provided AMS analyses of the TCN samples. Co-author, J. Gosse helped choose the subset of till samples to analyze and assisted with revision and focus of the manuscript.

Chapter 5 summarizes the conclusions for Chapters 2, 3 and 4 as well as uses these conclusions to discuss North American glacial erosion viewed in a context of polythermal continental ice cover during the last and preceding glaciations. A series of appendices follow the main text of the thesis and contain supplementary material and further explanation of details of TCN chemistry and ice sheet modeling procedures that were restricted by word count in the manuscripts that appear as Chapters 2, 3 and 4.

CHAPTER 2

ATMOSPHERIC SCALING OF COSMOGENIC NUCLIDE PRODUCTION:

THE CLIMATE EFFECT

Jane Staiger and John Gosse

Department of Earth Sciences, Dalhousie University, 3006 Life Sciences Centre, Edsell
Castle Circle, Halifax, Nova Scotia, B3H 4J1, Canada

Rick Toracinta

Byrd Polar Research Center, Ohio State University, 1090 Carmack Road, Columbus,
Ohio, 43210, U.S.A.

Bob Oglesby

MSFC, NASA, Huntsville, Alabama, U.S.A.

James Fastook

Department of Computer Science, University of Maine, Orono, Maine, 04469, U.S.A.

Jesse V. Johnson

Department of Computer Science, Social Science Building, Room 417, University of
Montana, Missoula, Montana, 59812, U.S.A.

2.1 ABSTRACT

Absorption of cosmic rays by atmospheric mass varies temporally due to a redistribution of atmospheric pressure by ice sheets during glaciations, the compression and expansion of the atmosphere due to cooling and warming, and changes in katabatic winds near large ice masses. This work examines the consequences of these atmospheric conditions on the production rates of cosmogenic nuclides at Earth's surface.

Combining a CCM3 model with imbedded ice sheets for 20 ka, production rates changes (relative to today) are greatest at high elevations (6-7% at 5 km altitude) due to atmospheric compression from decreased temperature. Production rates for sites near ice sheet margins, which are often targeted to exposure date deglaciation, can be reduced more than 10% due to a combination of katabatic winds draining off the ice sheet margins and atmospheric cooling. Time-integrated production rates that span both glacial and interglacial conditions should account for the duration of ice-margin proximity. Nunatak settings would also be significantly affected by the climate effect due to persistent glacial atmospheric conditions. Atmospheric variability may explain some of the disparities among cosmogenic nuclide production rate calibrations.

2.2 INTRODUCTION

The production rate of terrestrial in situ cosmogenic nuclides (TCN) varies spatially and temporally with geomagnetic field strength and atmospheric pressure (Lal, 1991). Production rates for six TCN (^3He , ^{10}Be , ^{14}C , ^{21}Ne , ^{28}Al , ^{36}Cl) have been determined for mid- and high-latitude sites at a range of atmospheric depths (from near sea-level to >3000 m above sea level (a.s.l.)). The cosmogenic exposure dating technique has been used to date surface exposure to cosmic radiation on surfaces spanning the elevations below sea level to >5000 m. Analytical measurements currently have routine precisions approaching 1% (1σ) but the uncertainty in time-averaged TCN production rates at some sites may be as large as 20%.

TCN production rates measured at calibration sites are normalized to production at sea level and high latitude using algorithms that have been derived mostly from detections of disintegrations (stars) produced in photographic film at different latitudes and altitudes (Lal and Peters, 1967; Lal, 1991), or from neutron flux measurements at different latitudes and altitudes (shipboard and monitor data) (e.g. Dunai, 2000; Desilets and Zreda, 2001, 2003). All empirical calibrations are a time-integrated measurement over the independently determined (typically with radiocarbon or $^{40}\text{Ar}/^{39}\text{Ar}$) exposure duration. Therefore, each calibration incorporates the time varying geomagnetic and atmospheric effects specific to that site. The normalized production rates are averaged and then scaled, using the same algorithms, to calculate the TCN production rate at any site on Earth's surface. Improved scaling methods incorporating better fits of the non-dipole geomagnetic field and non-standard atmospheric pressure anomalies have been suggested by Dunai (2000) and Stone (2000), respectively. Uncertainties in the

latitudinal scaling due to geomagnetic influences (especially due to temporal variations in paleointensity, secular variations in dipole position, and non-dipole features of the geomagnetic field) have been addressed by others (Gosse and Phillips, 2001; Masarik et al., 2001; Dunai, 2001; Desilets and Zreda, 2003) although there is no agreement on the actual influence of temporal variations in these geomagnetic field aspects. Uncertainty in atmospheric scaling has been assessed even less. Stone (2000) provided scaling factors for latitude and altitude based on those of Lal (1991) but recast the simple standard atmosphere approximation in terms of spatially variant atmospheric pressure. Even after rescaling the ^{10}Be production rates in quartz for a smaller muonic contribution (relative to Lal, 1991) there remains a slight positive correlation with calibration site elevation (Gosse and Stone, 2001).

This work examines the influences on TCN production rates of changes in the atmospheric density distribution during glaciations. Although the principal objective of this paper is to consider the potential sources of atmospheric-derived influences on TCN production rates, we have also attempted to quantify the effects. Interglacial and glacial conditions, discussed here as the difference between present-day and the Last Glacial Maximum (LGM) climate, affects the total atmospheric mass that shields surface samples from cosmic radiation. Four conditions that arise from a change in climate are (1) ice sheets displace atmospheric mass, (2) katabatic winds on the ice sheets produce quasi-stationary zones of low surface pressure (Stone, 2000), (3) cooler temperatures compress the atmosphere, and (4) decreased ocean degassing due to colder ocean temperatures decreases the global atmospheric mass (Mélières et al., 1991). Changes in the total mass of the atmosphere (4) are calculated to be approximately 0.1% of the total atmospheric

pressure (Mélières et al., 1991) so will not be treated further due to the insignificant impact on TCN production rates. We evaluate the potential influence of the first three conditions and show that climate change may explain residual disparities among production rate calibrations for ^{10}Be .

2.3 METHODOLOGY

We used a General Circulation Model (GCM) to provide climate simulations at two different climate scenarios—present-day conditions and LGM conditions—to determine the effect of large ice sheets on the atmosphere (Toracinta et al., 2004). Note that climate change without growth or decay of glaciers can have an impact on production rates, but the presence of ice sheets significantly adds to this effect and enables us to evaluate the effect of climate at two end-member climate regimes. The LGM GCM incorporated global glacier ice cover as calculated by the thermomechanical University of Maine Ice Sheet Model (2003 version) (UMISM: Fastook and Chapman, 1989; Fastook and Prentice, 1994). Full methodology for simulated LGM ice sheet surface elevations and simulated LGM atmospheric conditions from a GCM that includes a Land Surface Model are described elsewhere (CCM3: Kiehl et al., 1998a, 1998b; LSM: Bonan, 1998, *in* Toracinta et al., 2004). The following sections give an overview of the boundary conditions and nature of these models. Appendix 5 in this thesis extends the abbreviated description of UMISM in this chapter.

2.3.1 UMISM

UMISM is a time-dependant, momentum and mass-balance driven, finite-element model. Temperature proxy data from the GRIP ice core drives the ice sheet response and is extrapolated outward radially with lapse rates that govern temperature with altitude (Fastook and Chapman, 1989; Fastook and Prentice, 1994). Recent improvements in UMISM include additions of glacio-isostasy, thermodynamics of the temperature distribution within the ice sheet, and basal water algorithms (Johnson and Fastook, 2002). These improvements allow better control on ice-margin position and ice sheet surface elevation and are crucial to developing reasonable estimates of the effect of LGM climate on TCN production rates, especially at (calibration) sites that lie on the margins of paleo-ice sheets.

The surface elevations include an isostatic adjustment such that a pseudo-elastic, hydrostatically-supported crust is depressed by the weight of glacier ice. However, areas beyond the ice sheet margins are not isostatically compensated nor does the isostatic response create a forebulge. These temporary ice proximal depressions near ice margins are typically on the order of up to tens of meters and would not likely affect the climate simulations or TCN production rates. The climate in UMISM was controlled by the $\delta^{18}\text{O}$ curve from the GRIP ice core, central Greenland transformed to a temperature record (Johnsen et al., 1995). This record therefore forms the backbone of the temperature and precipitation calculation that drives the glacial cycle. The mean annual temperature for each node varies by specified altitudinal and latitudinal lapse rates.

For the LGM climate simulations, Laurentide, Fennoscandian and Antarctic ice sheet elevations are the glaciological model output from UMISM. The Patagonian Ice Sheet elevations are from model output by Hulton et al., (2002). Sea level during the LGM was lowered by 120 m, commensurate with the LGM ice sheet volume. Calculated sea level provides an additional check on global ice volume calculations.

2.3.2 CCM3

The NCAR Community Climate Model version 3 (CCM3: Kiehl et al., 1998a) is used to simulate the LGM climate over the ice sheets prescribed by UMISM. Boundary conditions other than UMISM ice elevations include 21-ka computed orbital-parameters for solar forcing, trace gases concentration (CO₂ concentration set to 180 ppm; CH₄ concentration set to 350 ppbv), sea level, and a modified version of the CLIMAP SSTs based on proxy data (a different temperature modeling scheme than UMISM). Modern vegetation was used due to uncertainty in global vegetation reconstructions for the LGM. The model employs a T42 spectral truncation (2.8° x 2.8° transform grid) with 18 levels in the vertical (Toracinta et al., 2004). Present-day topographic input is based on a 64 x 128-cell grid (2.8°x2.8°) that coarsely samples topography. The performance of CCM3 in simulating the present-day climate is described in several papers in the Journal of Climate special issue (June 1998). CCM3 produces a reasonable representation of the large-scale atmospheric circulation including the Northern Hemisphere longwave pattern and zonal wind structure (Kiehl et al., 1998a). Large-scale surface pressure features are well captured, as are the mid-latitude storm tracks (Hurrell et al., 1998; Kageyama et al.,

1998). Tropical inter-seasonal oscillations are simulated by CCM3, albeit with shorter than observed periodicities and somewhat damped amplitudes.

The simulated top-of-atmosphere radiative budget agrees well with observations, although deficiencies in the treatment of clouds in marine stratus regions and in the placement of atmospheric deep convection in the western Pacific result in large biases in shortwave fluxes at the surface and top-of-atmosphere (Kiehl et al., 1998b). The hydrologic cycle is generally well simulated, as is the Indian Monsoon, although CCM3 produces a lower tropospheric dry bias in the large-scale moisture field (Hack et al., 1998).

In polar regions, CCM3 exhibits deficiencies in the simulated radiation budget that are related to an excessive cloud fraction and cloud water path (Briegleb and Bromwich, 1998a). The resulting negative biases in solar radiation budget result in deep polar vortices and cold surface temperatures compared to observations (Briegleb and Bromwich, 1998b). Also, errors in surface albedo result from the lack of a meltwater pond representation in CCM3 and other atmospheric changes that may be specific to LGM conditions like the effect of large pro-glacial or pluvial lakes (Hoestetler et al., 2000). While CCM3 generally captures many important polar atmospheric features, there are errors in amplitude and placement of, for instance, the Northern Hemisphere Icelandic Low and Aleutian Low as well as the Antarctic circumpolar trough (Briegleb and Bromwich, 1998b). The Antarctic katabatic wind regime is well captured. A comparison of the atmospheric simulation for present-day and the 50-year averaged atmospheric data shown in Stone (2000) further demonstrates the reliability of the GCM model output

The LGM surface elevation input is based on the model output of UMISM and present-day elevations outside the margins of the ice sheets. Eustatic LGM sea level lowering is treated by raising the topography by 120 m and classifying sub-aerial regions between 0 and 120 m below sea level as new land surface. Although the simulation conforms to general knowledge of LGM climate, a thorough evaluation of the LGM simulation is not yet available. One simplistic test of the validity of the atmospheric compression produced by the CCM3 simulation is described in the CCM3 results (§2.4) section below.

2.3.3 PRODUCTION RATE CALCULATIONS

Sea level of the LGM model run is 120 m below present-day sea level. For the comparison of LGM and present-day surface pressures, adjustments to modeled pressure are unnecessary since surface pressure refers to the total mass above the surface. The calculations presented here build on the original altitude and latitude scaling method of Lal (1991), which assumed an atmosphere with a uniform pressure of 1013.5 hPa. Stone (2000) adjusted Lal's (1991) altitude and latitude scaling equations in terms of atmospheric pressure (P , in hPa) rather than altitude. Stone's (2000) scaling factor for production by spallation used in this calculation is:

$$S(P) = a + b \exp [-P/150] + cP + dP^2 + eP^3. \quad (\text{Eq. 2.1})$$

Coefficients 'a', 'b', 'c', 'd' and 'e' are given for latitudes of 0° – 60° in 10° increments (Table 1 in Stone, 2000). Values between the 10° increments are linearly interpolated.

The contribution of muons is considered negligible in this calculation in order to keep the results applicable to all TCN. This treatment of muons is warranted because muons contribute only a few percentage of the total surface production of TCN at sea level and decreases with decreasing atmospheric pressure or elevation (Stone, 2000; Kubik and Ivy-Ochs., 2004).

2.4 RESULTS

GCM output shows significant differences between the LGM, 200-hPa height field and the present-day, 200-hPa height field (Fig. 2.1). The majority of the atmospheric change during the LGM was a global compression of the atmosphere. Areas that are most affected by changes in pressure due to climate change are illustrated in the graphs of latitudinally averaged deviations of pressures (Fig. 2.2). These areas are located near the margins of paleo-ice sheets or latitudes with high average elevations. At the high-altitude sites, atmospheric compression during glaciation essentially results in a migration of atmospheric mass to lower elevations (Fig. 2.3), such that at sea level, the effect of atmosphere compression is negligible, but at 3.5 km above sea level, the TCN production rate can be 3-4% greater than the present-day atmosphere.

A rough estimate of the validity of the CCM3 atmospheric compression is supported by ELA (Equilibrium Line Altitude) changes during the LGM in the tropics. Porter et al. (2001) determined that the snowline depression in the tropics to be $900 \text{ m} \pm$

135 m during the LGM owing to lowered atmospheric temperatures. Using ELR (Environmental Lapse Rates) range of 6.5 °C/km or 10 °C/km, this change in the ELA corresponds to -10.4 to -4.9 °C of cooling in this area. Assuming that the ELA corresponds to the 0°C isotherm and using the universal gas law ($PV = nRT$), this results in a 1.8% to 3.8% decrease in the volume of the atmosphere. The CCM3 simulation of LGM climate cooling-induced atmospheric compression produces a 300 m decrease of the height of the 200-hPa isobar in this area, which is 3% of the average height of the 200-hPa isobar. This CCM3 simulation value lies within the range of compression supported by changes in the snowline altitudes (Porter et al., 2001).

The deviation of LGM production rates from present-day due to changes in atmosphere conditions is shown in Fig. 2.4. This result therefore incorporates the effect observed by Stone (2000) regarding the error in assuming a globally uniform standard atmosphere as well as the effect of the significant variations in atmospheric pressure distribution with time.

2.5 DISCUSSION

The deviations shown in Fig. 2.4 are maximum differences between the two end-member glacial and non-glacial modeled scenarios. Because TCN concentrations increase with exposure duration, a TCN exposure age reflects an integration of the time-varying production rates. To adjust the production rates over a glacial cycle, one must interpolate between the glacial production rate and the interglacial production rate by a fitting function that is appropriate to the glacial setting. For example, the production rate

interpolation from an LGM (+6.5% correction) to present-day (0% correction after Stone (2000) is applied) of a boulder on a terminal moraine of an ice sheet at 5.7 km altitude, which was occupied by an oscillating ice margin for 5 ka before rapid retreat would have to be adjusted for all three conditions (katabatic winds associated with the ice sheet for the first 5 ka of exposure, and the atmospheric variations due to cooling and the presence of ice sheets for the entire exposure duration, Fig. 2.5). On the other hand, a surface at sea level far removed from an ice sheet would experience a negligible integrated effect over the past 20 ka. The largest katabatic wind effect during a single glaciation would occur in areas where there has been a long-standing ice margin or on nunataks. Based on the distribution of erratic exposure ages from the front to rear of the broad moraine, Gosse et al. (1995) have shown that ice occupancy of the large LGM terminal moraine of the Fremont Lake lobe (Rocky Mountain Pinedale Glaciation type locality) may have persisted for more than 5 ka. Importantly, for exposure durations that span beyond the last 20 ka, the time integrated climate effect on production rate will be larger considering that ice sheets modified the atmosphere for the majority of the Pleistocene.

The influence of the climate conditions on TCN production rates can be evaluated for any calibration site. For example, Laurentide Ice Sheet ice at the New Jersey ^{10}Be production rate calibration site (Clark et al, 1996) may have remained at its terminal position for over 1 ka before retreating from that position over a period of several ka (Cotter, 1984, Cotter et al., 1986). The influence of katabatic winds may be significant (2-3%) when integrated over the entire exposure duration. Ackert et al. (2003) have also cited anomalies in their long-term ^3He production rates from Patagonian lava flows, independently dated by $^{40}\text{Ar}/^{39}\text{Ar}$ that are 11% higher than other published ^3He

production rates. They attributed the higher rate to atmospheric effects. Their long-term production-rate is supported by our model results, which show ~8% greater (glacial) production than modeled present-day production. When tuned to a $\delta^{18}\text{O}$ temperature-record and integrated over the duration of exposure, the production rate change in this area is 4-5% for the flows of different ages. An additional 4% greater production can be explained by the error related to using a standard atmosphere instead of a more realistic atmosphere (Stone, 2000).

After rescaling ^{10}Be production rates measured at calibration sites for a lower muonic contribution (Stone, 2000) than Lal (1991), Gosse and Stone (2001) noted a small, residual positive correlation between published ^{10}Be production rates and elevation. Fig. 2.6 illustrates the influence of time-integrated adjustments in production rates at sites where ^{10}Be has been measured. In the case of the New Jersey Laurentide Ice Sheet (LIS) calibration site adjustment, we report the production rate based on adjustments of the length of time the calibration site was in close proximity to the ice margin (Larsen, 1995, and references therein; Larsen et al., 1995). The production rates derived from UCSD and Echo Lake artificial targets (Nishiizumi, 1996) have not been adjusted for the climate effect but have been adjusted for the lowered (Stone, 2000) muonic contribution. The production rate adjustments due to atmospheric effects decrease the average production rate by 2% and slightly improve the standard deviation of the production rates. However, these adjustments are within 1- σ of the mean of the published calibrated ^{10}Be production rates, $5.1 \pm 0.3 \text{ atom g}^{-1}\cdot\text{a}^{-1}$ (Gosse and Stone, 2001). At this time, the topographic resolution of the CCM3 climate model inhibits more precise adjustments for site specific calibrations.

2.6 CONCLUSIONS

There are three climate controlled atmospheric conditions that induce temporal variability in TCN production rates. Changes in atmospheric pressure near large glaciers due to katabatic winds will increase production rates. The difference is present-day and LGM production rates due to katabatic winds may be as large as 10%. Changes in the altitudinal distribution of atmospheric mass due to cooling will have increasing influence with greater elevation. Changes in the synoptic atmospheric pressure distribution due to cooling and the increased volume of ice masses lead to worldwide effects that vary spatially due to complex atmospheric dynamics. The latter two conditions have caused LGM production rates to be as much as 7% higher than the present-day. The magnitude of the time-integrated changes in production rates will be proportional to the amount of the total exposure duration that experienced glaciation. The implication of climate-induced TCN production rate variability for published and future calibrations will require some consideration as the community continues to improve the technique.

2.7 ACKNOWLEDGEMENTS

We thank Greg Balco for the use of his online MATLAB scripts and Djordje Grujic and Rasmus C. Thiede for the use of the Excel spreadsheet for calculating mean linear regressions and Henry Osmaston for stimulating discussions on the appropriate

treatment of sea level lowering during the LGM. The Laurentide Ice Sheet research project was sponsored by NSF grant OPP- 9905381. The project was funded by ACOA-AIF grant 1001052 and OPP-9905381 to JG. Use of computer resources at NCAR and the Ohio Supercomputing Center was provided through grants 36091009 and PAS0045-1, respectively, to RT. JS thanks the Killam Trust for funding through a pre-doctoral Fellowship Award.

2.8 REFERENCES

- Ackert, R. P., Singer, B. S., Guillou, H., Kaplan, M. R., Kurz, M. D. 2003. Long-term cosmogenic ^3He production rates from $^{40}\text{Ar}/^{39}\text{Ar}$ and K-Ar dated Patagonian lava flows at 47°S. *Earth and Planetary Science Letters* **210**: 119-136.
- Bierman, P. R., Larsen, P., Clapp, E., Clark, D. 1996. Refining estimates of ^{10}Be and ^{26}Al production rates. *Radiocarbon* **38**: 149.
- Bonan, G.B. 1998. The land surface climatology of the NCAR land surface model (LSM1.0) coupled to the NCAR Community Climate Model (CCM3). *Journal of Climatology* **11**: 1307-1326.
- Briegleb, B. P., Bromwich, D. H. 1998a. Polar radiation budgets of the NCAR CCM3. *Journal of Climatology* **11**: 1246-1269.

- Briegleb, B. P., Bromwich, D. H. 1998b. Polar climate simulation of the NCAR CCM3. *Journal of Climatology* **11**: 1270-1286.
- Clark, D. H., Bierman, P., Gillespie, A. R. 1996. ^{10}Be and ^{26}Al production rates and a revised glacial chronology for the Sierra Nevada. *Radiocarbon* **38**: 152.
- Cotter, J. F. P. 1984. The minimum age of the Woodfordian deglaciation of northeastern Pennsylvania and Northwestern New Jersey, Ph.D. thesis, Lehigh University, Bethlehem.
- Cotter, J. F. P., Ridge, J. C., Evenson, E. B., Sevon, W., Sirkin, D. L., Stuckenrath, R. 1986. The Wisconsinan history of the Great Valley, Pennsylvania and New Jersey, and the age of the "terminal moraine", *Bulletin - New York State Museum*, (1976) **455**: 22-49.
- Desilets, D., Zreda M. 2001. On scaling cosmogenic nuclide production rates for altitude and latitude using cosmic-ray measurements. *Earth and Planetary Science Letters* **193**: 213-225.
- Desilets, D., Zreda, M. 2003. Spatial and temporal distribution of secondary cosmic-ray nucleon intensities and applications to in situ cosmogenic dating. *Earth and Planetary Science Letters* **206**: 21-42.

- Dunai, T. J. 2000. Scaling factors for production rates of in situ produced cosmogenic nuclides: A critical reevaluation. *Earth and Planetary Science Letters* **176**: 157-169.
- Dunai, T. J. 2001. Influence of secular variation of the geomagnetic field on production rates of in situ produced cosmogenic nuclides. *Earth and Planetary Science Letters* **193**(1-2): 197-212.
- Fastook, J., Chapman J. 1989. A map plane finite-element model: Three modeling experiments. *Journal of Glaciology* **35**(119): 48–52.
- Fastook, J., Prentice M. 1994. A finite-element model of Antarctica: Sensitivity test for meteorological mass balance relationship. *Journal of Glaciology* **40**(134): 167–175.
- Gosse, J. C., Stone, J. O. 2001. Terrestrial cosmogenic nuclide methods passing milestones of paleo-altimetry, *EOS* **82**(7): 82, 86, 89.
- Gosse, J. C., Phillips, F. M. 2001. Terrestrial in situ cosmogenic nuclides: theory and applications, *Quaternary Science Reviews* **40**(14): 1475-1560.

- Gosse, J. C., Klein, J., Evenson, E. B., Lawn, B., Middleton, R. 1995. Be-10 Dating of the duration and retreat of the last Pinedale Glacial Sequence. *Science* **268**(5215): 1329–33.
- Gosse, J. C., Klein, J., Evenson, E. B., Davis, P. T., Jull, A. T., Burr G. 2003. Production rate of ^{10}Be and ^{26}Al at mid-latitude high altitudes, *Earth and Planetary Science Letters*, resubmitted.
- Hack, J. J., Kiehl, J. T., Hurrell, J. W. 1998. The hydrologic and thermodynamic characteristics of the NCAR CCM3. *Journal of Climate* **11**: 1179-1206.
- Hostetler, S. W., Bartlein, P. J., Clark, P. U., Small, E. E., Solomon, A. M. 2000. Simulated influences of Lake Agassiz on the climate of central North America 11,000 years ago. *Nature* **405**: 334–337.
- Hulton, N. R., Purves, R. S. McColloch, R. D. Sugden, D. E., Bentley, M. J. 2002. The Last Glacial Maximum and deglaciation of southern South America. *Quaternary Science Reviews* **21**: 233-241.
- Hurrell, J. W., Hack, J. J. Boville, B. A. Williamson, D. L., Kiehl, J. T. 1998. The dynamical simulation of the NCAR Community Climate Model Version 3 (CCM3). *Journal of Climatology* **11**: 1207-1236.

- Johnsen S., Dahl-Jensen, D. Dansgaard, W., Gunderup N. 1995, Greenland paleotemperatures derived from GRIP bore hole temperature and ice core isotope profiles. *Tellus* **47B**: 624-629.
- Johnson, J. V., and Fastook, J. L. 2002. Northern Hemisphere glaciation and its sensitivity to basal melt water. *Quaternary International* **95-96**: 65-74.
- Kageyama, M., Valdes, P. J., Ramstein, G., Hewitt, C., Wyputta, U. 1998. Northern Hemisphere storm tracks in present day and last glacial maximum climate simulations: A comparison of the European PMIP models. *Journal of Climatology* **12**: 742-760.
- Kiehl, J. T., Hack, J. J., Bonan, G. B., Boville, B. A., Williamson, D. L., Rasch P. J. 1998a. The National Center for Atmospheric Research Community Climate Model: CCM3. *Journal of Climatology* **11**: 1131-1149.
- Kiehl, J. T., Hack, J. J., Hurrell, J. W. 1998b. The energy budget of the NCAR Community Climate Model: CCM3. *Journal of Climatology* **11**: 1151-1178.
- Kubik, P. W., Ivy-Ochs, S. 2004. A re-evaluation of the 0-10 ka ^{10}Be production rate for exposure dating obtained from the Kofels (Austria) landslide. *Nuclear Instruments and Methods B* **223-224**: 618-622.

- Lal, D. 1991. Cosmic ray labeling of erosion surfaces: In situ nuclide production rates and erosion models. *Earth and Planetary Science Letters* **104**: 424-439.
- Lal, D., Peters B. 1967. Cosmic-ray produced radioactivity on the earth. *Handbook of Physics* **46**(2): 551-12.
- Larsen, P. L., Bierman, P. R., Caffee, M. 1995. Preliminary in situ production rates of cosmogenic ^{10}Be and ^{26}Al over the past 21.5 ky from the terminal moraine of the Laurentide ice sheet, north-central New Jersey. *Geological Society of America Abstract with Programs* **27**: A59.
- Larsen, P. 1995. In situ production rates of cosmogenic ^{10}Be and ^{26}Al over the past 21,500 years determined from the terminal moraine of the Laurentide ice sheet, north central New Jersey, M.S. thesis, Univ. of Vermont, Burlington.
- Masarik, J., Frank, M. Schäfer, J.M., Wieler, R. 2001. Correction of in situ cosmogenic nuclide production rates for geomagnetic field intensity variations during the past 800,000 years. *Geochimica et Cosmochimica Acta* **65**(17): 2995-3003.
- Mélières, M. A., Martinerie. P., Raynaud, D., Lliboutry, L. 1991. Glacial-interglacial mean sea level pressure change due to sea level, ice sheet and atmospheric mass changes. *Palaeogeography Palaeoclimatology Palaeoecology* **89**: 333-340.

- Nishiizumi, K., Winterer, E. L., Kohl, C. P., Klein, J., Middleton R., Lal, D., Arnold, J. R. 1989. Cosmic ray production rates of ^{10}Be and ^{26}Al in quartz from glacially polished rocks. *Journal of Geophysical Research* **94**(B12): 17,907-17,915.
- Nishiizumi, K., Finkel, R. C. Klein, J., Kohl, C. P. 1996. Cosmogenic production of ^7Be and ^{10}Be in water targets. *Journal of Geophysical Research* **101**: 22,225-22,232.
- Porter, S. C. 2001. Snowline depression in the tropics during the last glaciation. *Quaternary Science Reviews* **20**: 1067-1091.
- Press, W. H., Teukolsky, S. A., Vetterling, W. T., Flannery, B. P. 1992. *Numerical recipes in FORTRAN: The art of scientific computing*, 963 pp., Cambridge University Press., New York.
- Stone J. O., Ballantyne, C. K., Fifield, L. K. 1998. Exposure dating and validation of periglacial weathering limits, NW Scotland. *Geology* **26**: 587-590.
- Stone, J. O. 2000. Air pressure and cosmogenic isotope production. *Journal of Geophysical Research* **105**(B10): 23,753-23,759.
- Toracinta, E. R., Oglesby, R. J., Bromwich, D. H. 2004. Atmospheric response to modified CLIMAP ocean boundary conditions during the Last Glacial Maximum. *Journal of Climatology* **17**: 504-522.

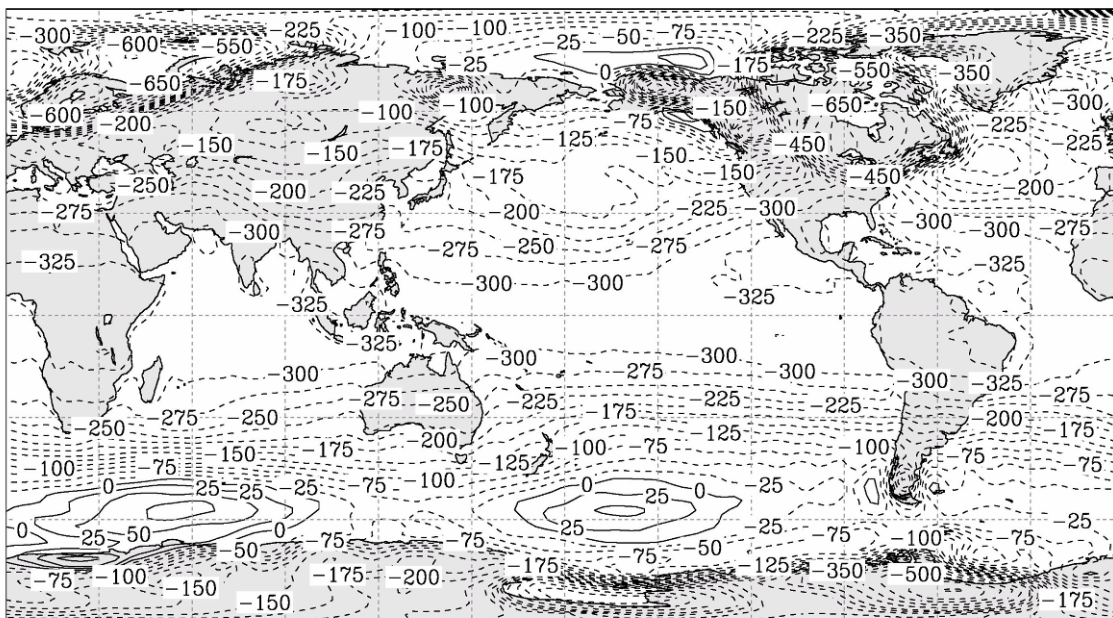


Figure 2.1 Difference in 200-hPa height field between 15-year average LGM and 15-year average (modeled) present day CCM3-simulation output. Dashed contours (m) reflect a compressed atmosphere; the deviation is greatest in areas near paleo-ice sheets. Solid contours signify a locally expanded atmosphere due to effects of glaciation.

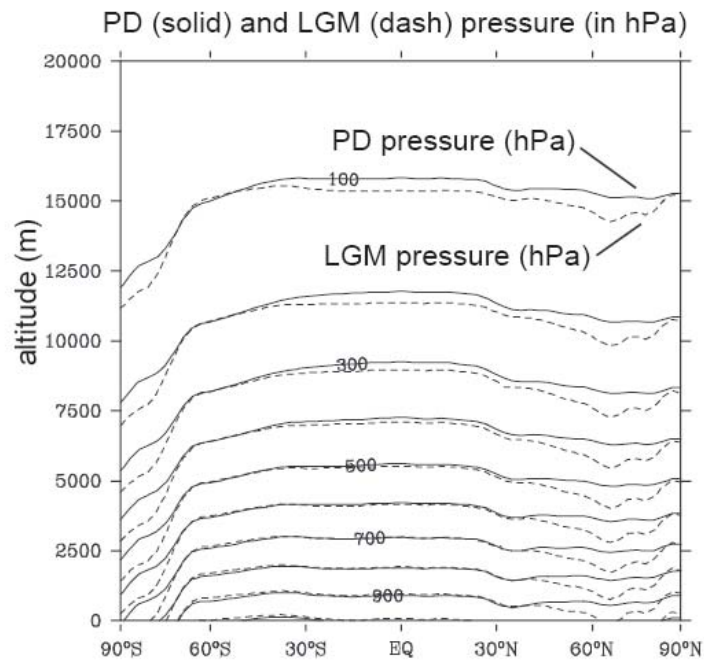


Figure 2.2 Longitudinal cross-section of average simulated pressure are contoured from 1000 to 100 (hPa) for present-day (solid lines) and LGM (dashed). Altitude represents height above the contemporaneous sea level.

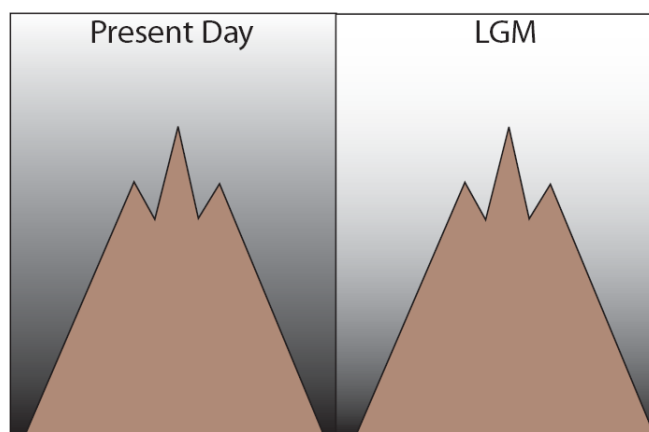


Figure 2.3 Illustration of atmosphere density redistribution due to cooling. The darkness of the shading of the background corresponds to atmospheric pressure (mass). Total mass is equal for both times. TCN production rates will not vary at sea level; but at high elevations, production rates will be greater during periods of glaciation.

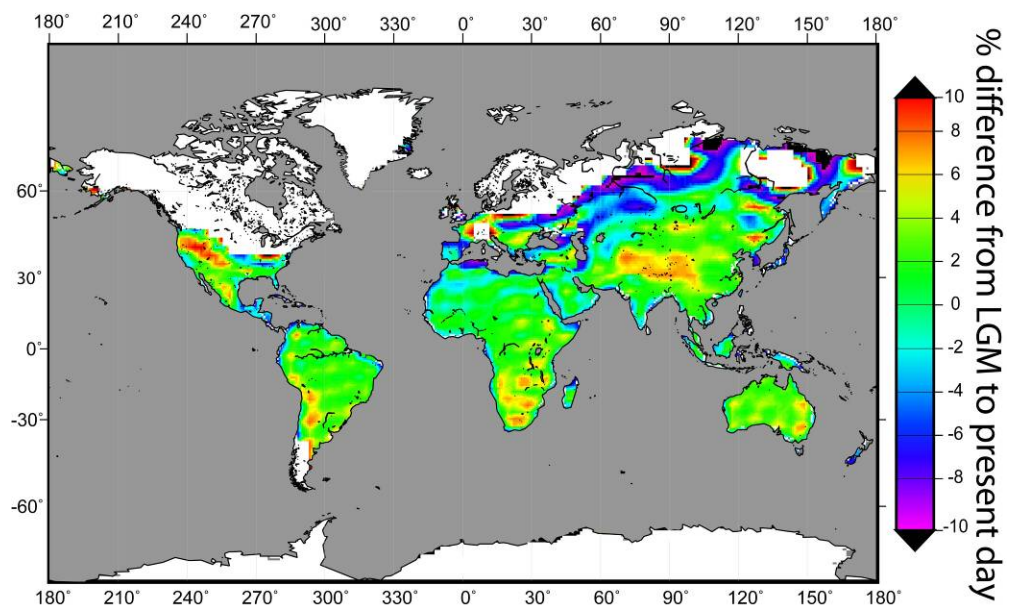


Figure 2.4 Percentage deviation of LGM production rates from present-day production rates. White areas were glaciated during the LGM and are excluded from the calculation.

Figure 2.5 a. Surface elevations (present-day) of the Himalaya used in the model climate simulations. **b.** Production rate percentage difference between present-day to LGM conditions. The area experiencing the greatest difference grossly matches the topography, illustrating the dominance of the atmospheric compression effect at high elevations. **c.** The 5720 m elevation site in (a) with a production rate increase of 6.5% during the LGM relative to present-day, may follow a $\delta^{18}\text{O}$ temperature curve to the present-day correction of 0%. The total effect on production rates in a sample deposited during the LGM follows the dashed line that essentially accumulates all the production rates to a final production rate adjustment of approximately 3% over that time of exposure.

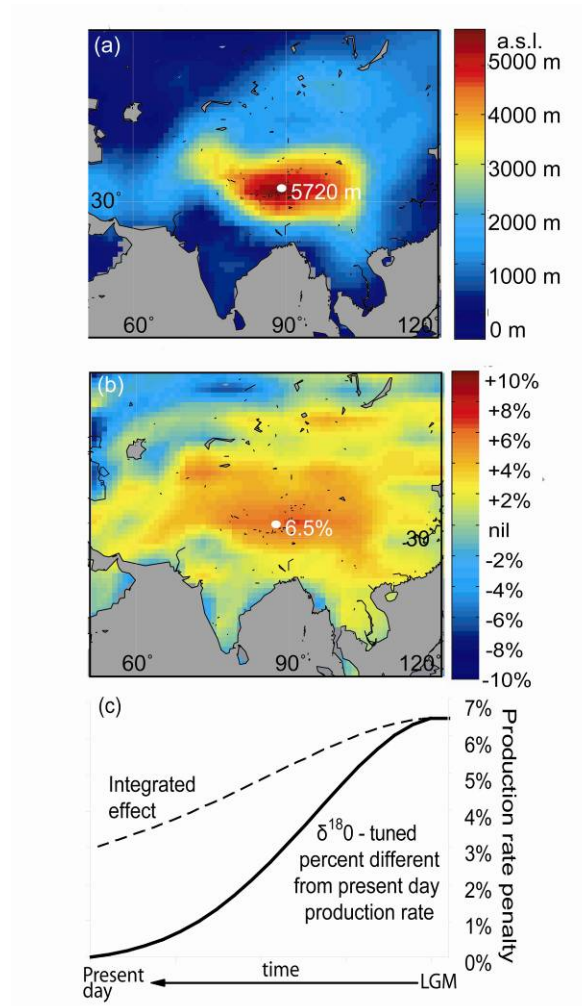


Figure 2.5

Figure 2.6 Calibrated and measured production rates of ^{10}Be (yellow squares) vs. altitude, adapted from Gosse and Stone (2001). LIS (Larsen et al., 1995; Bierman et al., 1996); An Teallach (Stone et al., 1998); Provo (Gosse et al., 1996); K fels (Kubik and Ivy-Ochs, 2004); Titcomb Basin (Gosse et al., 2003); and Sierra Nevada (Nishiizumi, 1989, Clark et al., 1995). These production rates are scaled by Lal's (1991) formulation to SLHL (sea level, high geomagnetic latitude) but uses a muonic contribution of 2.2% Stone (2000), except for the K fels site which uses a 3% muonic contribution. The green diamonds mark the correction of the ^{10}Be production rates for LGM atmospheric deviations from present day that includes a $\delta^{18}\text{O}$ curve-fit from LGM production rate deviation to present day, integrated over the period of exposure.

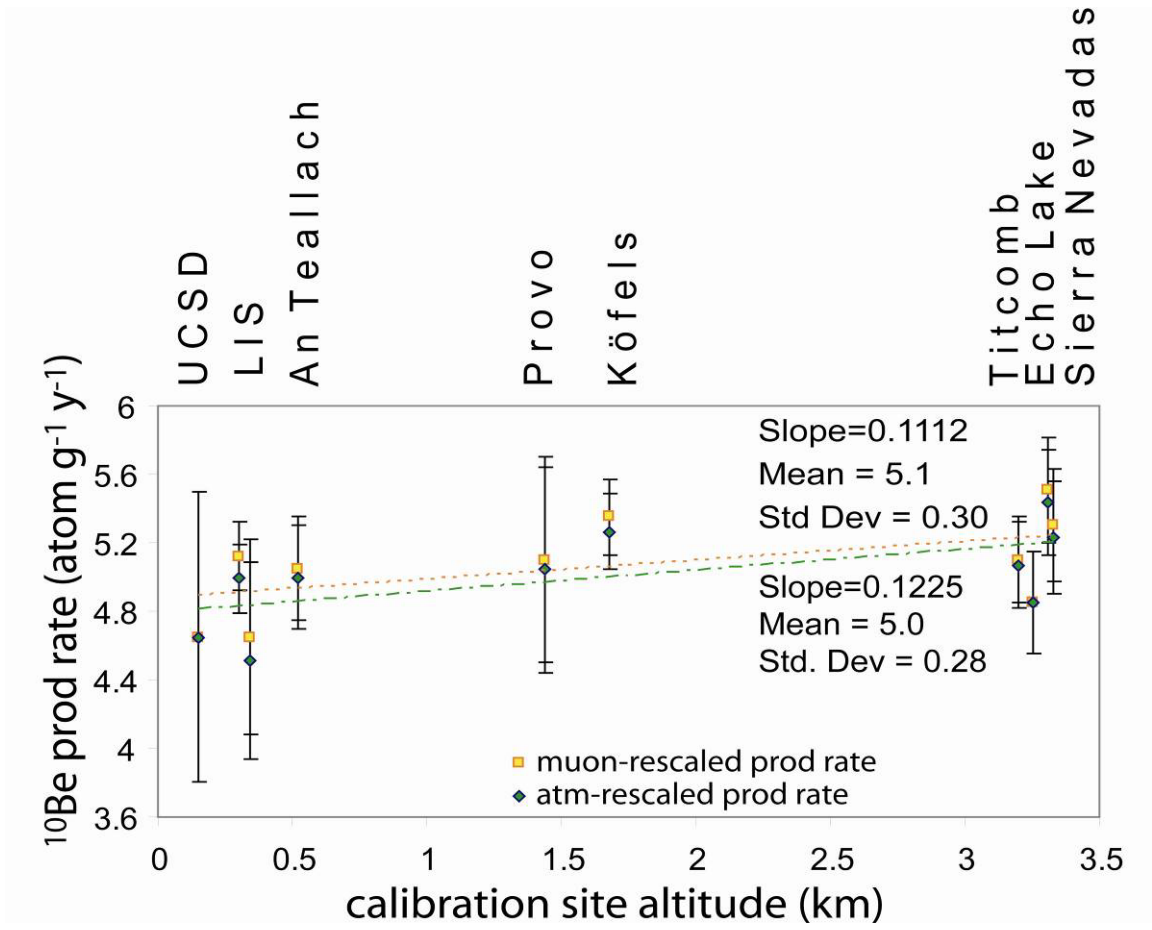


Figure 2.6

CHAPTER 3**QUATERNARY RELIEF GENERATION BY POLYTHERMAL GLACIER ICE****Staiger, Jane. K. W., Gosse, John C.**

Department of Earth Sciences, Dalhousie University, Halifax, Nova Scotia, CANADA

Johnson, Jesse V.

Department of Computer Science, University of Montana, Missoula, Montana 59812

Fastook, James

Department of Computer Science, University of Maine, Orono, Maine, 04469, U.S.A.

Gray, James T.,

Département de Géographie, Université de Montréal, Montréal, Québec, H3C 3J7,

Stockli, Daniel F., Stockli, Lisa

Department of Geology, University of Kansas, Lawrence, Kansas 66045, USA

Finkel, Robert

Lawrence Livermore National Laboratory, Center for Accelerator Mass Spectrometry

7000 East Ave, Livermore, California 94550, USA

3.1 ABSTRACT

The juxtaposition of wet-based erosive ice in valleys and cold-based, non-erosive ice atop felsenmeer-covered interfluvial plateaus has generated relief in the Torngat Mountains of northeastern Canada. Measurements of terrestrial in situ cosmogenic nuclide (TCN) concentrations from 31 bedrock sites, coupled with soils and geomorphology, indicate that erosion of the valleys has been > 2 m during a single glacial-interglacial cycle. However, on summit plateaus the long-term (over several glacial-interglacial cycles) erosion rate is < 1.4 m/Ma. TCN ratios reveal that the exposure plus ice cover history retained on some summit surfaces probably spans more than 800 ka despite complete ice cover as recently as 11 ka. A thermodynamic ice sheet model with a basal water calculation is used to calculate the sliding distance normalized by the duration of ice cover for the region. We formulate a general glacial erosion rule for the Torngat Mountains, which correlates TCN-derived erosion rates for terrain once partially covered by cold-based ice with modeled average ice basal sliding velocities. Erosion rates vary linearly with average sliding velocity by a glacial erosion coefficient of 5×10^{-7} . Due to the significant distribution of cold-based ice cover in this high latitude region, our estimates of net regional glacial erosion and glacial erosion coefficient are orders of magnitude lower than a previously published value.

3.2 INTRODUCTION

We begin with the premise that over several glacial cycles, glaciation can perturb topography and could cause climatic feedbacks (Molnar and England, 1990), relief-production feedbacks (Whipple et al., 1999, Small and Anderson, 1998), and preclusion of steady-state topography during changing climatic conditions (Peizhen et al., 2001). The principal purpose of this paper is to test this premise at the regional scale over interglacial-glacial cycles. Recent approaches to mineral exploration in glaciated terrains can also benefit from improvements in our understanding of the spatial variation of ice sheet erosion. Furthermore, from a regulatory perspective, better predictions of depth of glacial erosion are important to the geological assessment of potential nuclear waste repositories within the Canadian Shield where radioactive decay durations of 10^4 and 10^5 years are of interest.

Difficulties in documenting the rate and magnitude of glacial erosion over a glacial cycle are compounded by: (1) the spatial and temporal variability of subglacial erosion, (2) the apparent lack of a measurable quantity that records glacial erosion but is not intrinsically tied to transport and deposition of glacially-eroded debris (i.e. sediment flux), (3) the need for a monitor with a timescale similar to the characteristic timescales of glacial cycles (10^4 - 10^5 years: Harbor, 1995), and (4) the switch in erosive regime during an interglacial to glacial transition (Peizhen and Molnar, 2001).

The Torngat Mountains, situated on the Labrador Peninsula, Canada (Fig. 3.1), are well suited to a study of spatial patterns of differential glacial erosion over multiple glacial cycles. The Torngat Mountains have the essential components of Sugden's (1978)

landscape of selective linear erosion (extensive valley glacial erosion separating unscathed but ice-covered highlands). To aid others to recognize cold based ice conditions, the following observations are suggested. The presence of tors and lateral meltwater channels are pervasive features in areas at least partially covered by cold-based ice (Dyke, 1993). Marchant et al. (1993) outlined the following characteristics of cold-based ice based on observations near the East Antarctic Ice Sheet: (1) boulder-belt moraines or drift composed of angular englacial and supraglacial debris, (2) erratics and till veneers scattered passively by sublimation atop undisturbed bedrock and unconsolidated landforms; and (3) absence of outwash, pro-glacial lacustrine sediments, and associated meltwater channels. Notably, glacially-striated clasts have been found in actively-forming recessional boulder-belt moraines of Antarctic cold-based outlet glaciers (Atkins et al. 2002).

Despite the difficulties accessing the region, the glacial history of the Torngat Mountains has been examined extensively (Ives, 1958; Andrews, 1963; Ives, 1978; Bell, 1987; Clark, 1988). Importantly, the Torngat Mountains are one of the type-localities of classical weathering zones found in high latitude coastal regions (e.g. Ives, 1958 and 1978). This region is also unique because many aspects of the history of denudation since Mesozoic rifting have already been studied, including soil catenas at various landscape positions (Marquette et al. 2004), (U-Th)/He thermochronology from range-crossing and vertical transects (Centeno, 2005), lithospheric and geodynamic attributes (Funck et al., 2000), and the sedimentary record offshore (Balkwill et al., 1990; MacLean et al., 2001). Building on this foundation, we couple cosmogenic ^{10}Be and ^{26}Al with a thermo-mechanical ice sheet model to characterize the spatial variation and magnitude of erosion

over several glacial cycles on a mountain range scale. Then, we establish a glacial erosion relationship for similar lithological and glaciological environments. Spatial variation of TCN inheritance has been used to document glacial erosion rates on a valley scale (Fabel et al., 2004). Our mountain-range scale study builds on their results by allowing us to dismiss local small-scale variations of inheritance due to factors including variable snow or sediment cover, availability of bedrock outcrops, lithological and fracture density anomalies, and changes in shielding that might arise from a random sampling approach.

3.3 GEOMORPHIC SETTING

The Torngat Mountains form a narrow N-S ridge of peaks above 1600 m asl that protrude above a gently westward dipping (0.8°) subsummit plateau (Fig. 3.1). The plateau has been dissected by range-crossing E-W valleys that terminate as deep estuaries on both ends (Fig. 3.1a). The relief ranges from a few hundred meters along the west coast, to > 1800 m above submerged fiords in the center of the range. The valleys are cut into Archean Rae and Nain province gneisses and metasediments and have a periodic (ca. 10 km) spacing which may reflect obscured shear zones or some fundamental fluvial response to the physiographic conditions (Hovius, 2000) (Fig. 3.1c). Steep hillslopes of paraglacial origin have persisted in excess of the angle of repose due the competency of the highly resistant albeit pervasively sheared lithologies (Taylor, 1979)(Fig. 3.2). Rock structure is also the dominant control of several high peaks.

The regional climate undoubtedly plays a role in Torngat landscape evolution. An annual precipitation of 40-80 cm a⁻¹ arrives in low intensity storms with approximately 45% falling as snow (Environment Canada, 1991). Cirque glaciers in the Torngat Mountains are currently receding (Fahn, 1975). The relatively low and evenly distributed annual precipitation results in low stream discharge, inhibiting runoff atop the rough and porous felsenmeer-covered summits. Stream incision is currently ineffective in this region due to minimal precipitation and the low average grade of the longitudinal profiles of the mainstems (Fig. 3.2), which is a characteristic of persistent glacial erosion in valleys (MacGregor et al., 2000).

The antiquity of the large-scale landscape features is not debated, but the processes and timescales of landscape evolution are. The paleodrainage geometry, position of the divide, subsummit plateau, and preliminary (U-Th)/He results indicate that the plateau is mainly a palimpsest Mesozoic surface (Centeno, 2005) with antecedent drainage network influenced by rift flank uplift during the opening of the Labrador Sea (Odell, 1929; Twidale, 1976; Balkwill et al., 1990; Centeno, 2005). This setting is akin to the dissected paleosurfaces found throughout Fennoscandia (e.g. Lindmar-Bergstrom, 1995). It is possible that the topography has responded to isostasy during exhumation due to a thick, (maximum thickness of 52 km: Funck et al., 2000) remnant Paleoproterozoic crustal root (Mengel et al., 1991; Hall et al., 2002). However, the high flexural rigidity of the Labrador Peninsula lithosphere and wavelength of the topography could compensate the amount of isostatic uplift possible from removal of sediment during glaciations (Montgomery, 2002). Normal faults outboard of the continental shelf and slope in the Labrador Sea are unconformably overlain by up to 10 km of Mesozoic and

Cenozoic sediments, which record gradual subsidence because of post-rift thermal subsidence and sediment loading (Gradstein and Srivastava, 1980; Issler, 1987). Cooke (1929), McMillan (1973), Gradstein and Srivastava (1980), Chalmers (2000), and Japsen and Chalmers (2000) have proposed that the Torngat Mountain topography has been rejuvenated during Neogene time. We cannot preclude that minor subsummit plateau exhumation has continued in the Quaternary, especially considering that (1) the paleo-ELA based on average cirque floor elevation (ca. 800 m) in places is below the plateau, (2) the fracture density is locally high, and (3) the entire region falls within the zone of continuous permafrost activity which may contribute regolith and tools for efficient fluvial and glacial erosion.

The surficial geology mapping of the Torngat Mountains, although incomplete at the 1:50,000 scale, has revealed a lack of drumlins on all but the northernmost tip of the Labrador Peninsula. This drumlin-poor landform assemblage differs from the suite of landforms near Ungava Bay that is rife with flutes and drumlin fields. Absence of glacially molded landforms may indicate that the mode of glacial erosion was sediment limited (Dyke and Morris, 1988; Stokes and Clark, 2001) and spatially restricted. Within the Torngat Mountains, there is no evidence of pre-Wisconsinan tills; they may have been completely eroded or incorporated with regolith into the existing till veneers (Balco et al., 2003).

The weathering-zone type-locality of Ives (1958, 1978) in Saglek Fiord region of the Torngat Mountains exhibits 3 to 4 altitudinally separable zones of differential degrees of weathering. The highest surfaces on the peak summits comprise the Torngat Zone and exhibit a mature landscape characterized by thick weathering rinds, deep (>10 cm)

gnammas, rounded rock edges, and a complete lack of evidence of glaciation. Tors or tor-like knobs protrude above the broad, felsenmeer-covered plateaus (interfluvial surface seen in Fig. 3.2). In keeping with the notion that the boundaries between the weathering zones represent trimlines of successively older (and more voluminous) glaciations, Ives (1978) proposed that if the intermediate zones were ice covered, this ice must certainly be pre-Wisconsinan. Sub-rounded, pseudo-erratic boulders are found perched on angular felsenmeer slabs and tors. The intermediate zones can be characterized as zones with various thicknesses of incipient felsenmeer, lacustrine beach sediments, and glacial drift covering bedrock with scant evidence of glacial erosion. The valley bottoms have a strikingly different morphology. This lowest (Saglek) zone is characterized by fresh, glacially eroded landscapes (valley in Fig. 3.3), with glacial polish on roches moutonnées and relatively poorly developed soils (Marquette et al., 2004).

The highest weathering zones are usually interpreted as nunataks, not covered by ice during the Last Glacial Maximum (LGM) (Daly, 1902; Ives, 1958; and Clark, 1991). Others have suggested that the broad plateaus below the highest peaks represent areas protected from glacial erosion by cold-based ice, while the valley bottoms have been deeply scoured and the intermediate zone lies in a transition zone (Marquette et al., 2004). Evidence for the antiquity of the felsenmeer and support of complete ice cover atop the summit and sub-summit plateau surfaces includes: (1) TCN concentrations in locally erratic boulders on the interfluvial summits indicate that the erratics have been exposed since the Younger Dryas (YD) chron, (2) paired cosmogenic ^{26}Al and ^{10}Be ratios of bedrock tor-like features suggest minimum interruption of exposure for 200 ka, presumably by ice cover, and (3) the summit surface soils contain elevated concentrations

of gibbsite relative to the valley deposits from the same parent material. Gibbsite is thought to have been formed in a climate unlike any occurring during the Quaternary and preserved beneath cold-based ice throughout the Quaternary (Marquette et al., 2004).

3.4 TCN SURFACE EXPOSURE METHOD

The TCN method integrates exposure histories over the timescale of interest (10^4 - 10^6 years), which spans interglacial-glacial transitions. The method is based on the production of isotopes in rocks at the Earth's surface during the interaction of secondary cosmic radiation and atoms in exposed minerals (Gosse and Phillips, 2001). Although many other factors must be considered, the concentration of TCN in a given rock or mineral is mostly dependent upon (1) duration of exposure (or multiple exposures, in the instance of interruptions due to intermittent shielding from cosmic rays), (2) production rate at the site, which is a function of atmospheric shielding (altitude) and magnetic field effects (latitude), (3) environmental factors such as partial shielding by snow, ice, or till, (4) glacial and non-glacial erosion of the surface, and (5) radioactive decay of the cosmogenic isotopes. The secondary radiation responsible for these TCN (primarily fast neutrons and muons) attenuate exponentially with depth into rock (e-folding lengths of 150 and 1300 $\text{g}\cdot\text{cm}^{-2}$ respectively) so production at 3 m rock depth is only slightly more than 1% of surface production.

Glacial erosion of TCN bearing rocks may be incomplete under cold-based conditions. Evidence of inherited TCN in glacial deposits can be demonstrated when bedrock surface samples contain higher TCN concentrations than the surfaces of perched

erratics on the same bedrock surface (Gosse et al. 1995; Marsella et al., 2000; Briner et al., 2003). In this way, inheritance due to prior exposure may be exploited to qualitatively assess the degree of glacial abrasion and plucking (Briner and Swanson, 1998; Colgan et al., 2002) and to document the presence of non-erosive ice (Colgan et al., 2002).

Exposure of a surface may have been interrupted by an episode of shielding by non-erosive glacier ice. In this case, the apparent exposure ages will be less than a surface with continuous exposure because TCN production is reduced and radionuclides decay during the burial. In order to calculate an exposure duration that does not assume a simple history of steady exposure and constant erosion, it is necessary to use a ratio of two nuclides (Fig. 3.5). This history can be resolved by using a ratio of two isotopes with differences in decay rates (Nishiizumi et al., 1989). The ratio of the concentration of the short-lived isotope to that of the long-lived isotope will be lower in a surface that experienced a complete or partial burial. In the special case where the bedrock surface is episodically plucked or significantly abraded, the plucked (or abraded) surfaces of the bedrock and exhumed faces of the plucked boulder will have a lower ^{10}Be concentration than the continuously exposed surfaces (Macciaroli et al., 1994). Single nuclide concentrations may be used to estimate rock erosion rates if there is a reasonable inference of surface antiquity and that the concentration has attained a steady state for a particular constant erosion rate over that time (Lal, 1991). The calculated erosion rate is the rate required to maintain that concentration over long exposure durations, and is therefore a maximum limiting rate if the assumptions of continuous exposure and steady state concentration are invalid.

3.5 RESULTS

In total, 31 bedrock samples and 18 erratic boulder samples were collected over several field seasons. Table 3.1 gives the TCN bedrock and erratic sample site location, elevation, and TCN concentrations. Ages are scaled according to Lal (1991, his table 2) and modified according to Stone (2000) using new values for the muogenic contribution and a sea-level, high latitude (SLHL) production rate of $5.1 \text{ }^{10}\text{Be atoms g}^{-1} \text{ a}^{-1}$ (Gosse and Stone, 2001) and a $^{26}\text{Al}/^{10}\text{Be}$ production ratio of 5.94 (Gosse et al., 1995). ^{10}Be ($t_{1/2} = 1.5 \text{ Ma}$) and ^{26}Al ($t_{1/2} = 0.7 \text{ Ma}$) production rates were integrated over sample thicknesses (found in Appendix 3) using a simple exponential attenuation. Ages shown in Table 3.1 are calculated assuming a continuous exposure with no erosion, burial, or inheritance.

Some of the TCN results have previously been reported in Marquette et al., (2004). Because we have added additional samples and calculated erosion rates for these previously reported samples, we report the dataset in its entirety. The 58 targets were prepared at Dalhousie U. and the U. of Kansas, native element concentrations measured by ICP.AES at U. Kansas, and isotopic ratios measured at Lawrence Livermore National Lab. The ^{26}Al and ^{10}Be AMS measurements attained at least 4% precision at $1-\sigma$ and at least 10% at $2-\sigma$, except for 11 measurements. Samples of boulders and bedrock were collected from all four weathering zones (Ives, 1978) throughout the Torngat Mountains to detect inherited TCN signal, to date erratic boulders that are perched on bedrock, and to date summit bedrock and tor surfaces. The chemical data and calculation of exposure duration assuming simple exposure history are provided in Table 3.1. The effects of

snow cover, topography, and rock geometry influences on exposure were minimized by our sampling strategy but are reported in Table A3.1 in Appendix 3.

3.6 DISCUSSION

3.6.1 INTERPRETING TCN DATA IN GLACIATED TERRAINS

Assuming a simple exposure history, the TCN ages range from 340 ka on the Cirque Mountain felsenmeer summit to 8.5 ka on a bedrock protrusion rising a few m above the floor of Nakvak Valley (Table 3.1). The TCN concentrations and modeled exposure ages derived from these concentrations show a correlation with altitude (Fig. 3.3). Two end-member interpretations can explain the distribution of the concentration vs. elevation plot. (1) If all of the dated surfaces (valleys, plateaus and peaks) have simple exposure histories (i.e. no interruption of the exposure and negligible erosion), then the exposure ages help delineate trimline positions of each successively older (and thicker) valley glacier in accordance with Ives' (1978) interpretation of weathering zones (e.g. Gellatly et al., 1988, Brook et al., 1993, Stone et al., 1998, and Clark et al., 2003). (2) Alternatively, during the last glaciation, there may have been an extensive ice cover of all but the highest peaks, and surfaces that were not deeply eroded will retain an incomplete record of previous exposure, possibly with multiple interruptions (e.g. Gosse et al., 1993, Gosse et al. 1995; Gosse and Phillips, 2001; Marsella et al., 2000; Briner et al., 2003). The multiple-burial-with-little-erosion scenario is predicted by Sugden (1978) and Dyke (1993) for parts of Arctic Canada. TCN exposure ages of locally erratic boulders from summit surfaces and valley bottoms that cluster around the Younger Dryas (YD) chron

indicate that erratic-bearing ice covered the plateaus at least during the last glaciation (Fig. 3.4) and support the interpretation of Sugden (1978) and Dyke (1993).

In the valleys, bedrock TCN concentrations are indistinguishable (within $2\text{-}\sigma$ confidence) from the TCN concentrations of adjacent boulders so these concentrations may be interpreted as simple post-glacial exposure ages (i.e. with no record of exposure prior to the glaciation). The ages for the last deglaciation (8.5 to 11.5 ka) are consistent with the regional glacial geomorphology and radiocarbon chronology (Marquette et al., 2004). For example, sample LAB-00-23A, collected from the valley wall on the northwest side of the Mt. Haywood, plots on the continuous exposure line (Fig. 3.5), which also supports a simple exposure history. A nearby boulder sample, LAB-00-23-1A, matches this age within $2\text{-}\sigma$, but may contain several thousand years of inheritance.

On the summit plateaus and peaks, bedrock ages ranging from 10 to 340 ka are adjacent to younger boulders, so a simple exposure history is unlikely for these higher altitude samples. The $^{26}\text{Al}/^{10}\text{Be}$ of the bedrock samples from greater altitudes plot below the steady-state erosion island and have experienced a complicated exposure or erosion history (Fig. 3.5). Either > 8 m of ice ($\rho=0.92 \text{ g}\cdot\text{cm}^{-3}$) or >30 m of snow ($\rho=0.25 \text{ g}\cdot\text{cm}^{-3}$) are required can cause 100% shielding of the TCN production. However, because the summit plateaus have erratics, we will consider that the burial is due to ice cover. In the case of burial, the ^{26}Al concentration decays and is decreased faster than the ^{10}Be concentration, and the $^{26}\text{Al}/^{10}\text{Be}$ decreases. Note that in order to plot below the steady-state erosion island, the surface must have been exposed at least once prior to a shielding event. In the case of plucking, the surface of the rock after removal of the plucked block has significantly less ^{10}Be . An exposed - then buried - then plucked sample shifts the

graph to the left a distance proportional to the ^{10}Be removed during the plucking. Based solely on the $^{26}\text{Al}/^{10}\text{Be}$ ratio of the sample, we cannot distinguish between plucking and burial (Macciaroli et al., 1994, Gosse and Phillips, 2001). However, the high degree of weathering as indicated by the rounded edges and numerous gnammas on the plateau bedrock surfaces is much greater than valley outcrops, probably precluding plucking of the sampled summit surfaces during the last glaciation.

In summary, we interpret the TCN data from low elevations as simple exposure ages. However, the bedrock exposure ages on the higher surfaces must be considered minima owing to the decay of TCN during ice-cover burial. This last point is crucial and is discussed further below.

3.6.2 ESTIMATING GLACIAL EROSION RATES

In the glacial landscape of Torngat Mountains, the erosion rate calculation is complicated because the summit surfaces have been buried by ice. The TCN concentration will therefore be lower (owing to decay and stopped production during burial) for surfaces that were buried. Thus, the maximum possible erosion rate will be overestimated, but is nevertheless a maximum (Table 3.1). For samples from the Labrador Peninsula valley bottoms, we cannot assume long exposure durations. Considering the young exposure ages of the valley bedrock surfaces, the depth dependence of cosmogenic production, and the precision of our measurements, the amount of bedrock removed during the last glaciation was ≥ 250 cm. Assuming that the last glaciation was similar to previous glaciation, this erosion rate would have deepened

the valleys greater than 2.5 m per glacial cycle or greater than 62 m over 25 glacial cycles since the beginning of the Quaternary period.

3.6.3 ICE SHEET MODEL TESTS

We use University of Maine Ice Sheet Model (UMISM), a finite-element time-dependent ice sheet model (Fastook and Chapman, 1989, and Fastook, 1994) with an added basal water calculation (Johnson and Fastook, 2002) to simulate the ice dynamics in the Torngat Mountains over the last 100 ka. Appendix 5 expands on the abbreviated model descriptions in this section. The model's flow characteristics conform to the battery of European Ice Sheet Modelling Initiative project (EISMINT) experiments (Huybrechts et al., 1996). The bed topography is from a gridded inset ETOPO2 2-minute DEM, with coarser resolution topography that forms the ice flux boundary conditions for the inset model. A finer resolution is not supported by physics because of the assumptions in the shallow ice approximation and our estimates of realistic LGM ice thicknesses. The long-term paleoclimate was controlled by the $\delta^{18}\text{O}$ curve from the GRIP ice core, central Greenland, transformed to a temperature record (Johnson et al., 1995). This paleoclimate record drives the glacial cycle. The mean annual temperature for each node varies by specified altitudinal and latitudinal lapse rates. The temperature calculation is used to determine the positive degree days, which is assumed to be proportional to ablation. Accumulation is calculated from temperature and surface slope. A finite-element solver is coupled to an energy-, momentum-, and mass-balance solver to generate internal ice temperatures and accounts for diffusion, vertical advection, and

shear heating. Horizontal heat advection is not calculated but should not be a large contribution to the basal heat in areas of slow-moving ice. Geothermal heat flux is input as a basal boundary condition, but has been found to have a weak effect on ice sheet thickness or volume (Johnson and Fastook, 2002). Formulation of the hydrology model is summarized in Johnson and Fastook (2002).

Glacier thermodynamics predicts non-erosive basal ice on plateau interfluves at high elevations compared to deep valley floors (Sugden, 1978; Paterson, 1994). Long-term frozen-bed conditions at high elevations could have facilitated summit preservation during glacial cycles (Kleman et al., 1997). We have attributed the relationship between elevation and TCN concentration (Fig. 3.3) to the differential preservation of pre-glacial inheritance under cold-based ice. Although there is glaciological basis for using altitude as a first-order proxy for sliding velocity, the TCN age vs. altitude relationship does not consider features such as low-altitude areas that might lie beneath semi-permanent ice centers. These factors could greatly affect the degree of subglacial erosion or subglacial preservation, but do not scale with ice thickness. It is necessary to account for these complications when relating the Torngat Mountain TCN measurements with subglacial erosion over a glacial cycle; we address this issue by simulating ice dynamics..

Näslund et al. (2003) outlined a method of quantifying integrated ice-sliding speeds by using the distance that the ice that has passed over an area (in any direction). This value was calculated by multiplying the basal ice sliding velocity by the amount of time that that velocity persisted. Their pattern of high basal ice sliding distances correlated broadly with zones of bare bedrock outcrop. We use an adaptation of Naslund et al.'s (2003) approach in order to distinguish zones in the model that are covered by fast

moving ice for a short amount of time from sites that were always covered by slow-moving, relatively non-erosive ice. In our study, we normalize the distance of sliding by the duration of ice cover. In this case, sliding distance normalized by time is equivalent to average basal sliding speed. We use this value in order to compare our results with models of glacial erosion in which glacial erosion scales directly with ice velocity.

Because the regional ice configuration is intrinsically linked to the basal thermal regime, the first priority in adjusting the model was to match known ice margins and basic flow patterns by adjusting parameters that are considered unknowns for the region such as the amplitude of the GRIP temperature record in this region and the LGM lapse rate. The persistent features that were reproduced independently of parameter adjustments include: (1) local thin, slow-moving ice cover on summit surfaces preceding ice cap formation similar to ice-fields and lichen-kill zones for short-lived Holocene cold-periods (Dyke, 1978), (2) an early-forming Torngat Mountain ice cap, (3) complete ice cover transforming during glaciation to valley ice and small isolated summit ice caps and cirque glaciers, (4) cold-based ice covering the banks of the continental shelf, (5) the most pervasive sliding at the time of maximum ice extent and thickness (see Paterson, 1994) and (6) areas of highest basal sliding grossly matching areas of scoured bedrock (Klassen et al. 1992).

The simulations reveal the patterns of basal ice sliding distance normalized by duration of ice cover (Fig. 3.6). We compare these modeled sliding distance normalized by ice duration with TCN concentration derived erosion rates. A note of caution should be added in interpreting this coarse scale of the ice sheet model with respect to the real

topography such that each model pixel that records the calculated sliding speeds covers several TCN sample sites over a range of altitudes.

3.6.4 RELIEF GENERATION BY GLACIERS

Epeirogenic peak uplift may occur in regions where valleys are sufficiently denuded. Relatively short-term sediment yields (Hallet et al., 1996) and valley morphology (Montgomery, 2002) have indicated that valley glacier erosion can result in greater sediment flux than fluvial erosion for similar climatic conditions. Our results show that even areas that were completely covered by polythermal ice sheets or ice caps, differential rates of glacial erosion will tend to complement valley deepening. Bed erosion in the Torngat Mountains is inferred to depend on the basal thermal regime of the ice-substrate interface.

We suggest that relief generation is owing to two linked processes, although the influence of bedrock lithology and post-glacial climate cannot be understated: (1) while the summits were protected by cold-based ice, the faster moving wet-based ice deepened the valleys greater than 2.5 m per glacial cycle. Although the exposure clock was reset on valley floors, the resetting on valley walls and summit shoulders is partial, so erosion in these higher areas averages less than 2.5 m per glacial cycle, (2) felsenmeer inhibits summit plateau erosion. Felsenmeer is a distinct regolith in which the porosity is maintained due to frost sorting and slow rates of weathering, while most other regoliths succumb to soil development and lose porosity. Following deglaciation, the high

connectivity and surface roughness of the felsenmeer could prevent overland flow on the summits. In places, the summit surfaces were eroded a maximum of 1.4 m/Ma.

Given that the summit surfaces were minimally eroded (< 1.4 m/Ma) and the valleys were pervasively eroded (> 250 cm/glacial advance), we can recast the cosmogenic exposure age vs. normalized sliding distance plot into terms of maximum possible erosion and minimum possible erosion for an average sliding speed (Fig. 3.7). We subtracted post-glacial TCN accumulation from all of the sites. In all cases, we used the TCN concentration as it was 11 ka ago – although a few of the valley bottom samples likely have less than 11 ka post-glacial exposure and some of the highest peaks may have greater than 11 ka of post-glacial exposure. This correction is small compared to the other sources of uncertainty, such as the effect of TCN decay during glacial cover. To correlate these maximum erosion rates in order to constrain relief generation, we have made two assumptions. First, all bedrock erosion recorded by the TCN is glacial. This assumption is valid because the valley floor bedrock samples are from glacially-striated knobs. The summit erosion could be either glacial or non-glacial because the calculated maximum erosion rate does not depend on the style of erosion. Despite the style of erosion, the erosion rate is still a maximum for glacial erosion. Second, we assume a linear relationship between basal sliding speed and glacial erosion (ϵ_g). In doing so, we ignore the effects of abrasion that may vary with some power of velocity.

Consider that integrated sliding distance normalized by ice cover duration is comparable to basal ice sliding velocity, u_s . We constrain a simple empirical erosion rule over an interglacial-glacial cycle for areas that have been covered by polythermal ice. The slope of the best-fit line (glacial erosion coefficient) of Fig. 3.7 yields:

$$\varepsilon_g = 5 \times 10^{-7} | \mathbf{u}_s | \quad (\text{Eq. 3.1})$$

This glacial erosion coefficient, K_g , is three orders of magnitude lower than the glacial erosion coefficient of Hallet's (1979) abrasion law ($K_g=10^{-2}$) as applied by Tomkin and Braun (2004). Our estimate is closer to the empirically derived Humphrey and Raymond (1994) K_g value of 10^{-4} . This discrepancy in the values of K_g may indicate that our maximum and minimum erosion rate estimates are extremes. Our approach to constrain a glacial erosion rate is simplistic and is not intended to be transferred to other areas with dissimilar lithologies, fracture densities, climate, and geothermal flux. However, our low value of K_g of 5×10^{-7} seems appropriate considering that the summits are particularly durable in this region. It allows a minimum end-member for a value of K_g for geodynamics models that consider the role of glacial erosion in orogenic evolution.

The generation of relief by glaciers has been described previously in tectonically diverse regions (e.g. Southern Alps (Koons, 1989), and Wind River Range (Small and Anderson, 1998)). However, relief due to the preservation of glaciated summits under cold-based ice has not been previously described.

3.7 SUMMARY

1. Complete interpretation of differentiate exposure, burial, and erosion signals from TCN data in glacial landscapes must consider the soils, geomorphology, and double nuclide ratios.

2. TCN data suggest > 2.5 m of erosion per single glacial-interglacial cycle occurred within Torngat Mountain valleys. On summit plateaus, the long-term (over several glacial-interglacial cycles) erosion rates are < 1.4 m/Ma. Therefore, in the Torngat Mountains, glacial erosion may have generated > 62 m of relief over ~ 25 glacial cycles since the Quaternary.
3. In contrast to landscapes dominated by hillslope processes, denudation in glaciated regions is controlled mostly by the basal thermal regime of ice throughout glaciation, not slope or elevation. A thermodynamic ice sheet model that calculates normalized sliding distance can be used to distinguish zones of past non-erosive and highly erosive ice. Numerical models of landscape erosion that incorporate glacial erosion should consider environmental factors, such as rock type and climate, or risk grossly overestimating the amount of erosion by glaciation.

3.8 ACKNOWLEDGEMENTS

The authors thank G. Marquette and J.-P. Centeno for field assistance and G. Yang for valuable laboratory assistance. We are grateful to the GSC TFSS for field equipment during mapping and sample collection. Field access was partly supported by the Canadian Coast Guard. This research was supported by a Killam Fellowship to JWS and a NSF-OPP (Grant OPP-9906280) and ACOA-AIF (Grant 1005052) to JCG. Thanks to John Stone and Bernard Hallet for their helpful and thorough reviews of the manuscript.

3.9 REFERENCES

- Andrews, J. T. 1963. End moraines and late-glacial chronology in the northern Nain-Okak section of the Labrador coast. *Geografiska Annaler* **45**(2-3): 158-171.
- Ahnert, F. 1994. Equilibrium, scale and inheritance in geomorphology. *Geomorphology* **11**: 125-140.
- Atkins, C. B., Barrett P. J., Hicock, S.R. 2002. Cold-based glaciers erode and deposit: Evidence from the Allan Hills, Antarctica. *Geology* **30**(7): 659–662.
- Balco G., Patterson C.J., Stone, J.O. 2003. The fate of preglacial regolith beneath the Laurentide Ice Sheet; XVI INQUA congress; shaping the earth; a Quaternary perspective. *Congress of the International Union for Quaternary Research* **16**: 189.
- Balkwill, H.R., McMillan, N.J., MacLean, B., Williams, G.L., Srivastava, S.P. 1990. Geology of the Labrador Shelf, Baffin Bay, and Davis Strait. in *Geology of the Continental Margin of Eastern Canada*. Keen MJ, Williams GL (eds). The Geology of North America **I-1**: 295-348.

- Bell, T. 1987. Quaternary geomorphology, glacial history and relative sea level change in outer Nachvak Fiord, northern Labrador. M.Sc. thesis, Memorial University of Newfoundland, St. John's Newfoundland.
- Briner, J., Swanson, T. 1998: Using inherited cosmogenic ^{36}Cl to constrain glacial erosion rates of the Cordilleran ice sheet. *Geology* **26**(1): 3-6.
- Briner, J. P., Miller, G. H., Davis, P. T., Bierman, P. B., Caffee, M. 2003. Last Glacial Maximum ice sheet dynamics in arctic Canada inferred from young erratics perched on ancient tors. *Quaternary Science Reviews* **22** (5-7): 437-444.
- Brook, E. J., Nesje, A., Lehman, S. J., Raisbeck, G. M., Yiou, F. 1996. Cosmogenic nuclide exposure ages along a vertical transect in western Norway - implications for the height of the Fennoscandian ice sheet. *Geology* **24**(3): 207-210.
- Centeno, J. P. 2005. Exhumation of the Torngat Mountains, northern Labrador, Canada. M.Sc. thesis, University of Kansas, Lawrence, Kansas.
- Chalmers, J. A. 2000. Offshore evidence for Neogene uplift in central West Greenland. *Global and Planetary Change* **24**: 311-318.
- Clark, P. U. 1988. Glacial geology of the Torngat Mountains, Labrador. *Canadian Journal of Earth Sciences* **25**: 1184-1198.

- Clark, P. U. 1991. Landscapes of glacial erosion, Torngat Mountains, Northern Labrador - Ungava. *The Canadian Geographer* **35**: 208-213.
- Clark, P. U., Brook, E. J., Raisbeck, G. M., Yiou, F., Clark, J. 2003. Cosmogenic ^{10}Be ages of the Saglek Moraines, Torngat Mountains, Labrador. *Geology* **31**: 617-620.
- Colgan, P. M., Bierman, P. R., Mickelson, D. M., Caffee, M. 2002. Variation in glacial erosion near the southern margin of the Laurentide Ice Sheet, south-central Wisconsin, USA: Implications for cosmogenic dating of glacial terrains. *Geological Society of America Bulletin* **114**(12): 1581–1591.
- Cooke, H. C. 1929. Studies of the physiography of the Canadian Shield: I, Mature valleys of the Labrador Peninsula. *Transactions of the Royal Society of Canada*, **23**(24): 91-120.
- Daly, R. A. 1902. The Geology of the northeast coast of Labrador. *Bulletin of the Museum of Comparative Zoology at Harvard College* **38**(5): 203-270.
- Dyke, A. S. 1978. Indications of neoglaciation on Somerset Island, District of Franklin. *Paper - Geological Survey of Canada* **78-1B**: 215-217.

Dyke, A. S. 1993. Landscapes of cold-centred late Wisconsin ice caps, arctic Canada.

Progress in Physical Geography **17**(2): 223-247.

Dyke, A. S., Morris, T. F. 1988. Canadian Landform examples .7. drumlin fields,

dispersal trains, and ice streams in arctic Canada. *Canadian Geographer* **32**(1):

86-90.

Environment Canada. 1991. Canadian Climate Normals. 1961-1990. [http://climate.](http://climate.weatheroffice.ec.gc.ca//climate_normals_1990)

[weatheroffice.ec.gc.ca//climate_normals_1990.](http://climate.weatheroffice.ec.gc.ca//climate_normals_1990)

Fabel, D., Harbor, J., Dahms, D., James, A., Elmore, D., Horn, L., Daley, K., Steele, C.

2004. Spatial patterns of glacial erosion at a valley scale derived from terrestrial cosmogenic ^{10}Be and ^{26}Al concentrations in rock. *Annals of the Association of American Geographers* **94**(2): 241-255.

Fastook, J. L. 1994. Modelling the Ice Age: the finite element method in glaciology.

Computational Science and Engineering **1**(1): 55-67.

Fastook, J. L., Chapman, J. E. 1989. A map plane finite-element model: three modelling

experiments. *Journal of Glaciology* **35**(119): 48-52.

- Fahn, C. 1975. Glaciers of northern Labrador. in *Mountain glaciers of the Northern Hemisphere*. Field WO (eds). Hanover, N.H., U.S. Army Cold Regions Research and Engineering Lab **2**: 673–682.
- Funck, T., Loudon, K. E., Wardle, R. J., Hall, J., Hobro, J. W., Salisbury, M. H., Muzzati, A. M. 2000. Three-dimensional structure of the Torngat Orogen (NE Canada) from active seismic tomography. *Journal of Geophysical Research* **105**(B10): 23 403-23 420.
- Gellatly, A. F., Whalley, W. B., Gordon, J. E., Hansom, J. D. 1988. Thermal regime and geomorphology of plateau ice caps of northern Norway: observations and implications. *Geology* **16**: 983-986.
- Gosse, J. C., Evenson, E. B., Klein, J., Lawn, B., Middleton, R. 1995. Precise cosmogenic ^{10}Be measurements in western North America; support for a global Younger Dryas cooling event. *Geology* **23**(10): 877-880.
- Gosse, J. C., Phillips, F. M. 2001. Terrestrial in situ cosmogenic nuclides: theory and application (Reviews). *Quaternary Science Reviews* **20**: 1475-1560.
- Gosse, J. C., Stone, J. O. 2001. Terrestrial cosmogenic nuclide methods passing milestones toward paleo-altimetry. *EOS* **82**(7): 82, 86, 89.

- Gradstein, F. M., Srivastava, S. P. 1980. Aspects of Cenozoic stratigraphy and paleoceanography of the Labrador Sea and Baffin Bay. *Palaeogeography, Palaeoclimatology, Palaeoecology* **30**: 261-295.
- Hall, J., Loudon, K. E., Funck, T., Deemer S. 2002. Geophysical characteristics of the continental crust along the Lithoprobe Eastern Canadian Shield Onshore-Offshore Transect (ECSOOT): a review. *Canadian Journal of Earth Sciences* **39**: 569-587.
- Hallet, B. 1979. A theoretical model of glacial abrasion. *Journal of Glaciology* **23**(89): 39-50.
- Hallet, B. 1996. Glacial quarrying; a simple theoretical model. *Annals of Glaciology* **22**: 1-8.
- Hallet, B., Hunter, L., Bogen, J. 1996. Rates of erosion and sediment evacuation by glaciers; a review of field data and their implications; impact of glaciations on basin evolution; data and models from the Norwegian margin and adjacent areas. *Global and Planetary Change* **12**(1-4): 213-235.
- Harbor, J. M. 1995. Development of glacial-valley cross sections under conditions of spatially variable resistance to erosion; glacial geomorphology; process and form development. *Geomorphology* **14**(2): 99-107.

- Hovius, N. 2000, Macro scale process systems of mountain belt erosion, in,
Geomorphology and Global Tectonics. Summerfield M (eds). New York, John
Wiley and Sons: 77- 105.
- Humphrey, N. F., Raymond, C. F. 1994. Hydrology, erosion and sediment production in
a surging glacier; the Variegated Glacier surge, 1982-83. *Journal of Glaciology*
40(136): 539-552.
- Huybretchs P., Payne, T., Abe-Ouchi, A., Calov, R., Fabre, A., Fastook, J., Greve, R.,
Hindmarsh, R., Hoyddal, O., Johannesson, T., MacAyeal, D., Marsiat, I., Ritz,
C., Verbitsky, M., Waddington, E., Warner, R. 1996. The EISMINT benchmarks
for testing ice-sheet models. *Annals of Glaciology* **23**: 1-12.
- Issler, D. R. 1987. The thermal and subsidence history of the Labrador Margin. Ph. D.
thesis, Dalhousie University, Halifax, Nova Scotia, Canada: 1-235.
- Ives, J. D. 1958. Mountain-top detritus and the extent of the last glaciation in northeastern
Labrador-Ungava. *The Canadian Geographer* **12**: 25-31.
- Ives, J. D. 1978. The maximum extent of the Laurentide Ice Sheet along the east coast of
North America during the last glaciation. *Arctic* **31**(1): 24-53.

- Japsen, P., Chalmers, J.A. 2000. Neogene uplift and tectonics around the North Atlantic: overview. *Global and Planetary Change* **24**: 165-173.
- Johnsen, S., Dahl-Jensen, D., Dansgaard, W., Gunderup, N. 1995. Greenland paleotemperatures derived from GRIP bore hole temperature and ice core isotope profiles. *Tellus* **47B**: 624-629.
- Johnson, J. V., Fastook, J. L. 2002. Northern Hemisphere glaciation and its sensitivity to basal melt water. *Quaternary International* **95-96**: 87-98.
- Klassen, R. A., Paradis, S., Bolduc, A. M., Thomas, R. D. 1992. Glacial landforms and deposits, Labrador, Newfoundland and eastern Quebec. *Geological Survey of Canada, Map 1814A*, scale 1:1000000.
- Kleman, J., Hättestrand, C., Borgström, I., Stroeven, A. P. 1997. Fennoscandian palaeoglaciology reconstructed using a glacial geological inversion model. *Journal of Glaciology* **43**: 283-299.
- Koons, P. O. 1989. The topographic evolution of collisional mountain belts: a numerical look at the southern Alps, New Zealand. *American Journal of Science* **289**: 1044-1069.

- Lal, D. 1991. Cosmic ray labelling of erosion surfaces: in situ nuclide production rates and erosion rates. *Earth and Planetary Science Letters* **104**: 424-439.
- Lidmar-Bergström, K. 1995. Relief and saprolites through time on the Baltic Shield. *Geomorphology* **12**: 45-61.
- Macciaroli, P., Giegengack, R., Klein, J., Middleton, R., Lawn, B. 1994. Late Quaternary glaciation of exposed rock surfaces along a ridge of the Appalachian Mountains, dated using ^{26}Al and ^{10}Be produced in situ. *Geological Society of America. Abstracts with Programs* **26**: A-125.
- MacGregor, K. R., Anderson R. S., Anderson, S. P., Waddington, E. D. 2000. Numerical simulations of glacial-valley longitudinal profile evolution. *Geology* **28**: 1031–1034.
- MacLean, B., Andrews, J. T., Gray, J. T., Hall, F. R., Hardy, I., Jennings, A. E., Manley, W. F., Pfeffer, W. T., Vilks, G. 2001. Late Quaternary sediments, depositional environments, and late glacial-deglacial history derived from marine and terrestrial studies. in *Marine geology of Hudson Strait and Ungava Bay, eastern Arctic Canada*; MacLean, B. (eds) Bulletin of the Geological Survey of Canada, Report: **566**: 181-191.

- Marchant, D. R., Denton, G. H., Swisher, C. C. 1993. Miocene-Pleistocene glacial history of Arena Valley, Quartermain Mountains, Antarctica. *Geografiska Annaler* **75A**: 269-302.
- Marquette, G. C., Gray, J. T., Gosse, J. C., Courchesne, F., Stockli, L., Macpherson, G., Finkel, R. 2004. Felsenmeer persistence under non-erosive ice in the Torngat and Kaumajet mountains, Quebec and Labrador, as determined by soil weathering and cosmogenic nuclide exposure dating. *Canadian Journal of Earth Sciences* **41**(1): 19-38.
- Marsella, K. A., Bierman, P. R., Davis, P. T., Caffee, M. W. 2000. Cosmogenic ^{10}Be and ^{26}Al ages for the last glacial maximum, eastern Baffin Island, Arctic Canada. *Geological Society of America Bulletin* **112**(8): 1296-1312.
- McMillan, N. J. 1973. Shelves of Labrador Sea and Baffin Bay, Canada. *in*: McCrossan, R. G. (ed.), *The Future Petroleum Provinces of Canada*, 473–517. Canadian Society of Petroleum Geologists, Calgary.
- Mengel, F., Rivers, T., Reynolds, P. 1991. Lithotectonic elements and tectonic evolution of the Torngat Orogen, Saglek Fiord, northern Labrador. *Canadian Journal of Earth Sciences* **28**: 1407-1423.

- Molnar, P., England, P. 1990. Late Cenozoic uplift of mountain ranges and global climate change: Chicken or egg? *Nature* **346**: 29-34.
- Montgomery, D. R. 2002. Valley formation by fluvial and glacial erosion. *Geology* **30**(11): 1047-1050.
- Näslund, J. O., Rodhe, L., Fastook, J. L., Holmlund, P. 2003. New ways of studying ice sheet flow directions and glacial erosion by computer modelling – examples from Fennoscandia. *Quaternary Science Reviews* **22**: 245-258.
- Nishiizumi, K., Winterer, E. L., Kohl, C. P., Klein, J., Middleton, R., Lal, D., Arnold, J. R. 1989. Cosmic ray production rates of ^{10}Be and ^{26}Al in quartz from glacially polished rocks. *Journal of Geophysical Research, B, Solid Earth and Planets* **94**(12): 17 907-17 915.
- Odell, N. E. 1933. The mountains of Labrador (continued), *The Geographical Journal* **82**(4): 315-325.
- Paterson, W. S. B. 1994. *The Physics of Glaciers*. Elsevier Science Ltd., Trowbridge.
- Peizhen, Z., Molnar, P., Downs, W. R. 2001. Increased sedimentation rates and grain sizes 2-4 Myr ago due to the influence of climate change on erosion rates. *Nature* **410**: 891-896.

- Small, E. E., Anderson, R. S. 1998. Pleistocene relief production in Laramide Mountain ranges, western United States. *Geology* **26**: 123-126.
- Stokes, C. R., Clark, C. D. 2001. Palaeo-ice streams. *Quaternary Science Reviews* **20** (13): 1437-1457.
- Stone, J. O. 2000. Air pressure and cosmogenic isotope production. *Journal of Geophysical Research* **B105**(10): 23 753 - 23 759.
- Stone, J. O., Ballantyne, C. K., Fifield, L. K. 1998. Exposure dating and validation of periglacial weathering limits, Northwest Scotland. *Geology* **26** (7): 587-590.
- Sugden, D. E. 1978. Glacial erosion by the Laurentide ice sheet. *Journal of Glaciology* **20**: 367-391.
- Taylor, F. C. 1979. Reconnaissance geology of a part of the Precambrian shield, northeastern Quebec, northern Labrador and Northwest Territories. *Geological Survey of Canada Memoir* **393**: 1-99.
- Tomkin, J. H., Braun, J. 2002. The influence of alpine glaciation on the relief of tectonically active mountain belts. *American Journal of Science* **302**(3): 169-190.

Twidale, C. R. 1976. On the survival of paleoforms. *American Journal of Science* **276**: 77-95.

Whipple, K. X., Kirby, E., Brocklehurst, S. H. 1999. Geomorphic limits to climate-induced increases in topographic relief. *Nature* **401**: 39-43.

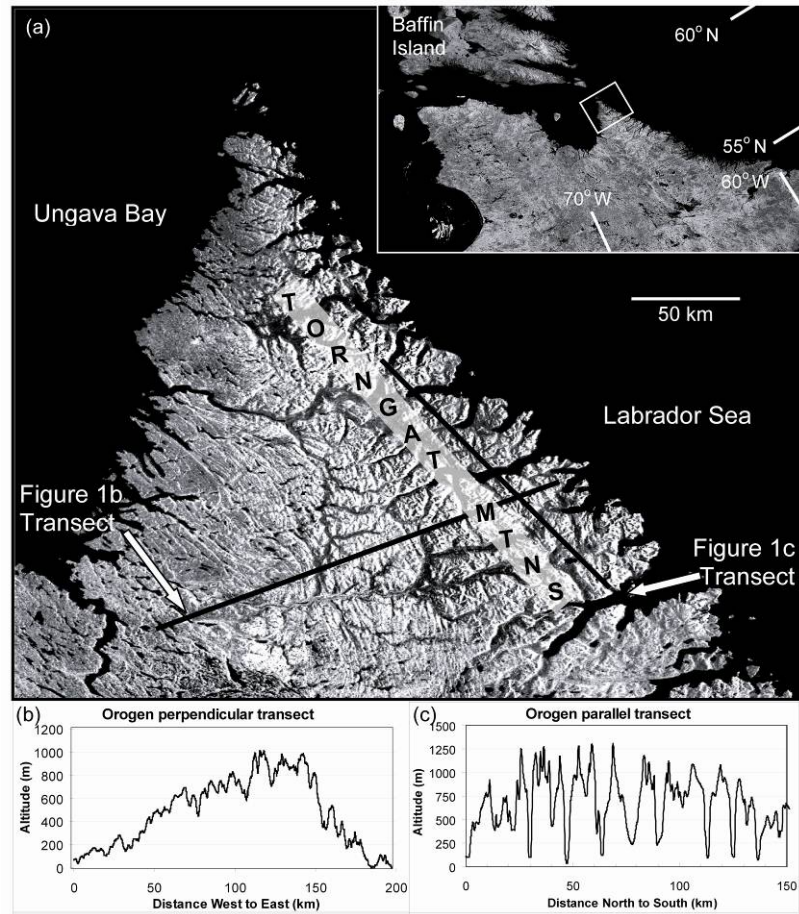


Figure 3.1 a. The Torngat Mountains on the Labrador Peninsula, eastern Canada form a narrow N-S ridge of peaks that protrude above a gently westward dipping (0.8°) subsummit plateau. The positions of the orogen-parallel and perpendicular cross-sections are marked. **b.** Transect of the mean topographic profile across the Labrador Peninsula reveal a distinct asymmetry to Torngat Mountain cross-section morphology. **c.** Range parallel topographic profile reveals a periodic (ca. 10 km) spacing of valleys that may reflect obscured shear zones or some fundamental fluvial response to the physiographic conditions (Hovius, 2000).

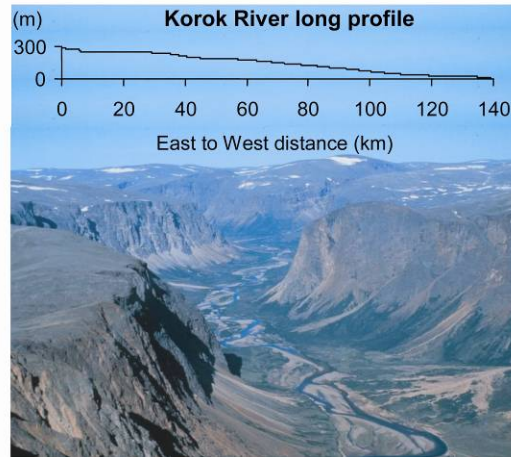


Figure 3.2 Low angle photograph of the Korok River valley. The valley position is inherited from ancestral fluvial erosion (Ahnert, 1994; Centeno, 2005) and probably only modified by glacial erosion (MacGregor et al., 2000). Highly-sheared, resistant bedrock lithologies maintain the 800 m relief. Inset long profile of the Korok River with 20x vertical exaggeration.

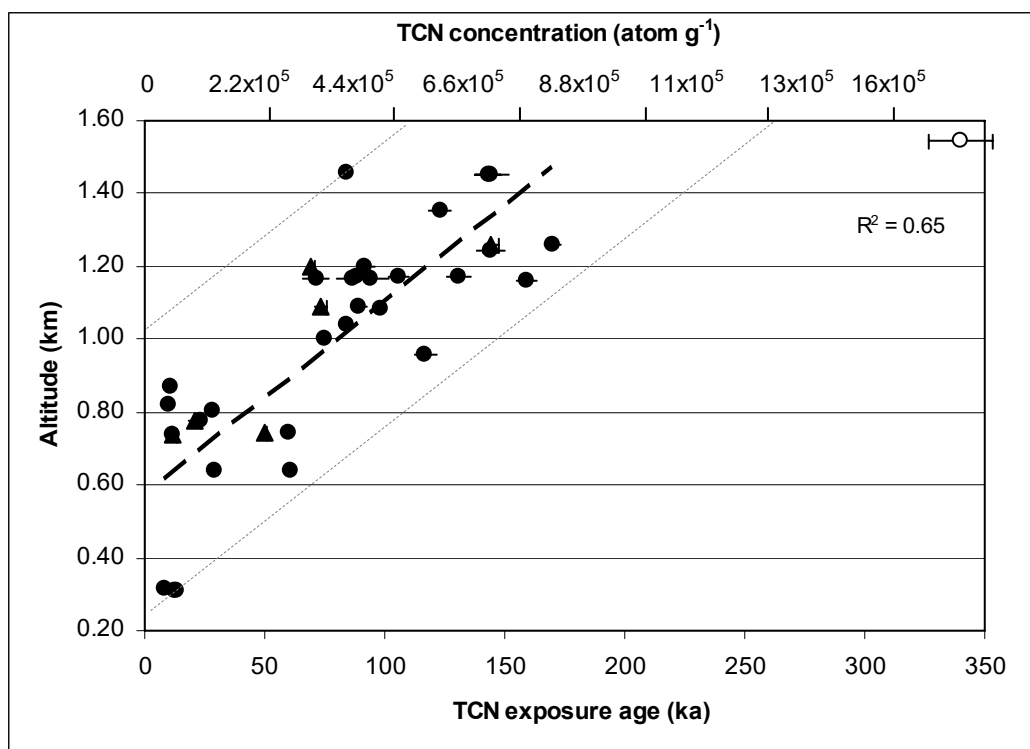


Figure 3.3 Apparent exposure age plotted vs. altitude for bedrock samples in the Torngat Mountains. This plot suggests there is a linear relationship between elevation and TCN concentrations that are proportional to age by a production rate (given in Table 3.1). Solid circles represent ¹⁰Be data; solid triangles represent ²⁶Al data on the same bedrock sample. The open circle is an outlier. The thick dashed line shows the best-fit line through the ¹⁰Be data points. The thin dashed line marks the boundaries of the 1- σ confidence level.

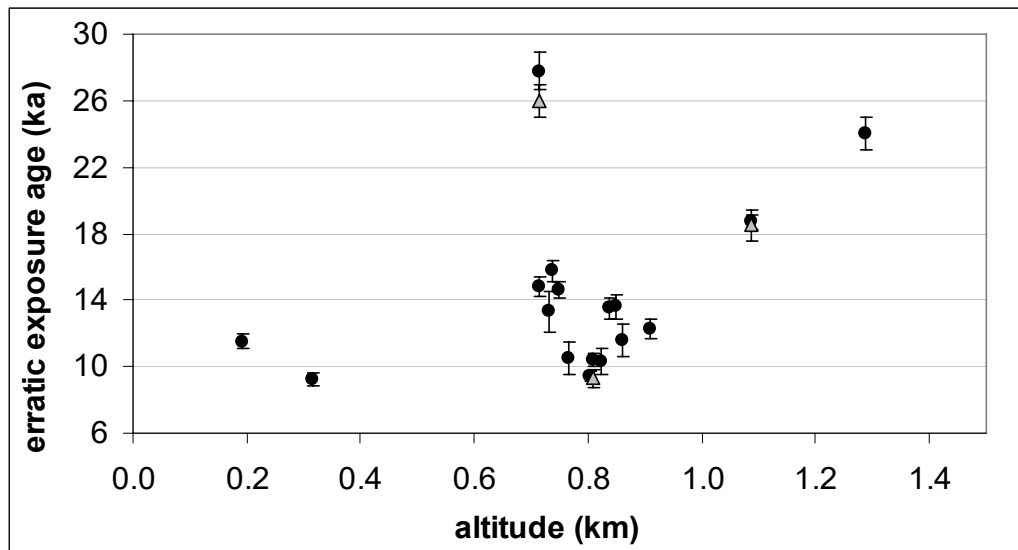


Figure 3.4 Exposure ages of erratic boulders found at elevations ranging from high summits to lowest valley bottom samples on the right side of the graph. Elevations of the boulder samples displayed on this graph range from 200 m to 1400 m asl. Black circles represent ^{10}Be data; gray triangles represent ^{26}Al data on the same boulder sample.

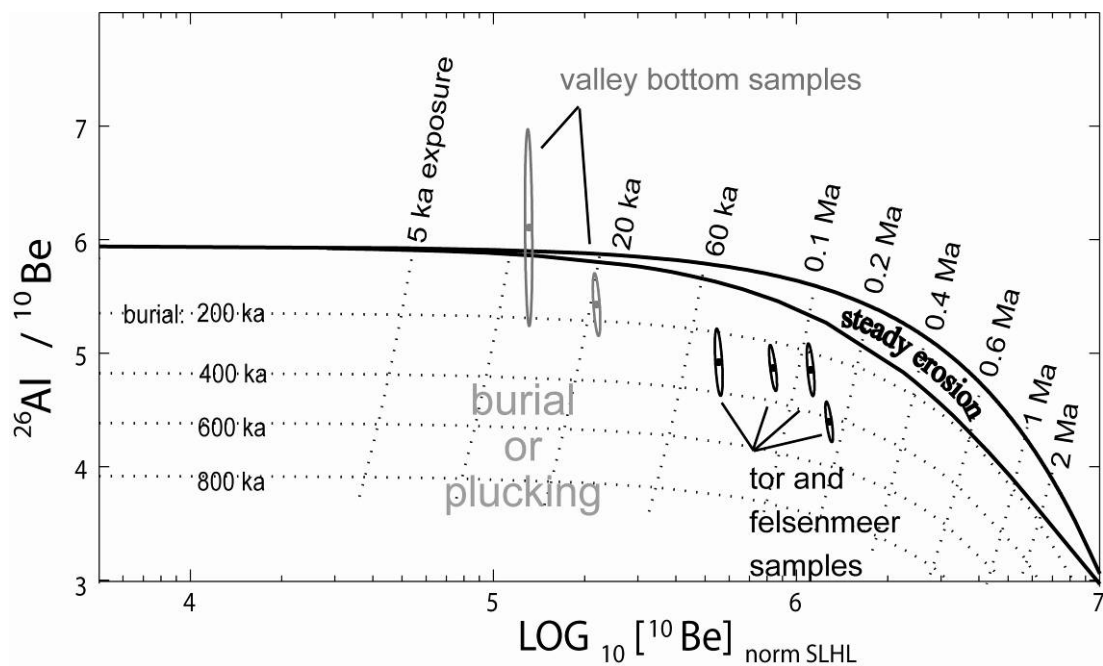


Figure 3.5 Exposure-erosion diagram of $^{26}\text{Al}/^{10}\text{Be}$ vs. $\log^{10}\text{Be}$ normalized for production at sea level high latitude (SLHL). Samples that plot below the lower curve have experienced an interruption in their exposure history, by burial or deep plucking. The uncertainties reflect 1- σ analytical precision in the AMS measurements.

Figure 3.6 UMISM results over a 100-ka cycle for the Labrador Peninsula. Bed topography is input into the model and is derived from the ETOPO2 2-minute gridded dataset. The edge of the modeled region in a and b can be affected by the ice fluxes dictated by boundary condition derived from the coarser resolution ice sheet simulations for the entire Laurentide Ice Sheet and gradually scaled down to the 2-minute topography. **a.** Plan view of the duration (ka) of ice cover over the last glacial cycle. Summit plateaus grow ice relatively quickly in the model as a response to cooler temperatures forced by GRIP. **b.** Spatial variation in the modeled basal sliding distance normalized by duration of ice cover. The ice simulation shows that the plateau and peak surfaces likely were positioned below slow-moving cold-based ice whereas lower altitude surfaces were overridden by faster, thicker, warm-based ice.

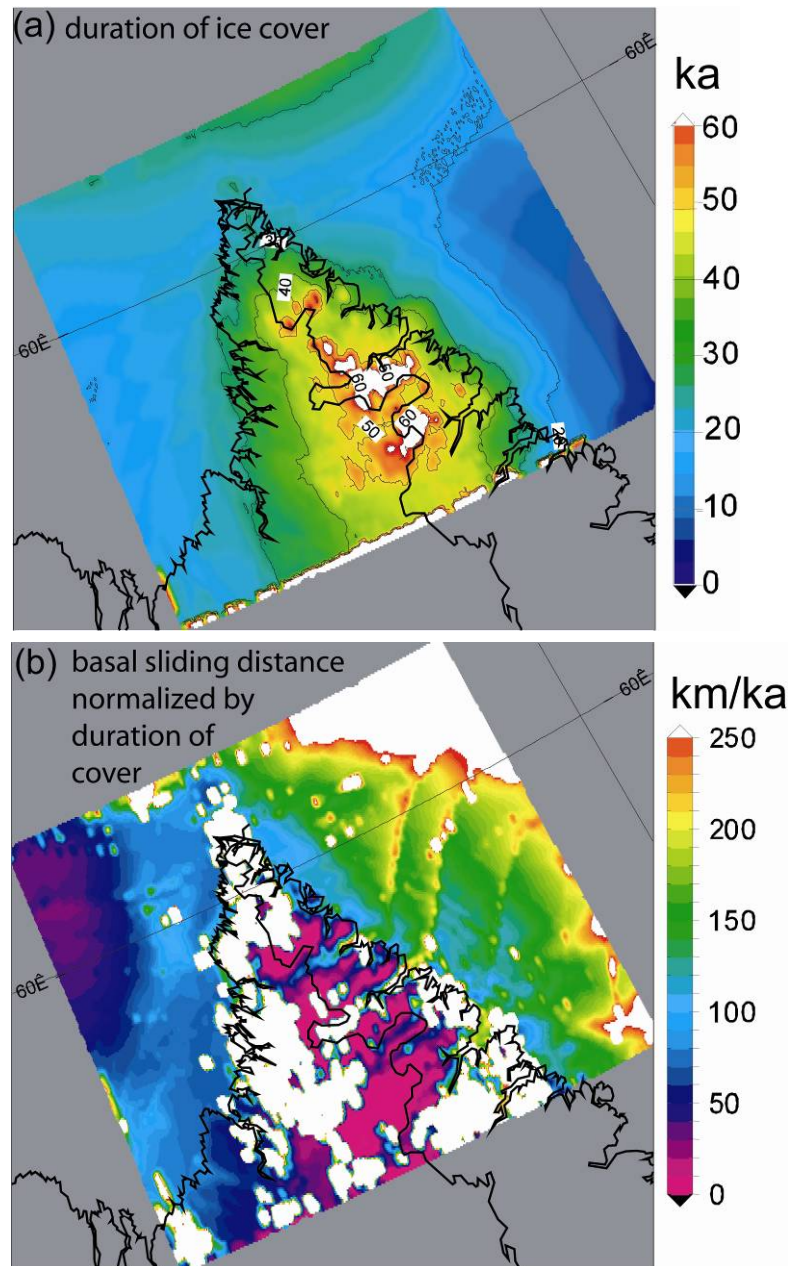


Figure 3.6

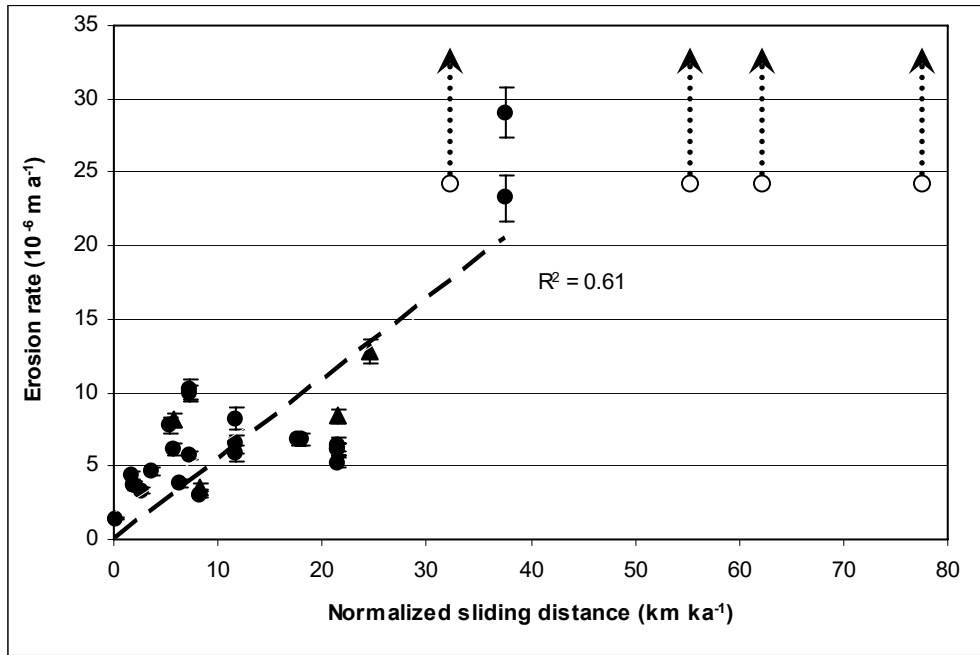


Figure 3.7 Erosion rate vs. normalized sliding distance based on the 100 ka UMISM simulation for the Torngat Mountains. Sliding distance is normalized by ice cover and represents average ice speed for each 30 arc-second pixel. Post-glacial TCN concentrations were subtracted from the measured TCN concentrations before calculating erosion rates (see text). The slope of this line is the glacial erosion constant in Equation 3.1.

Table 3.1 Sample location and exposure age data. Uncertainties reflect 1- σ analytical uncertainties in the AMS analyses. For the $^{26}\text{Al}/^{10}\text{Be}$ ratio uncertainty, we report the 1- σ uncertainty by adding the Be and Al AMS precisions in quadrature. ^9Be carrier is from a shielded beryl, prepared by J. Klein. ^{27}Al carrier is from a SPEX ICP standard. Chemical blanks ranged from 1.9×10^5 to 3.9×10^5 ^{10}Be atoms. AMS was completed at Lawrence Livermore National Lab (LLNL). ¹These data were originally reported in Marquette et al. (2004). AMS targets for these samples were prepared at University of Kansas, all other targets were prepared at Dalhousie University. ²Previously reported ages were re-calculated and scaled according to Lal (1991, his table 2) and modified for muon fraction according to Stone (2000) using a high-latitude sea-level production rate of 5.1 ^{10}Be atoms $\text{g}^{-1} \text{a}^{-1}$ (Gosse and Stone, 2001). ³C concentrations were normalized to sea level, high-latitude (SLHL) production rate in order to compare samples from differing locations. ⁴Ages are calculated assuming a continuous exposure with no erosion or burial, therefore they may be considered minimum exposure durations.

Table 3.1

field ID	nuc.	site specific data			cosmogenic concentrations					ratio		age ⁴		max erosion rate	
		lat deg	alt. km	prod rate ² atom g ⁻¹ a ⁻¹	measured atom g ⁻¹	meas err atom g ⁻¹	prec %	norm SLHL ³ atom g ⁻¹	wo post-glac atom g ⁻¹	²⁶ Al/ ¹⁰ Be	unc	ka	err ka	calc cm/100ka	error cm/100ka
summit and subsummit plateau bedrock	¹⁰ Be	58.92	1.547	18.10	5.7E+06	2.3E+05	4%	1.6E+06	1.5E+06	---	---	340.0	26.7	14.1	1.1
	¹⁰ Be	59.03	1.460	17.27	1.4E+06	2.4E+04	2%	4.2E+05	3.6E+05	---	---	84.0	2.7	67.9	3.7
	¹⁰ Be	58.69	1.453	16.79	2.3E+06	8.8E+04	4%	7.1E+05	6.5E+05	---	---	143.3	10.6	36.9	2.5
	¹⁰ Be	58.69	1.453	17.23	2.4E+06	1.2E+05	5%	7.1E+05	6.6E+05	---	---	144.6	13.5	36.5	2.7
	¹⁰ Be	58.69	1.355	15.79	1.9E+06	7.1E+04	4%	6.1E+05	5.5E+05	---	---	123.0	9.0	43.9	2.9
	¹⁰ Be	59.29	1.257	14.49	2.4E+06	4.9E+04	2%	8.4E+05	7.8E+05	---	---	170.0	6.9	30.5	1.8
	²⁶ Al	59.29	1.257	86.21	1.2E+07	2.3E+05	2%	4.1E+06	6.3E+05	4.7	3%	144.2	5.7	35.8	2.2
	¹⁰ Be	57.88	1.245	14.68	2.0E+06	7.8E+04	4%	6.8E+05	6.2E+05	---	---	144.0	11.2	38.5	2.6
	¹⁰ Be	58.70	1.200	14.11	1.3E+06	5.1E+04	4%	4.6E+05	4.1E+05	4.4	4%	92.0	7.3	60.7	4.1
	²⁶ Al	58.70	1.200	83.81	5.6E+06	1.1E+05	2%	2.0E+06	2.9E+05	---	---	69.5	2.7	84.1	4.8
	¹⁰ Be	58.69	1.173	13.69	1.2E+06	6.2E+04	5%	4.4E+05	3.8E+05	---	---	88.0	9.0	64.1	4.8
	¹⁰ Be	58.70	1.172	13.68	1.2E+06	4.9E+04	4%	4.6E+05	4.0E+05	---	---	130.9	10.3	61.0	4.0
	¹⁰ Be	58.69	1.170	13.69	1.4E+06	5.3E+04	4%	5.2E+05	4.7E+05	---	---	106.0	7.8	52.0	3.4
	¹⁰ Be	58.70	1.169	13.58	1.3E+06	9.4E+04	8%	4.7E+05	4.2E+05	---	---	94.4	13.9	58.9	5.5
	¹⁰ Be	58.70	1.169	13.58	9.6E+05	7.3E+04	8%	3.6E+05	3.0E+05	---	---	71.5	10.6	81.9	7.7
	¹⁰ Be	58.70	1.169	13.58	1.2E+06	8.8E+04	8%	4.3E+05	3.8E+05	---	---	86.8	12.9	64.9	6.1
	¹⁰ Be	59.48	1.162	13.29	2.0E+06	5.3E+04	3%	7.8E+05	7.3E+05	---	---	159.0	8.0	32.8	2.0
	¹⁰ Be	58.60	1.090	12.83	1.1E+06	4.4E+04	4%	4.4E+05	3.9E+05	---	---	89.0	6.9	60.9	4.2
	²⁶ Al	58.60	1.090	76.20	5.4E+06	1.6E+05	3%	2.1E+06	3.1E+05	4.8	5%	73.4	4.3	81.2	4.9
	¹⁰ Be	59.25	1.086	12.70	1.2E+06	2.3E+04	2%	4.9E+05	4.3E+05	---	---	98.0	3.7	57.0	3.2
	¹⁰ Be	58.88	1.041	12.23	1.0E+06	2.9E+04	3%	4.2E+05	3.6E+05	---	---	84.0	4.7	67.7	4.0
	¹⁰ Be	59.47	1.000	11.84	8.7E+05	3.4E+04	4%	3.7E+05	3.2E+05	---	---	75.0	5.7	77.9	5.1
	¹⁰ Be	59.61	0.960	12.29	1.4E+06	5.6E+04	4%	5.8E+05	5.2E+05	---	---	117.0	9.2	46.5	3.1
	¹⁰ Be	59.32	0.870	10.91	1.2E+05	7.7E+03	6%	5.7E+04	6.2E+02	---	---	11.2	1.4	---	---
	¹⁰ Be	58.98	0.822	11.10	1.1E+05	3.2E+03	3%	5.1E+04	0.0E+00	---	---	10.0	0.6	---	---
	¹⁰ Be	58.98	0.803	11.01	3.1E+05	8.3E+03	3%	1.4E+05	8.7E+04	---	---	28.2	1.5	290.5	16.6
	¹⁰ Be	58.50	0.741	9.42	5.5E+05	2.2E+04	4%	3.0E+05	2.4E+05	---	---	60.0	4.7	101.9	6.7
	²⁶ Al	58.50	0.741	55.96	2.7E+06	8.2E+04	3%	1.5E+06	1.9E+05	4.9	5%	49.9	2.9	127.8	7.7
¹⁰ Be	59.05	0.639	7.93	2.6E+05	1.0E+04	4%	1.6E+05	1.1E+05	---	---	29.5	2.3	232.3	15.1	
¹⁰ Be	59.05	0.639	8.72	5.2E+05	1.3E+04	3%	3.1E+05	2.5E+05	---	---	60.8	3.0	99.6	5.8	

Table 3.1 (continued)

	field ID	nuc.	site specific data			cosmogenic concentrations					ratio		age ⁴		max erosion rate	
			lat deg	alt. km	prod rate ² atom g ⁻¹ a ⁻¹	measured atom g ⁻¹	meas err atom g ⁻¹	prec %	norm SLHL ³ atom g ⁻¹	wo post-glac atom g ⁻¹	²⁶ Al/ ¹⁰ Be	unc	age ka	err ka	calc cm/100ka	error cm/100ka
valley bedrock	LAB-00-25B ¹	¹⁰ Be	58.70	0.776	9.71	2.2E+05	6.6E+03	3%	1.2E+05	6.0E+04	5.4	4%	23.0	1.4		
		²⁶ Al			57.68	1.2E+06	3.6E+04	3%	6.3E+05	5.0E+04			20.9	1.2		
	LAB-00-23A ¹	¹⁰ Be	58.60	0.740	9.49	1.1E+05	4.5E+03	4%	5.8E+04	2.1E+03	6.1	11%	11.4	0.9		
		²⁶ Al			56.39	6.6E+05	6.6E+04	10%	3.5E+05	3.5E+03			11.7	2.3		
	LAB-00-24D	¹⁰ Be	58.61	0.316	6.46	5.5E+04	2.2E+03	4%	4.3E+04	0.0E+00	---	---	8.5	0.7		
	LAB-02-STK-228	¹⁰ Be	58.83	0.312	6.50	8.3E+04	2.5E+03	3%	6.5E+04	9.5E+03	---	---	12.9	0.8		
LAB-02-STK-229	¹⁰ Be	58.85	0.311	6.72	9.2E+04	4.8E+03	5%	7.0E+04	1.4E+04	---	---	13.7	1.4			
Perched and (Pseudo)erratic boulders	LAB-00-29B	¹⁰ Be	58.88	1.289	14.98	3.6E+05	1.5E+04	4%	1.2E+05	6.7E+04	---	---	24.0	2.0		
	LAB-02-NACH-222	¹⁰ Be	59.26	1.086	12.59	2.3E+05	5.9E+03	3%	9.5E+04	3.9E+04	5.8	6%	18.7	0.9		
		²⁶ Al			74.78	1.4E+06	6.9E+04	5%	5.6E+05	3.8E+04			18.5	1.8		
	MTH-99-01 ¹	¹⁰ Be	56.92	0.908	10.91	1.3E+05	6.5E+03	5%	6.2E+04	6.2E+03	---	---	12.3	1.2		
	LAB-00-16B	¹⁰ Be	58.71	0.859	10.50	1.2E+05	1.0E+04	9%	5.9E+04	2.8E+03	---	---	11.6	2.0		
	KAU-99-02A ¹	¹⁰ Be	57.87	0.850	10.38	1.4E+05	7.3E+03	5%	6.9E+04	1.3E+04	---	---	13.6	1.4		
	LAB-00-20A ¹	¹⁰ Be	58.62	0.838	10.37	1.4E+05	6.2E+03	4%	6.9E+04	1.3E+04	---	---	13.5	1.2		
	LAB-02-NACH-201	¹⁰ Be	58.98	0.822	10.19	1.0E+05	8.2E+03	8%	5.2E+04	0.0E+00	---	---	10.3	1.6		
	Lab-00-15A	¹⁰ Be	58.70	0.809	10.20	1.1E+05	4.2E+03	4%	5.3E+04	0.0E+00	5.3	7%	10.4	0.8		
		²⁶ Al			60.59	5.6E+05	3.4E+04	6%	2.8E+05	0.0E+00			9.3	1.1		
	LAB-02-NACH-204	¹⁰ Be	58.98	0.803	11.01	1.0E+05	3.2E+03	3%	4.8E+04	0.0E+00	---	---	9.4	0.6		
	LAB-99-23-1A ¹	¹⁰ Be	59.31	0.766	9.61	1.1E+05	1.0E+04	10%	5.6E+04	0.0E+00	---	---	10.5	2.0		
	LAB-00-14B	¹⁰ Be	58.70	0.748	9.60	1.4E+05	4.5E+03	3%	7.4E+04	1.8E+04	---	---	14.6	0.9		
	LAB-00-14A	¹⁰ Be	58.70	0.736	9.47	1.5E+05	6.0E+03	4%	8.0E+04	2.4E+04	---	---	15.8	1.2		
	LAB-97-24A ¹	¹⁰ Be	59.32	0.730	59.90	7.9E+05	7.1E+04	9%	4.0E+05	1.1E+04	---	---	13.3	2.4		
	LAB-00-11B	¹⁰ Be	58.70	0.715	9.38	1.4E+05	5.5E+03	4%	7.5E+04	1.9E+04	---	---	14.8	1.2		
	LAB-00-17A ¹	¹⁰ Be	58.64	0.713	9.28	2.6E+05	1.0E+04	4%	1.4E+05	8.5E+04	5.5	6%	27.8	2.2		
		²⁶ Al			55.12	1.4E+06	5.4E+04	4%	1.3E+05	7.4E+04			26.0	2.0		
LAB-00-27C	¹⁰ Be	59.06	0.530	8.72	2.6E+05	1.0E+04	4%	1.5E+05	9.6E+04	---	---	33.1	2.6			
LAB-00-24C	¹⁰ Be	58.61	0.316	6.38	5.9E+04	2.3E+03	4%	4.7E+04	0.0E+00	---	---	9.2	0.7			
LAB-00-28A	¹⁰ Be	59.00	0.191	5.87	6.7E+04	2.7E+03	4%	5.9E+04	2.6E+03	---	---	11.5	0.9			

CHAPTER 4**GLACIAL EROSION AND SEDIMENT DISPERSION FROM DETRITAL COSMOGENIC
NUCLIDE ANALYSES****Jane Willenbring Staiger, John Gosse,**

Department of Earth Sciences, Dalhousie University, Halifax, Nova Scotia B3H 4J1,
Canada

Edward C. Little, Dan Utting

Canada–Nunavut Geoscience Office, P.O. Box 2319, Iqaluit, Nunavut X0A 0H, Canada

Robert Finkel

Lawrence Livermore National Laboratory, Center for Accelerator Mass Spectrometry
7000 East Ave, Livermore, California 94550, USA

Jesse V. Johnson

Department of Computer Science, University of Montana, Missoula, Montana, 59812,
U.S.A.

James Fastook

Department of Computer Science, University of Maine, Orono, Maine, 04469, U.S.A.

4.1 ABSTRACT

Glacial erosion and till production are a function of the thermal regime at the base of a glacier. We suggest a new means to identify paleo-glacier polythermal conditions from the measurement of terrestrial in situ cosmogenic nuclides (TCN). The premise is that during non-glacial times TCN will be produced in exposed minerals in the upper few meters of regolith (e.g. bedrock, saprolite, previous tills). During glacial times, areas of warm (wet) basal conditions will strip the upper few m of regolith and effectively remove the previous TCN. Under cold-based conditions the ice is frozen to the bed so much of the previous TCN concentration survives (except a small amount due to radioactive decay). In areas that were classified as warm-based or cold-based (end member) systems based on sedimentology, geomorphology, and the presence of exotic erratics, concentrations of ^{10}Be and ^{26}Al on 19 till samples mimic the pattern. In three localities that resembled intermediate cases, i.e. cold-based conditions but with exotic clasts in the till, the ^{10}Be and $^{26}\text{Al}/^{10}\text{Be}$ reveal that the surface experienced a combination of cold-based ice burial and glacial erosion, but the minimal burial duration was shorter than the minimal burial durations for the cold-based ice end members. An ice sheet simulation of bed conditions reflects the same pattern. An important implication for mineral exploration in glaciated terrain is that the till TCN method can help to identify cold-based anomalies in basal sliding, a major obstacle in interpreting glacial dispersal patterns. Patterns in subglacial erosion and till production can also be inferred, and the data suggest that preservation of till and regolith is possible under > 3 Ma of glacial cover.

4.2 INTRODUCTION

Glacial erosion of bedrock and the movement and deposition of entrained basal detritus is linked to the basal thermal regime of the ice (Boulton, 1972; Hallet, 1979; 1996; Alley et al., 2003), which depends on the distance from the ice divide, a dampened air temperature signal, and the underlying bed topography. Glaciers are cold-based when the ice-substrate interface temperature is lower than the pressure-melting point. Thin, cold-based ice inhibits glacial erosion and may protect rock from periglacial processes (Whipple et al., 1999). Warm-based ice (i.e. the basal temperature is greater than the pressure-melting point) has a much higher potential for eroding the substrate due to a mobile layer of water. Thick ice lowers the pressure-melting point and effectively insulates geothermal heat from Arctic air temperatures. Heat is also produced by frictional or strain heating, prevalent in areas with converging ice flow. Except near the ice sheet or glacier terminus, ice velocities generally increase with distance from the ice divide, owing to the advection or “downwelling” (Marshall and Clark, 2002) of cold surface ice at the ice dome. Basal sliding velocity is enhanced by increased basal water that can result from raising the ice temperature above the pressure-melting point.

As a function of the heat distribution and production, the ice at a glacier bed can (1) be completely melted throughout the glaciation, (2) be completely frozen throughout the glaciation, (3) alternate between melting and freezing cycles and, (4) effectively conduct heat such that there is little freezing or melting (Boulton, 1972). Beneath a polythermal ice sheet, the basal thermal regimes and associated glacial erosional and depositional processes vary spatially (Paterson, 1994). Climate-induced changes in ice thickness and glaciological or climatical shifts in ice dispersal centers can induce

temporal variations in thermal regime and contribute to the spatial variation in erosional and depositional processes (Moore, 1990).

Basal thermal regime, physical properties of the regolith, transport distance and distance from the ice center are reflected in the textural characteristics of tills. Tills associated with cold-based ice have short transport distances (“short distance tills”) and have less silt and clay than tills from warm-based ice because the latter have experienced more comminution. Short distance tills contain clasts that are angular, locally-derived, and rarely striated. Fine-grained, silt-rich tills with striated, subrounded clasts and a wide variety of clast lithologies are indicative of “long distance tills” associated with warm-based conditions. The decrease in particle size fraction and increase and clast lithology variation with ice-transport distance has been well-documented (Shilts, 1976).

Areas of cold-based ice cover can be difficult to differentiate from areas that have not been covered by ice because cold-based ice cover leaves only scant, cryptic evidence of glaciation, such as lateral meltwater channels (Dyke, 1993) and tills with angular clasts. The temporal variation in the thermal regime can be inferred from the presence of palimpsest and preserved landforms. For example, drumlins are thought to form by fast ice flow and are therefore prime candidates for erosion; yet, they remain.

Many studies in polar landscapes reveal that TCN concentrations in bedrock and boulders are often greater than that corresponding to independently dated exposure durations (i.e. radiocarbon dated ice-marginal positions). The excessive concentration can also be demonstrated in areas where erratic boulder TCN concentrations are consistently lower than TCN concentrations in the bedrock that the boulders rest on. The difference in concentration is interpreted to be due to differential erosion under a glacier,

due to physical properties of bedrock and to glaciological factors. These studies imply that in glaciated landscapes there are regions where bedrock erosion is less than 1.4 m/Ma and that an inventory of the TCN across a landscape would be indicative of minimal glacial erosion (Fabel et al., 2002; Stone et al., 2003; Briner et al., 2003; Marquette et al., 2004; Hilchey, 2004, Briner et al., 2005). TCN concentrations in ca. 6 ka old glaciolacustrine deltaic sediment in the Ravn River valley, northern Baffin Island, have a high inherited TCN budget (equivalent to > 25 ka of exposure) and thus also reflect the lack of glacial erosion of the bed until deglacial conditions induce basal thawing (Hilchey, 2004). Yet, in mid-latitude alpine regions with warm-based conditions, <3% of moraine boulders contain discernable amounts of inherited TCN concentrations (Gosse and Phillips, 2001; Putkonen and Swanson, 2003). These observations provide the proof of concept for our hypothesis that the TCN concentration in till should allow us to differentiate regions with low and high amounts of glacial erosion.

The purpose of this paper is to show that TCN can be used to determine spatial and temporal variations in glacial erosion that are not solely dependent upon landscape position (elevation) or physical properties of the underlying bedrock and regolith. We first use geomorphological and sedimentological descriptions to classify and select regions in northern Baffin Island where end-member cold-based or warm-based conditions persisted through most of the last glaciation. We test the hypothesis that TCN concentrations should reflect those basal thermal regimes at 19 sites with different bedrock lithologies. We then use a thermomechanical ice sheet model to help evaluate

our interpretation that basal thermal regime is a primary control of the spatial and temporal variability in glacial erosion.

4.3 PHYSIOGRAPHY OF THE STUDY AREA

The study area is situated to the north and east of the Barnes Ice Cap (Fig. 4.1). Physiographic zones broadly correspond to bedrock lithologies and probably their resistance to erosion (Little et al., 2004). The Davis Highlands zone in the north is a fiord-dissected elevated plateau composed of metamorphosed Archean rocks of the Mary River Group (Little et al., 2004). The Ice Bound Lakes region of this highland has small, decaying cold-based ice caps and ice patches (Andrews et al., 1976). The Davis Highlands are bordered to the southwest by the Baffin Uplands, beginning at the heads of the fiords to the north and east. The Baffin Uplands consists of broad hills composed of Proterozoic siliciclastic and carbonate rocks and generally slope to the southwest from >900 m to <300 m (Ives and Andrews, 1963). Wide, deep (>300 m) valleys dissect the region, including the Ravn River Valley, which flows westward onto the lakes, bogs, flat rolling till plains, and subdued non-metamorphosed carbonate and siliciclastic bedrock ridges of the lower Lancaster Plateau (Fig. 4.1). To the south, the Lancaster Plateau is a graben structure defined by the Central Baffin Fault line escarpment. In the south, the Lancaster Plateau is bordered by the Foxe Plain in the south, which dips gently towards Foxe Basin.

4.4 GLACIAL HISTORY

Briner et al. (2003, 2005) and Kaplan et al. (2003) concluded from their TCN data that at the last glacial maximum (LGM), relatively fast-flowing, warm-based ice filled valleys, and cold-based, slow-moving ice was present on upland, felsenmeer surfaces in Baffin Island. Barring a few coastal nunataks, glacier ice completely covered Baffin Island and deposited erratic boulders that yield exposure ages of the regional LGM even at high elevations (Steig et al., 1998; Bierman et al., 1999; Marsella et al., 2000; Davis et al., 2002; Kaplan et al., 2003, Briner et al., 2003 and Briner et al., 2005). Some of this ice was inferred to have been cold-based owing to the preservation of nearby tors with pre-glacial exposure histories. The inland areas are now thought to have been inundated by ice until the early Holocene (Dyke and Hooper, 2001). The easternmost coastal forelands of Baffin Island may have remained ice-free (Briner et al., 2005, Davis et al., 2002; Kaplan et al., 2003, Briner et al., 2005) or may have been inundated to the shelf break (Jennings et al., 1996; Andrews et al., 1998). This ice margin is still debated, but the ice configuration above the study area is not.

Within the study area, the ice cover is believed to have been complete, although the paleo-glacier dynamics not only responded to climatically-driven changes in ice thickness but also controls on ice flow by high relief (> 1000 m in places). Relative paleo-ice flow indicators in the area suggest that four main regional ice flow phases took place during the last deglaciation (Little et al., 2003). The overall pattern of deglaciation given in Little et al. (2005) is similar to previously published patterns by Ives and Andrews (1963) and Hodgson and Haselton (1974). The ages of ice margin positions

have been interpolated to modern termini by Dyke et al. (2003, See Fig. 4.2) from radiocarbon age constraints on the Cockburn Moraine (Falconer, 1965) and shell-bearing marine sediments.

4.5 METHODOLOGY

TCN are rare isotopes produced in regolith at the Earth's surface during the interaction of secondary cosmic radiation and atoms in exposed minerals (Lal, 1991; Gosse and Phillips, 2001). The concentration of TCN in a given rock or mineral is primarily dependent upon (1) duration of exposure (or multiple exposures, in the instance of interruptions due to intermittent shielding from cosmic rays), (2) production rate at the site, which is a function of atmospheric shielding (altitude) and magnetic field effects (latitude), (3) environmental factors such as partial shielding by snow, ice, or till, (4) glacial and non-glacial erosion of the surface, and (5) radioactive decay of the cosmogenic isotopes. The secondary radiation responsible for these TCN (primarily fast neutrons and muons) attenuate exponentially with depth into rock (e-folding lengths of 150 and 1300 g cm⁻², respectively) so production at 3 m rock depth is only slightly more than 1% of surface production. Therefore, more than 99% of the TCN concentration is removed when > 3 m of rock is eroded. However, under cold-based or quasi-cold-based subglacial ice conditions, removal of this surface layer may be incomplete, resulting in inheritance from the previous exposure production profile. In an area that is thought to have experienced cover by partly cold-based ice such as north-central Baffin Island, the interpretation of a single TCN concentration in bedrock or till as a simple exposure age

can be misleading. However, TCN inheritance due to prior exposure may be exploited to qualitatively assess the degree of glacial abrasion and plucking (e.g., Briner and Swanson, 1998).

We sampled till sites (n=19; See Fig. 4.4a) that were classified as predominantly cold-based or warm-based end-members based on geomorphology, sedimentology (Fig. 4.5), and presence of clasts of exotic lithologies. We assume that TCN concentrations in surface till samples represent a glacially-mixed till blanket that was derived from regolith containing a pre-glacial TCN production profile and have been exposed for the last 4-9 ka of the Holocene period (Fig. 2). For simplicity, we use the term regolith to include rock, saprolite, and sediment including previous tills that may be susceptible to glacial erosion. The TCN concentrations should be highest in short distance tills where an inherited exposure signal has been preserved beneath slow-moving, non-erosive ice (Fig. 4.3a) and lowest in long distance tills comprising regolith from deeper excavation by highly-erosive, fast-flowing ice (Fig. 4.3b).

Initial mineral separation (heavies from lights) was conducted at the Geological Survey of Canada-Ottawa. Concentration of the quartz from the light fractions was completed at Dalhousie University. Nineteen Be-oxide and 15 Al-oxide targets were prepared at Dalhousie University using standard procedures and an average of 20 g of quartz concentrate. Native element concentrations were measured by ICP.AES at U. Kansas and Tailored Polymers Group at DRDC, and isotopic ratios were measured at Lawrence Livermore National Lab. Data reduction and assumptions in the interpretation of the TCN data used standard procedures (no correction for geomagnetic field effects) and production rates and scaling according to Lal (1991) and Stone (2000).

Prior to Quaternary glaciations, a ^{10}Be production profile would have existed in the upper meters of the Earth's surface. The maximum concentration (N_{max}) at the surface of this pre-Quaternary profile was dependant on the erosion rate for the site. In lower elevation site, this scenario was more complicated due to possible deposition of alluvium. Quaternary glaciations cause a decrease in this concentration by decay from burial and/or erosion into the top of the pre-Quaternary ^{10}Be profile. In any sample, the inherited (pre-Quaternary remnant) TCN concentration is the measured concentration (N_{meas}) minus the concentration produced during post-glacial exposure (N_{post}). The inherited concentration in a sample is a function of the depth of erosion into the pre-Quaternary production profile. The eroded regolith thickness can be estimated by assuming a pre-Quaternary TCN concentration that once existed at the top of the bedrock surface of the production profile (Fig. 4.6a):

$$z = -\frac{\Lambda_{\text{spall}}}{\rho} \ln \frac{N_{\text{meas}} - N_{\text{post}}}{N_{\text{max}}} \quad (\text{Eq. 4.1})$$

where z is the depth of the surface eroded (cm), Λ_{spall} is the attenuation length for the exponential decrease of cosmogenic nuclide spallogenic production with depth ($\text{g}\cdot\text{cm}^{-2}$), ρ is the bulk density ($\text{g}\cdot\text{cm}^{-3}$), N_{meas} is the measured concentration of cosmogenic nuclides in quartz that is that is a function of the depth in the inherited profile and the post-glacial exposure ($\text{atom}\cdot\text{g}^{-1}$), N_{post} is the post-glacial component of the total measured concentration in quartz ($\text{atom}\cdot\text{g}^{-1}$), and N_{max} is the inherited initial concentration in quartz prior to glacial erosion ($\text{atom}\cdot\text{g}^{-1}$) (Davis et al., 1999).

Tills deposited by non-erosive ice are incorporating only the upper portion of a bedrock production profile; tills deposited by erosive ice are excavating and mixing a greater bedrock depth. Till samples derived from wet-based, erosive ice should not

contain a TCN concentration greater than that produced from post-glacial exposure. An inherited TCN concentration in till represents a greater depth of erosion than the same inherited TCN concentration in bedrock because TCN concentrations in till reflect a mixture (or integration) of the upper portion of the depth profile (Fig. 4.6b). We can estimate minimum thickness eroded in tills by defining the pre-Quaternary TCN signal (N_{\max}) as the highest levels of inheritance found in the sample with the highest TCN concentration. This definition assumes that this till still retains the inherited ^{10}Be signal plus the relatively small post-glacial ^{10}Be concentration and that the $^{26}\text{Al}/^{10}\text{Be}$ ratio indicates the portion that was lost to decay under ice cover. We then calculate the amount of erosion in a mixed sample that integrates a portion of the bedrock TCN production profile by:

$$z = -\frac{\Lambda_{spall}}{\rho} \ln \left(1 - \frac{\rho_{till}}{\Lambda} \frac{N_{meas} - N_{post}}{N_{\max}} \right) \quad (\text{Eq. 4.2})$$

Tills in our area might represent a continuum between the bedrock (Eq. 4.1) and mixed till end-members (Eq. 4.2). These two erosion scenarios form the range of thicknesses eroded for each inherited TCN concentration in till (See Appendix 7 for derivation of the depth calculations).

Equations 4.1 and 4.2 assume only one TCN production mechanism, thus assume only one attenuation length. TCN production by muons contributes only a small portion of the total production at the surface, but muons contribute a larger portion of total production at depth owing to the longer attenuation length. Total production is described by the equation:

$$P(z) = P_n e^{-z\rho/\Lambda_{spall}} + P_{s1} e^{-z\rho/\Lambda_{s1}} + P_{s2} e^{-z\rho/\Lambda_{s2}} + P_f e^{-z\rho/\Lambda_f} \quad (\text{Eq. 4.3})$$

where P_{s1} and P_{s2} are constants related to production by slow muons (0.096 and 0.21 for ^{10}Be), P_f is a constant related to production by fast muons (0.026 for ^{10}Be), and Λ_{s1} , Λ_{s2} , and Λ_f are mass attenuation lengths (738, 2688, 4360 $\text{g}\cdot\text{cm}^{-2}$) (Granger and Muzikar, 2001; Granger and Smith, 2000).

One source of uncertainty introduced by sampling surface tills is that surface cryoturbation (meaning post-glacial frost churning), which only affects the portions of the measured TCN signal produced after deglaciation. Surface cryoturbation is a more significant uncertainty in long-distance tills in which the post-glacial TCN contribution is the major portion of the total TCN and a smaller source of uncertainty in short-distance tills that should contain a larger inherited contribution. The sampling depth was an average of 30 cm. In all cases, the N_{post} and N_{meas} were corrected for the sampling depth. Cryoturbation depths are typically 30 cm on Baffin Island, but can range from 0 to 90 cm below the surface (Bockheim and Tarnocai, 1998). Because of this cryoturbation uncertainty and uncertainties stemming from post-glacial erosion and shielding by Holocene snow cover, till matrices cannot be used for TCN exposure dating of till blankets or moraines. The magnitude of the difference in the till TCN concentrations from warm-based ice versus cold-based ice still must be greater than these uncertainties.

Radioactive TCN, such as ^{26}Al ($t_{1/2}=0.7$ Ma) and ^{10}Be ($t_{1/2}=1.5$ Ma), can be lost not only by erosion of the surface that concentrates the TCN, but also by decay. Such decay is particularly evident when glacier ice shields the regolith from cosmic radiation because shielding halts TCN production. Therefore, regolith that has been overridden by glacier ice may have lost TCN to both glacial erosion and burial/decay effects. The use of two radionuclides with different half-lives (e.g. ^{10}Be and ^{26}Al) may be used to determine

the discrepancy between the two concentrations once the differences in production rates are accounted for (Nishiizumi et al., 1989). This discrepancy is directly related to how long the material was buried and related to the initial concentration. In this way, we are able to decipher complex erosion and preservation histories with only a sample of quartz from till. This history can be resolved by using a ratio of two isotopes with differences in decay rates. The ratio of the concentration of the short-lived isotope to that of the long-lived isotope will be lower than the production ratio in a surface that experienced a complete or partial burial. In the case of burial, the ^{26}Al decays faster than the ^{10}Be and the $^{26}\text{Al}/^{10}\text{Be}$ ratio decreases. Cryoturbation at the surface does not affect the ratio because $^{26}\text{Al}/^{10}\text{Be}$ is almost invariant at depths on the 1-10 meter scale. Decay of cosmogenic radionuclides can also better constrain the theoretical maximum N_{max} possible in any area, which may be greater than the greatest measured sample. The theoretical limit of N_{max} is the equilibrium concentration of ^{10}Be and ^{26}Al , which is an eventual balance of TCN production and decay after exceptionally long exposure at a given erosion rate.

4.6 RESULTS

TCN measured concentrations for the till samples are given in Table 4.1. The ^{10}Be AMS measurements attained at least 4% precision at $1-\sigma$. The ^{26}Al AMS measurements have better than 5% precision at 1σ except for measurements on the extremely low ^{26}Al concentrations. The ^{26}Al measurements have an additional uncertainty associated with the measurement of native Al concentration by ICP-AES.

ICP-AES measurements on Aluminum have a coefficient of variation that is typically <1%. The reported uncertainty for TCN measurements reflects random Poisson errors. Normalized concentrations in Table 4.1 are scaled according to Lal (1991, his table 2) and modified according to Stone (2000) using new values for the muogenic TCN contribution and a sea-level, high latitude (SLHL) production rate of $5.1 \text{ }^{10}\text{Be atoms g}^{-1}\text{ a}^{-1}$ (Gosse and Stone, 2001) and a $^{26}\text{Al}/^{10}\text{Be}$ production ratio of 5.94 (Gosse et al., 1996).

4.7 DISCUSSION

^{10}Be and ^{26}Al concentrations (Fig. 4.4 and Table 4.1) are largely consistent with deposition by erosive and non-erosive ice, which suggests a link of TCN to basal thermal regime. Samples that were classified to have been deposited by non-erosive ice have high TCN concentrations (Fig. 4.4). Samples from warm-basal zones have low TCN concentrations. In most instances, the TCN concentrations in samples classified as warm-based tills are equal to the post-glacial exposure with the related Holocene snow cover and erosion uncertainties and indicate negligible presence of the inherited TCN preserved in the tills classified as cold-based. We can also use the $^{26}\text{Al}/^{10}\text{Be}$ ratio to further distinguish tills with more complicated exposure histories from cases with simple exposures that lack any inheritance of pre-glacial TCN. The samples classified as warm-based have a $^{26}\text{Al}/^{10}\text{Be}$ 1- σ error ellipse that spans the production ratio of 5.94 (Fig. 4.7) consistent with a single, uncomplicated exposure history since deglaciation.

Unlike the till derived from warm-based ice, $^{26}\text{Al}/^{10}\text{Be}$ of samples classified as cold-based plot within the burial field (Fig. 4.7). Note that in order to plot below the

steady exposure line, the surface must have been exposed at least once prior to a shielding event. In the most extreme case, the ratio in short distance tills represent a minimum of 800 ka of exposure followed by one or more burial episodes, presumably by cold-based ice, for a minimum of 3 Ma. Samples predicted to have been deposited by non-erosive ice have a complex and long exposure history despite being recently deglaciated (4-9 ka). Samples predicted to have been deposited by non-erosive ice but that contain low ^{10}Be also plot below the $^{26}\text{Al}/^{10}\text{Be}$ production ratio. Assuming there is no chemical error that would cause a decreased ^{26}Al concentration, two possibilities exist for this $^{26}\text{Al}/^{10}\text{Be}$ ratio. The first possibility is that these samples represent tills with an initially small inherited TCN, but then were covered by cold-based ice for a minimum of 800 ka. The alternative possibility is that the samples had been exposed for >2 Ma followed by plucking of the top >3 m (Macciaroli et al., 1994).

The interpretations of the TCN results are based on fundamental tenets of glaciology that would require non-erosive ice on plateau interfluves at high elevations compared to erosive ice overriding deep, constricted valleys (Sugden, 1978; Paterson, 1994). We have attributed the trend in elevation and TCN concentration (Fig. 4.8b) to the preservation of pre-glacial inheritance under thin, largely non-erosive, cold-based ice. However, four of the warm-based tills with low TCN concentrations were sampled from high elevations. In some areas beneath an ice sheet, even high elevation sites can experience basal sliding depending on the thickness of the ice.

Areas that experiences ice cover by both cold-based ice and warm-based ice at different times can contain palimpsest forms or relict warm-based depositional features that can be difficult to interpret (Kleman et al., 1994). Interpreting TCN in tills is also

best done considering that even samples that have low inherited signals may be reflecting warm-based conditions during only part of a glaciation. This last case bears on the interpretation of three tills classified as intermediate tills. In the field, these sites appeared consistent with high elevation cold-based zones, but the clast lithologies that were smaller than the cobbles were more consistent with warm-based, far-traveled tills, possibly indicating a previous warm-based phase. The $^{26}\text{Al}/^{10}\text{Be}$ ratio also confirms that two of these intermediate samples were not warm-based or cold-based end members. Hence, TCN is a very useful tool for addressing the thermal conditions over time, especially when coupled with geomorphology, till sedimentology and clast lithological data.

4.7.1 ICE SHEET MODEL TESTS

One strategy for addressing these temporal and spatial variations in basal thermal regime described in the previous section is to simulate ice flow over a 100 ka period to assess how temperature distribution within the ice sheet reacts to time-dependant climate change, geothermal heat insulation and the latent heat of melting and freezing. These simulated basal thermal conditions can be used to elucidate the role of thermal regime in glacial erosion and transport and assess the possibility of relict surface exposure remnants on the margin of present-day cold-based ice caps.

We use University of Maine Ice Sheet Model (UMISM), a finite-element time-dependent ice sheet model (Fastook and Chapman, 1989, and Fastook, 1994) with a coupled basal water calculation (Johnson and Fastook, 2002) to simulate the ice

dynamics in the study area over the last 100 ka. The bed topography is from a gridded inset ETOPO2 dataset, with coarser resolution topography for the larger LIS simulation that forms the ice flux boundary conditions for the inset model. A finer resolution is not supported by the assumptions in the shallow ice approximation, which only applies to ice masses of a small aspect ratio (ice thickness divided by the horizontal extension). The long-term paleoclimate was controlled by the $\delta^{18}\text{O}$ curve from the GRIP ice core, central Greenland, transformed to a temperature record (Johnsen et al., 1995). The mean annual temperature for each node varies by specified altitudinal and latitudinal lapse rates. The temperature calculation is used to determine the positive degree days, which is assumed to be proportional to ablation. Accumulation is calculated from temperature. A finite-element solver is coupled with a mass-balance solver to generate internal ice temperatures and accounts for diffusion, vertical advection, and shear heating. Formulation of the hydrology model is summarized in Johnson and Fastook (2002) and in Appendix 5.

To investigate the importance of external boundary conditions and the sliding formula, a series of sensitivity tests and EISMINT (European Ice Sheet Modelling INiTiavite) ice sheet model intercomparisons were conducted and reported in Johnson (2002) and Huybrechts et al. (1995, 1996). EISMINT considered applications to the Greenland and Antarctic ice sheets, the only extant terrestrial analogs for the LIS. This battery of tests was particularly important for assessing the results of UMISM on these areas where characteristics of the ice dynamics can be checked. Although the basal water model can reproduce the spatial pattern and velocities of West Antarctic ice streams (Johnson, 2002) and can reproduce and predict the presence of Antarctic large sub-glacial

lakes (Johnson, 2002), there are some limitations to this model. Horizontal heat advection is not calculated, but should not be a large contribution to the basal heat in areas of slow-moving ice on Baffin Island. Another limitation is the difference in temporal and spatial scales between the water model and the ice sheet model. The spatial scale issue also prohibits any attempt to link TCN derived of subglacial thermal regimes on an outcrop scale to the dynamic behavior of basal water and ice on the coarse topographic scale.

Surfaces on the northern and eastern margins of the map sheet record the most variation in basal melt production and the number of thawed to frozen basal cycles from high elevation sites to low elevation sites (Fig. 4.9). Large variations over short distances are not completely resolved in the model compared to the TCN variations in field sites over similarly short distances. The northeast corner of the Ice Bound Lakes region has always experienced persistent frozen bed conditions with negligible basal transport potential in the model and is consistent with the highest TCN concentrations. On the other hand, many of the tills with low TCN concentrations have experienced one or more cycles of basal freezing of previously thawed basal water. One of the most striking features of the model simulations was the stark contrast between warm-based and cold-based ice near the northeastern margin that is proximal to the coast, while the inland area basal ice experienced few switches from melted bed to frozen bed conditions. The model simulation output of basal melt production (Fig. 4.9b) does reproduce positive basal melt production over the high elevation warm-based till site as the TCN concentration would predict.

The study area has deposition potential during ice retreat phases either by surface ice sublimation or melt production at the base or surface of the ice. However, if the

overriding LGM ice deposited a significant portion of till derived from deeply eroded areas and containing low inherited TCN, the $^{26}\text{Al}/^{10}\text{Be}$ ratios of the upland till samples would be closer to the $^{26}\text{Al}/^{10}\text{Be}$ production ratio and would have a lower total TCN concentration. High TCN concentrations are consistent with little interaction with the cold-based ice cap and any far-traveled ice was probably funneled through the constricted valleys and fiords.

4.7.2 SHORT AND LONG TILL TRANSPORT DISTANCES

The interpretation of boulder trains and geochemical anomalies in till has had, and still has, important implications for the mineral exploration in glaciated areas. Though these indicators of dispersal distance can be crucial to finding source rocks or kimberlite zones, transport distance depends on transport velocity, transport duration, erosion rate and in the case where flows may overlap, flow direction and timing of transport (Puranen, 1988). Substrate lithology plays some role in the erosion rate and in the differences in observed inheritance preservation due to different resistance to erosion and in the renewal distance of till dispersion (Dremanis and Vagners, 1969; Clark, 1987).

Past studies have shown that rock or substrate strength has an impact on differences in enlargement and widening of glacial valleys in alpine settings (Harbor et al., 1995; Augustinus, 1992). Colgan et al. (2002) found that Wisconsin bedrock that had been overridden by Laurentide ice contained greater residual inherited ^{10}Be with increasing rock compressive strength. Their results showed a greater correlation with

bedrock lithology than with distance from the ice margin, which they used as a proxy for basal thermal regime and erosivity.

However, in our study where both cold-based and warm-based sample predictions often lie within the same bedrock unit, there is neither correlation with ^{10}Be concentration and underlying bedrock lithology (corr. coeff. <0.4) nor correlation between ^{10}Be and clast lithology (corr. coeff. <0.3). The TCN concentrations correlate (corr. coeff. 0.6) with the percentage of exotic clasts that are not of the same lithology as the underlying bedrock. The lithologies within the lowest ^{10}Be concentrations are the most cosmopolitan; highest ^{10}Be concentrations have lower percentage of exotic clasts (Fig 4.8a). This relationship is consistent with a prediction that slow moving, non-erosive local ice will preserve an inherited TCN signal. Clasts that have the lowest ^{10}Be concentrations are consistent with the idea of fast-moving, erosive ice eroding to greater depths. Tills that were predicted to be deposited by warm-based ice that had low TCN concentrations were not within more-friable bedrock, but contain greater percentages of exotic clasts, implying greater transport distances.

4.7.3 DEPTH OF GLACIAL EROSION

We use equation 4.1 and 4.2 to calculate the thickness of material that has been removed from a pre-Quaternary surface exposure. Average wet bulk densities for these tills is assumed to be $2.2 \text{ g}\cdot\text{cm}^{-3}$, which is appropriate given that the wet bulk density of sand is $2.13 \pm 0.16 \text{ g}\cdot\text{cm}^{-3}$ and the wet bulk density of clay-rich till is $2.24 \pm 0.07 \text{ g}\cdot\text{cm}^{-3}$ (Balco, 2004). The samples have probably been nearly water saturated since deglaciation

as is common for mud or frost boils (Shilts, 1978). We combined the uncertainty in the depth calculation owing to a range of possible densities (3%) with the ^{10}Be AMS precision (2-4%) to calculate the total uncertainty for the thickness calculation in Table 4.1. Although Eq. 4.1 and 4.2 neglect the contribution of muogenic TCN production, Eq. 4.3 was used in concert with Eq. 4.1 and 4.2 to include muogenic production in the reported thicknesses in Table 4.1.

Other unknown variables needed to calculate the thickness eroded using Equations. 4.1 and 4.2 include N_{post} and N_{max} . In order to bound the range for N_{post} , we use the lowest concentration for any warm-based ice deposit. This estimate can be interpreted as an age of ~ 4 ka using a production rate that integrates over the ca. 30 cm sampling thickness. This estimate could be >1 ka less than the estimated minimum age of deglaciation for this area based on Dyke et al. (2003) regional deglaciation isochrons (See Fig. 4.2). Although lower than the regional-scale deglaciation timing would predict, we feel this lowest TCN concentration is appropriate as an estimate of the post-glacial TCN contribution because away from the Cockburn moraine system, high-resolution deglaciation timing is poorly constrained. However, >1 ka of exposure discrepancy could be explained by post-glacial erosion, Holocene snow cover or widespread Little Ice Age (LIA) ice.

In order to bound the range for N_{max} , we use the largest value of inheritance as the initial concentration N_{max} in the study area, scaled for the production rate at each till sample's elevation (Table 4.1). As stated above in the methodology section, the largest possible TCN concentration at the top of a pre-Quaternary production profile is the concentration representing secular equilibrium between decay and production, not the

largest measured concentration. The time necessary to reach secular equilibrium and the maximum concentration of secular equilibrium is dependant on the erosion rate of the surface (Fig. 10). For the till sample with the largest measured concentration corrected for burial (Table 4.1, Fig. 4.4), the maximum possible erosion rate prior to burial could have been up to 0.4 m/Ma. At this erosion rate, the TCN had reached secular equilibrium; at lower erosion rates, it had not yet reached secular equilibrium. This erosion rate assumes that the surface has experienced only one episode of glacial cover. For multiple periods of glacial cover, the maximum possible erosion rate would have been higher because the TCN production was increased, the TCN decay was decreased. However, multiple burial episodes would require total burial time to extend through the Pliocene climatic optimum. An erosion rate significantly lower than 0.4 m/Ma is improbable because this erosion rate is lower than in all landscapes but the driest (Summerfield et al. 1999; Dunai et al., 2005). If 0.4 m/Ma is the maximum erosion rate on the high elevation surface, areas at lower elevations may have had higher erosion rates prior to burial or may have complicated depositional sequences instead of a simple ^{10}Be profile. Therefore, this thickness calculation is most applicable to determine the maximum thickness removed for the cold-based samples and the high elevation warm-based sample and only these cases are given in Table 4.1.

4.8 CONCLUSIONS

^{10}Be in sand-sized particles of quartz extracted from 19 till sample matrices was used to mark the change in basal thermal regime in overriding paleo-ice. This new

technique for assessing glacial erosion uses till matrix TCN inheritance to average the inheritance values in the till samples by analyzing thousands of sand grains (amalgamated) as if they were individual clasts at each site to reduce the range of variability possible for a given sample. If the glacial history of a region is well known, the inherited TCN signal can be used as an indicator of cold-based ice over a landscape.

High inherited TCN concentrations in tills that originate from pre-glacial exposure were used to understand sub-glacial preservation. Tills with textural characteristics of cold-based ice deposits sometimes had TCN concentrations of 2-50 times greater than tills with textural characteristics of warm-based, erosive ice. Cold-based tills had lower concentrations of exotic lithologies that attest to short transport distances of these tills. Till samples found on the margin of small cold-based ice caps indicate that some of these samples have been buried by cold-based ice for a minimum of millions of years following an initial period of exposure. Tills that were predicted to have been deposited from warm-based ice consistently had a ^{10}Be inventory of less than 10^5 $\text{at}\cdot\text{g}^{-1}$ and contained negligible inheritance based on the $^{26}\text{Al}/^{10}\text{Be}$ ratio. Tills with low TCN concentrations had larger percentages of clasts of exotic lithologies that indicate greater till transport distances. TCN concentrations used in conjunction with till sedimentology, and exotic clast lithology and can be used to decipher till transport distances and complex exposure histories.

4.9 ACKNOWLEDGEMENTS

For discussions and support in the field, we thank Art Dyke, Andrew Hilchey, Mike Young, and Phil Holme. G. Yang's and E. Willenbring's help in the laboratory is greatly appreciated. Helicopter support was provided by Custom Helicopters Ltd. We thank Gary Fisher (Tailored Polymers Group at DRDC) and Gwen MacPherson (U. Kansas) for ICP-AES analyses. Funding for this project was provided by the ACOA Atlantic Innovation Fund 1001052 and NSERC Discover Grant to JCG, and Canada–Nunavut Geoscience Office (Project 040001) and the Polar Continental Shelf Project (03-2) support to ECL. JWS acknowledges the Izaak Walton Killam Foundation for a pre-doctoral fellowship.

4.10 REFERENCES

- Alley R. B., Lawson D. E., Larson G. J., Evenson E. B., Baker G. S. 2003. Stabilizing feedbacks in glacier-bed erosion. *Nature* **424**(6950): 758-760.
- Andrews, J. T., Davis, P.T., Locke, C., 1976, Little Ice Age permanent snowcover in the eastern Canadian Arctic—Extent mapped from Landsat-1 satellite imagery: *Geografiska Annaler* **58A**(1–2): 71–81.
- Andrews, J.T., Kirby, M.E., Aksu, A., Barber, D.C., Meese, D. 1998. Late Quaternary detrital carbonate (DC-) layers in Baffin Bay marine sediments (67 degrees-74 degrees N); correlation with Heinrich events in the North Atlantic. *Quaternary Science Reviews* **17**(12): 1125-1137.

- Augustinus, P.C. 1992. The influence of rock mass strength on glacial valley cross-valley profile morphometry: A case study from the Southern Alps, New Zealand. *Earth Surface Processes and Landforms* **17**: 39-51.
- Balco, G. 2004. *The sedimentary record of subglacial erosion beneath the Laurentide Ice Sheet*. Unpublished Ph.D. thesis, University of Washington. 153 pp.
- Bierman, P. R., Marsella, K. A., Patterson, C., Davis, P. T., Caffee, M. 1999. Mid-Pleistocene cosmogenic minimum-age limits for pre-Wisconsin glacial surfaces in southwestern Minnesota and southern Baffin Island: a multiple nuclide approach. *Geomorphology* **27**: 25–39.
- Bierman, P. R., Marsella, K. A., Davis, P. T., and Caffee, M. W. 2001. Response to Discussion by Wolfe et al. on Bierman et al. (*Geomorphology* **27** (1999) 25–39). *Geomorphology*, **39**: 255–260
- Bockheim, J. G. 1979: Properties and relative ages of soils of southwestern Cumberland Peninsula, Baffin Island, N.W.T., Canada; *Arctic and Alpine Research* **11**: 289-304.
- Bockheim, J. G., Tarnocai, C.. 1998. Recognition of cryoturbation for classifying permafrost-affected soils. *Geoderma* **81**: 281–293.

- Boulton, G. S. 1972. The role of thermal regime in glacial sedimentation. *in*: Price, R. J. and Sugden, D. E. (eds), *Polar Geomorphology*, 1–19. Special Publication No. 4, Institute of British Geographers, London.
- Briner, J., Swanson, T. 1998: Using inherited cosmogenic ^{36}Cl to constrain glacial erosion rates of the Cordilleran ice sheet. *Geology* **26**(1): 3-6.
- Briner, J. P., Miller, G. H., Davis, P. T., Bierman, P. R., Caffee, M. 2003: Last Glacial Maximum ice sheet dynamics in Arctic Canada inferred from young erratics perched on ancient tors. *Quaternary Science Reviews* **22**: 437-444.
- Briner, J. P., Miller, G. H., Davis, P. T., Finkel, R. C. 2005. Cosmogenic exposure dating in arctic glacial landscapes: implications for the glacial history of northeastern Baffin Island, Arctic Canada. *Canadian Journal of Earth Sciences* **42**: 67-84.
- Briner, J. P., Kaufman, D. S., Manley, W. F., Finkel, R. C., Caffee, M. W. 2005. Cosmogenic exposure dating of late Pleistocene moraine stabilization in Alaska. *Geological Society of America Bulletin* **117**: 1108-1120.
- Cerling, T. E., Craig, H. 1994. Geomorphology and in situ cosmogenic isotopes. *Annual Reviews of Earth and Planetary Science* **22**: 273-317.

- Clark, P. U., 1987. Subglacial sediment dispersal and till composition. *Journal of Geology* **95**, 527–541.
- Colgan, P. M., Bierman, P. R., Mickelson, D. M., Caffee, M. 2002. Variation in glacial erosion near the southern margin of the Laurentide Ice Sheet, south-central Wisconsin, USA: Implications for cosmogenic dating of glacial terrains. *Geological Society of America Bulletin* **114**(12): 1581-1591.
- Davis, P. T., Bierman, P. R., Marsella, K. A., Caffee, M. W., Southton, J. R., 1999, Cosmogenic analysis of glacial terrains in the eastern Canadian Arctic: A test for inherited nuclides and the effectiveness of glacial erosion. *Annals of Glaciology* **28**: 181–188.
- Davis, P. T., Briner, J. P., Miller, G. H., Coulthard, R. D., Bierman, P., Finkel, R. W. 2002. Huge >54,000 yr old glaciomarine delta on northern Baffin Island overlain by boulders with <20,000 yr old cosmogenic exposure ages: implications for non-erosive cold-based ice on Baffin Island during the LGM. *Geological Society of America Annual Meeting* (October 27-30, 2002) Denver Colorado.
- Dreimanis, A. and Vagners, U. J. 1969. Lithologic relation of till to bedrock, in Wright, H. E., Jr., ed. *Quaternary Geology and Climate*: Washington, National Academy of Sciences: 93-98.

- Dunai, T. J., Lopez, G. A. G., Juez-Larre, J. 2005. Oligocene-Miocene age of aridity in the Atacama Desert revealed by exposure dating of erosion-sensitive landforms. *Geology* 33(4): 321 - 324.
- Dyke, A. S. 1993. Landscapes of cold-centred Late Wisconsinan ice caps, Arctic Canada. *Progress in Physical Geography* 17: 223-247.
- Dyke, A. S. 1999. Last glacial maximum and deglaciation Devon Island, arctic Canada: Support for an Innuitian Ice Sheet. *Quaternary Science Reviews* 18: 393–420.
- Dyke, A. S., Hopper, J. M. G. 2001: Deglaciation of northwest Baffin Island, Nunavut, Geological Survey of Canada, A-Series Map 1999A, scale 1:500,000.
- Dyke, A. S., Prest, V. K. 1987. Late Wisconsin and Holocene history of the Laurentide Ice Sheet. *Géographie physique et Quaternaire* 41: 237–263.
- Dyke, A. S., Andrews, J. T., Clark, P. U., England, J. H., Miller, G. H., Shaw, J., Veillette, J. J. 2002. The Laurentide and Innuitian Ice Sheets during the Last Glacial Maximum. *Quaternary Science Reviews* 21: 9–31.
- Dyke, A. S., Moore, A., Robertson, L. 2003: Deglaciation of North America. Geological Survey of Canada, Open File 1574. Thirty-two maps at 1:7,000,000 scale with

accompanying digital chronological database and one poster (in two sheets) with full map series.

England, J. 1987. Glaciation and the evolution of the Canadian high arctic landscape.

Geology **15**: 419-424.

England, J. 1996. Glacier dynamics and paleoclimatic change during the last glaciation of eastern Ellesmere Island, Canada. *Canadian Journal of Earth Sciences* **33**: 779–799.

England, J. 1998. Support of the Innuitian Ice Sheet in the Canadian High Arctic during the Last Glacial Maximum. *Journal of Quaternary Science* **13**: 275–280.

England, J. 1999. Coalescent Greenland and Innuitian ice during the Last Glacial Maximum: Revisiting the Quaternary of the Canadian High Arctic. *Quaternary Science Reviews* **18**: 421–456.

Fabel D., Stroeven, A. P., Harbor, J., Kleman J., Elmore, D., Fink, D. 2002. Landscape preservation under Fennoscandian ice sheets determined from in situ produced ^{10}Be and ^{26}Al . *Earth and Planetary Science Letters* **201**: 397-406.

Falconer, G., Ives, J. D., Løken, O. H., Andrews, J. T. 1965. Major end moraines in eastern and central arctic Canada. *Geographic Bulletin* **7**(2): 137-153.

Gosse, J. C., Phillips, F. M. 2001: Terrestrial in situ cosmogenic nuclides: Theory and applications. *Quaternary Science Reviews* **20**: 1475-1560.

Gosse, J. C., Stone, J. O. 2001. Terrestrial cosmogenic nuclide methods passing milestones toward paleo-altimetry. *Eos (Transactions, American Geophysical Union)*: **82**: 82, 86, 89.

Gosse, J., Klein, J., 1996. Production rate of in situ cosmogenic ^{10}Be in quartz at high altitude and mid-latitude. *Radiocarbon* **38** (1): 154-155.

Granger, D. E., Muzikar, P. F. 2001. Dating sediment burial with in situ-produced cosmogenic nuclides: theory, techniques, and limitations. *Earth and Planetary Science Letters* **188(1-2)**: 269-281.

Granger, D. E., Smith, A. L., 2000. Dating buried sediments using radioactive decay and muogenic production of ^{26}Al and ^{10}Be . *Nuclear Instruments and Methods in Physics Research B* **172(1-4)**: 822-826.

Hallet, B. 1979. A theoretical model of glacial abrasion. *Journal of Glaciology* **23(89)**: 39-50.

Hallet, B. 1996. Glacial quarrying; a simple theoretical model. *Annals of Glaciology* **22**: 1-8.

Harbor, J. M. 1995. Development of glacial-valley cross sections under conditions of spatially variable resistance to erosion; glacial geomorphology; process and form development. *Geomorphology* **14**(2): 99-107.

Hilchey, A. 2004. Holocene Deglacial Geologic History of the Ravn River Valley, Northern Baffin Island, Nunavut. Honours thesis, Dalhousie University, Halifax. 99 pp.

Hodgson, D. A., Haselton, G. M. 1974. Reconnaissance glacial geology, northeastern Baffin Island. *Geological Survey of Canada Paper* **74-20**: 1-10.

Hooyer, T. S., Iverson, N. R. 2000. Diffusive mixing between shearing granular layers: constraints on bed deformation from till contacts. *Journal of Glaciology* **46**: 641–651.

Huybrechts, P., Payne, T., Abe-Ouchi, A., Calov, R., Fastook, J., Greve, R., Hindmarsh, R., Hoydal, O., Johannesson, T., MacAyeal, D., Marsiat, I., Ritz, C., Verbitsky, M., Waddington, E., Warner, R. 1995. The EISMINT benchmarks for testing ice-sheet models. In *Annals of Glaciology Volume 23*, Chamonix, France. IGS/EISMINT International Conference on Ice Sheet Modelling.

- Huybrechts, P., Payne, T., Abe-Ouchi, A., Calov, R., Fabre, A., Fastook, J., Greve, R., Hindmarsh, R., Hoydal, O., Johannesson, T., MacAyeal, D., Marsiat, I., Ritz, C., Verbitsky, M., Waddington, E., Warner, R. 1996. The EISMINT benchmarks for testing ice-sheet models. *Annals of Glaciology* **23**:1–12.
- Ives, J. D., Andrews, J. T. 1963: Studies in the physical geography of north-central Baffin Island, N.W.T.. *Geographical Bulletin* **19**: 5-48.
- Ives, J. D. 1978. The maximum extent of the Laurentide Ice Sheet along the east coast of North America during the last glaciation. *Arctic* **31**: 24–53.
- Jennings, A. E., Tedesco, K. A., Andrews, J. T., Kirby, M. E. 1996: Shelf erosion and glacial ice proximity in the Labrador Sea during and after Heinrich events (H-3 or H-4 to H-0) as shown in foraminifera; in Andrews et al. eds., Late Quaternary Paleooceanography of the North Atlantic Margins: *Geological Society of America Special Publication* **111**: 29-49.
- Johnsen, S., Dahl-Jensen, D., Dansgaard, W., Gunderup, N. 1995. Greenland paleotemperatures derived from GRIP bore hole temperature and ice core isotope profiles. *Tellus* **47B**: 624-629.

Johnson, J. V., Fastook, J. L. 2002. Northern Hemisphere glaciation and its sensitivity to basal melt water. *Quaternary International* **95-96**: 87-98.

Johnson, J. V. 2002. A basal water model for ice sheets. Ph.D. thesis, University of Maine, Orono. 187 pp.

Kaplan, M. R., Miller, G. H., Steig, E. J. 2001. Low-gradient outlet glaciers (ice streams?) drained the northeastern Laurentide Ice Sheet. *Geology* **29**: 343–346.

Klassen, R. 1998. Geological factors affecting the distribution of trace metals in glacial sediments of central Newfoundland. *Environmental Geology* **33**(2-3): 154-169.

Kleman, J. 1994. Preservation of landforms under ice sheets and ice caps. *Geomorphology* **9**: 19–32.

Kurz, M. D., Brook, E. J. 1994: Surface exposure dating with cosmogenic nuclides, in Beck, C., ed., *Dating in exposed and surface contexts*: Albuquerque, University of New Mexico Press, p. 139-159.

Lal, D. 1991: Cosmic ray labeling of erosion surfaces: in situ production rates and erosion models. *Earth and Planetary Science Letters* **104**: 424-439.

- Larsen, N. K., Piotrowski, J. A., Kronborg, C. 2004. A multiproxy study of a basal till: a time-transgressive accretion and deformation hypothesis. *Journal of Quaternary Science* **19**: 9–21.
- Larson, P. C., Moores, H. D. 2004. Glacial indicator dispersal processes: a conceptual model. *Boreas* **33**: 238-249.
- Little, E. C., Holme, P., Hilchey, A., Young, M. 2004. Glacial Geology, Ice- Movement Chronology and Drift Prospecting in the Vicinity of Icebound Lakes (NTS 37G), Northern Baffin Island, Nunavut. Geological Survey of Canada Current Research.
- Little, E. C., Young, M., Utting D. J. 2005. Preliminary bedrock geochemistry and drift prospecting results from the North Baffin Project (NTS 37F, 37G, 47E), Northern Baffin Island, Nunavut. Geological Survey of Canada Open File Report.
- Macciaroli P, Giegengack R, Klein J, Middleton R, Lawn B. 1994. Late Quaternary glaciation of exposed rock surfaces along a ridge of the Appalachian Mountains, dated using ^{26}Al and ^{10}Be produced in situ. *Geological Society of America. Abstracts with Programs* **26**: A-125.
- Mäkinen, J. 2003. A mathematical model to explain the effect of comminution, re-sedimentation and outwashing on the finest fractions of till in four test areas in

central Finland, in Räisänen, M.L. and Nikkarinen, M. eds., Complexity of glacial dispersal and hydromorphic processes in till geochemistry, *Geological Survey of Finland, Special Paper 34*: 43-69.

Marquette, G. C., Gray, J. T., Gosse, J. C., Courchesne, F., Stockli, L., Macpherson, G., Finkel, R. 2004. Felsenmeer persistence under non-erosive ice in the Torngat and Kaumajet Mountains, Quebec and Labrador, as determined by soil weathering and cosmogenic nuclide exposure dating. *Canadian Journal of Earth Sciences* **41**: 19–38.

Marsella, K. A., Bierman, P. R., Davis, P. T., Caffee, M. W. 2000: Cosmogenic ^{10}Be and ^{26}Al ages for the Last Glacial Maximum, eastern Baffin Island, Arctic Canada. *Geological Society of America* **112**(7): 1296-1312.

Marshall, S. J., Clark, P. U. 2002. Basal temperature evolution of North American ice sheets and implications for the 100-kyr cycle. *Geophysical Research Letters* **29**(24): 2214-2218.

Moores, H. D. 1990. A glacial-process model: The role of spatial and temporal variation in glacier thermal regime. *Geological Society of America Bulletin* **102**(2): 243-251.

- Nishiizumi, K., Winterer, E. L., Kohl, C. P., Klein, J., Middleton, R., Lal, D., Arnold, J. R. 1989. Cosmic ray production rates of ^{10}Be and ^{26}Al in quartz from glacially polished rocks. *Journal of Geophysical Research, B, Solid Earth and Planets* **94**(12): 17 907-17 915.
- Paterson, W. S. B. 1994. The physics of glaciers. Elsevier, New York, N.Y., 480 pp.
- Puranen, R., 1988. Modelling of glacial transport of basal tills in Finland. Report of Investigation 81, Geological Survey of Finland. 36 pp.
- Putkonen, J., Swanson, T. 2003. Accuracy of cosmogenic ages for moraines. *Quaternary Research* **59**: 1-7.
- Shilts, W. W. 1976. Glacial till and mineral exploration. in Legget, R. F. ed. Glacial Till: *Royal Society of Canada Special Publication* **12**: 205-224.
- Shilts, W. W. 1978. Nature and genesis of mudboils, central Keewatin, Canada. *Canadian Journal of Earth Science* **15**: 1053-1068.
- Steig, E. J., Wolfe, A. P., Miller, G. H. 1998: Wisconsinan refugia and the glacial history of eastern Baffin Island, Arctic Canada: coupled evidence from cosmogenic isotopes and lake sediments. *Geology* **26**: 835-838.

- Stone J. O., Balco G. A., Sugden D. E., Caffee M. W., Sass L.C. III, Cowdery S. G., Siddoway, C. 2003. Holocene deglaciation of Marie Byrd Land, West Antarctica. *Science* **299** (5603): 99-102.
- Sugden, D. 1978. Glacial erosion by the Laurentide Ice Sheet. *Journal of Glaciology* **20**: 367–391.
- Sugden, D. E., Balco, G., Cowdery, S. G., Stone, J. O., Sass, L.C. III. 2005. Selective glacial erosion and weathering zones in the coastal mountains of Marie Byrd Land, Antarctica. *Geomorphology* **67**(3-4): 317-334.
- Summerfield, M. A., Stuart, F. M., Cockburn, H. A. P., Sugden, D. E., Denton, G. H., Dunai, T., Marchant, D. R. 1999. Long-term rates of denudation in the Dry Valleys, Transantarctic Mountains, southern Victoria Land, Antarctica based on in-situ-produced cosmogenic ^{21}Ne . *Geomorphology* **27**(1-2):113-129.
- Whipple, K. X., Kirby, E., Brocklehurst, S. H. 1999. Geomorphic limits to climate-induced increases in topographic relief. *Nature* **401**: 39-43.

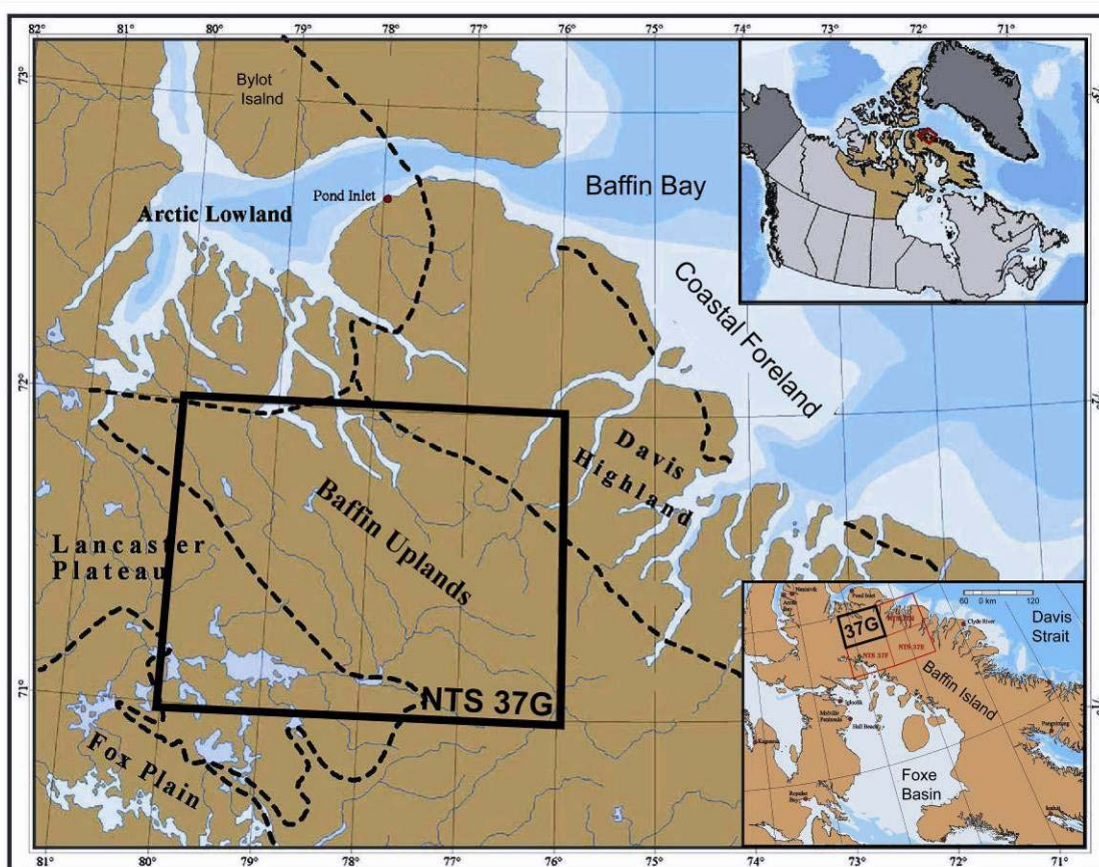


Figure 4.1 Study area in north-central region of Baffin Island, Nunavut. The thick-line box shows the location of NTS sheet 37G “Ice Bound Lakes.” Physiographic zones of Northern Baffin Island. Adapted from Little et al. (2004). Top inset map: location of Baffin Island in relation to Nunavut (shaded), the rest of Canada, Greenland and Alaska. Bottom inset map: Foxe Basin, the location of a proposed paleo-ice dome lies to the south of the study area.

Figure 4.2 Figures are adapted from Dyke et al. (2003). Ice margin positions are based on ice margin indicators and ^{14}C chronologies wherever available. Study area 37G is outlined in the black box. Ice configuration at **a.** ca. 9 ka. Ice is thought to have covered the study area completely from LGM to ca. 9 ka. This configuration is similar to the LGM extent. **b.** Ice configuration at ca. 8 ka. and at **c.** ca. 5 ka. **d.** At ca. 4 ka, the paleo-Barnes Ice Cap may have completely receded to the south of the study area.

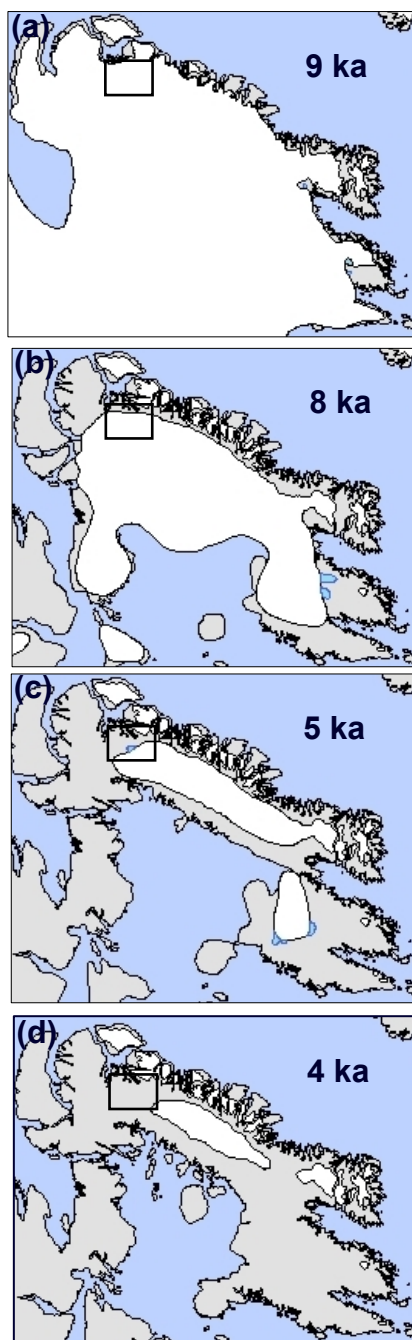


Figure 4.2



Figure 4.3 a. Till sample site from a deposit that was predicted to have been deposited by cold-based non-erosive ice. Note the similarity of clast lithology in this deposit and angular clasts. **b.** Sample pit from a deposit thought to have been entrained originally by warm-based erosive ice. Sample depths in both cases were typically 30 cm deep.

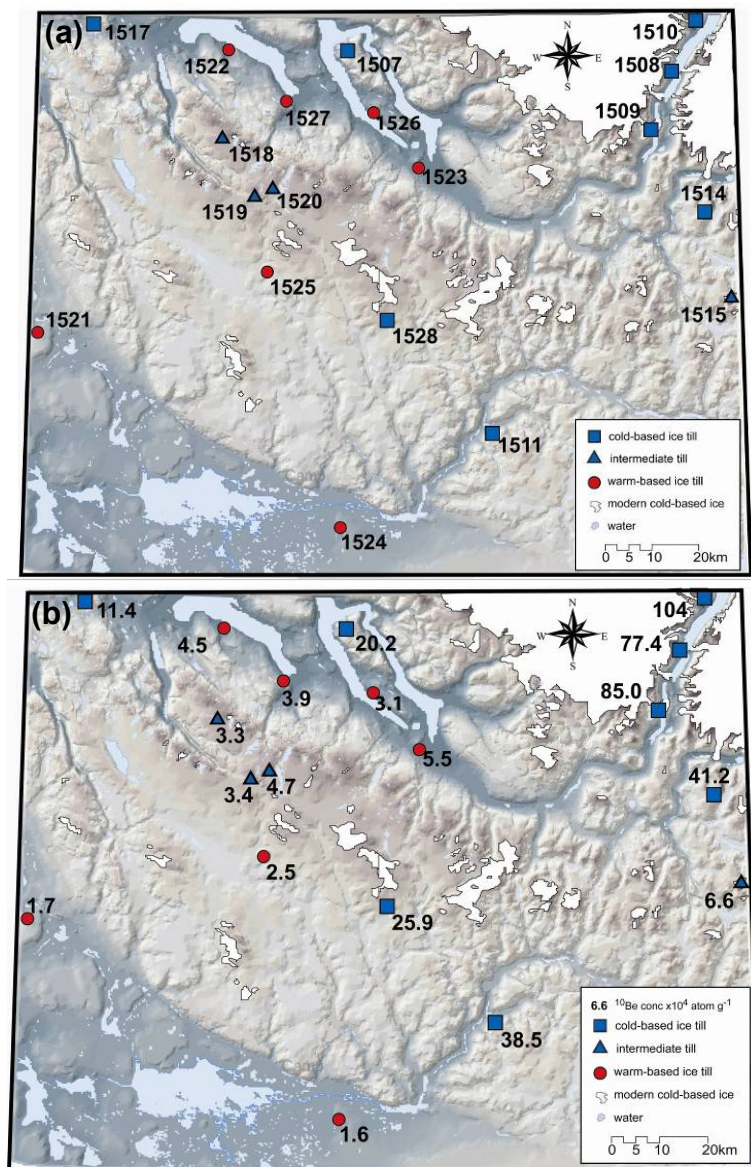


Figure 4.4 a. Map of 37G area showing surface till sites predicted to be deposited by either cold-based (blue) or warm-based (red) ice. **b.** ^{10}Be concentrations in 10^4 atom g^{-1} . Four samples termed intermediate were classified as cold-based tills, but have low ^{10}Be concentrations. Sample symbols (red circles – warm-based; blue squares – cold-based; blue triangles – intermediate) will be used consistently throughout Chapter 4.

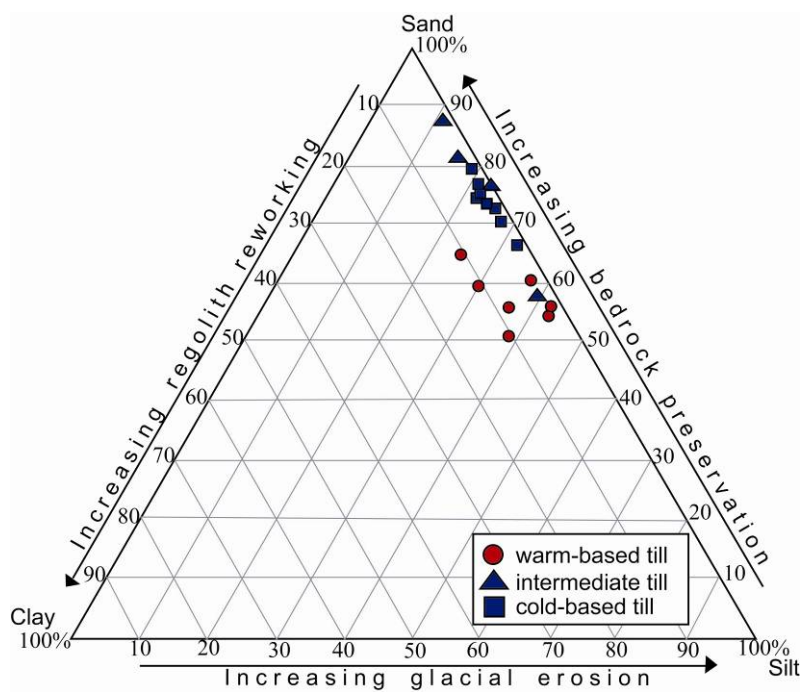


Figure 4.5 Sedimentology of till samples. All of the samples shown on this sediment grain-size ternary diagram can be classified as silty sands. The percentages of clay and silt are probably higher in mudboils than for other nearby areas (Shilts, 1978).

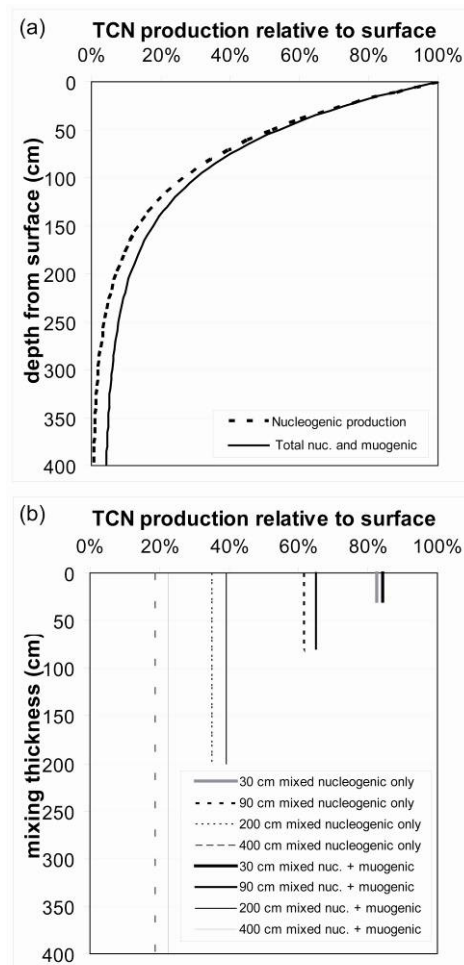


Figure 4.6 a. The dashed line shows the exponential production profile from the surface to 4 m depth for nucleogenic production only. The solid curve shows the decreasing total production with depth. **b.** The dashed lines represent the effect of mixing the in situ produced spallation production profile to a specific thickness. The solid lines represent the effect of mixing the in situ produced total production profile to a specific thickness. In mixed samples, inheritance is distinguishable at a greater depth than in the bedrock profile.

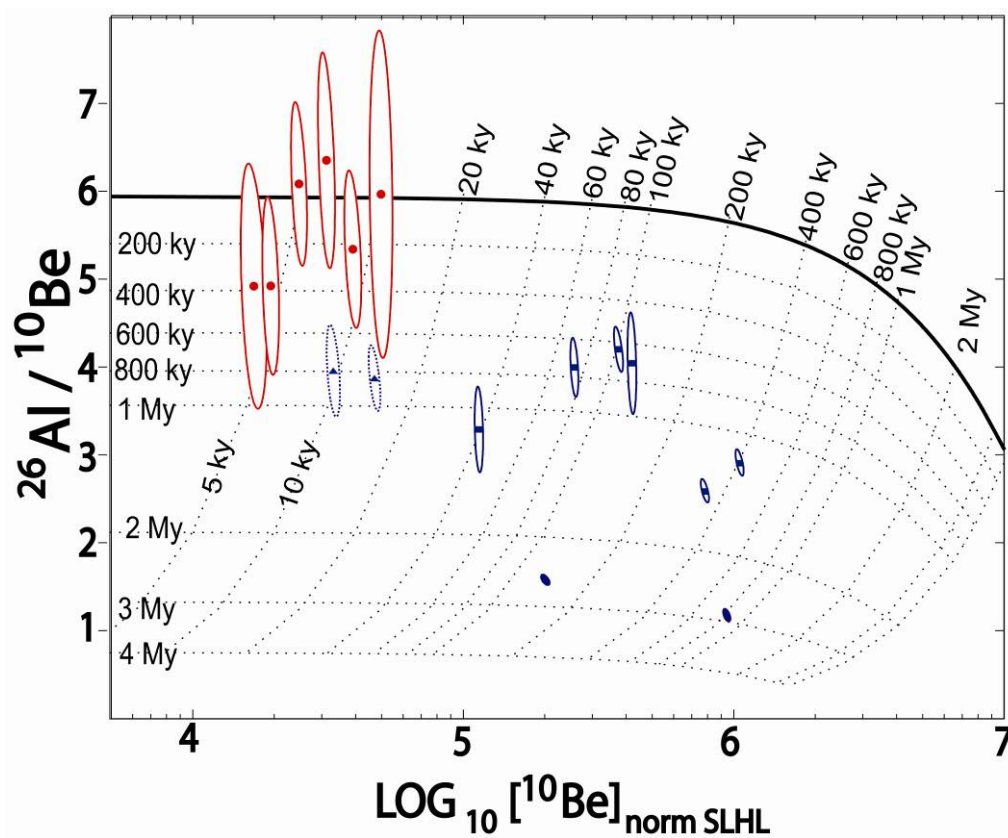


Figure 4.7 Exposure-erosion diagram of $^{26}\text{Al}/^{10}\text{Be}$ vs. $\log^{10}\text{Be}$ normalized for production at sea level high latitude (SLHL). Samples that plot below the lower curve have experienced an interruption in their exposure history, by burial or deep plucking. The uncertainties ellipses reflect 1- σ analytical precision in the AMS measurements.

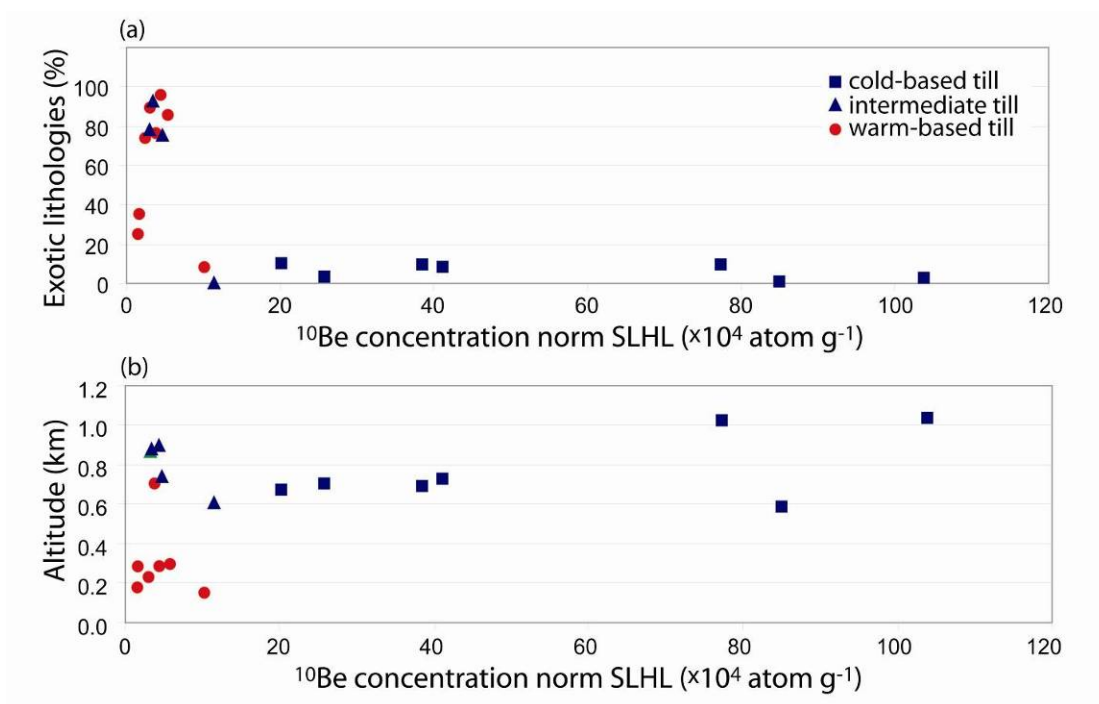


Figure 4.8 a. Plot of ^{10}Be concentrations versus clast exotic lithology. **b.** Plot of ^{10}Be concentration versus sample altitude.

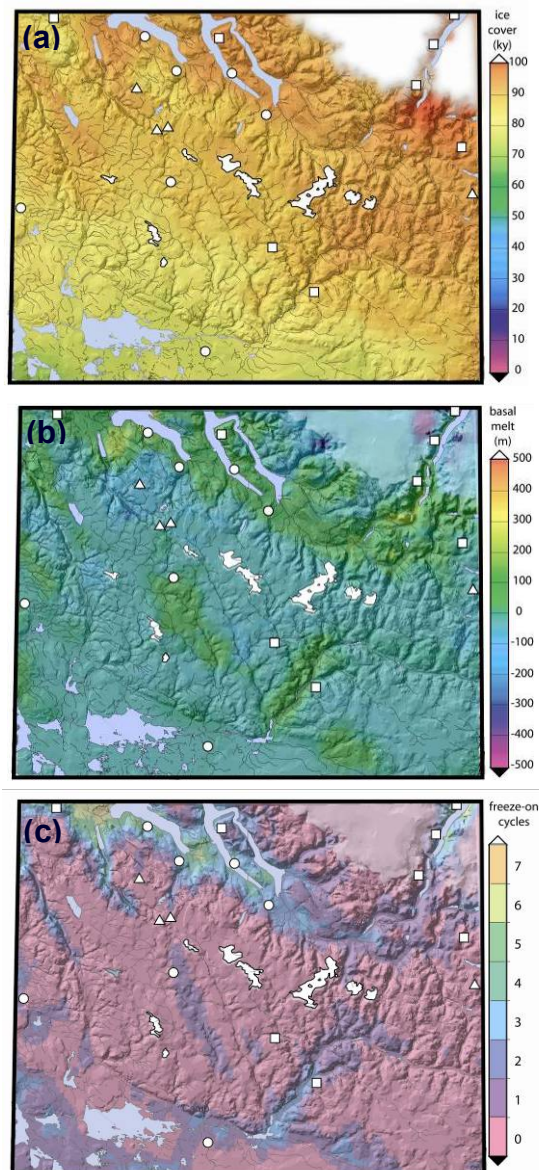


Figure 4.9 **a.** Modeled ice cover in a 100-ka cycle. **b.** Modeled basal melting water production in 100-ka. Basal melt water plot reflects net melt, thus basal freezing decreases the net basal melt. **c.** The number of cycles of freezing during the model simulation. A freezing cycle is defined as a switch from warm-based conditions to cold-based conditions during the next 10-year timestep.

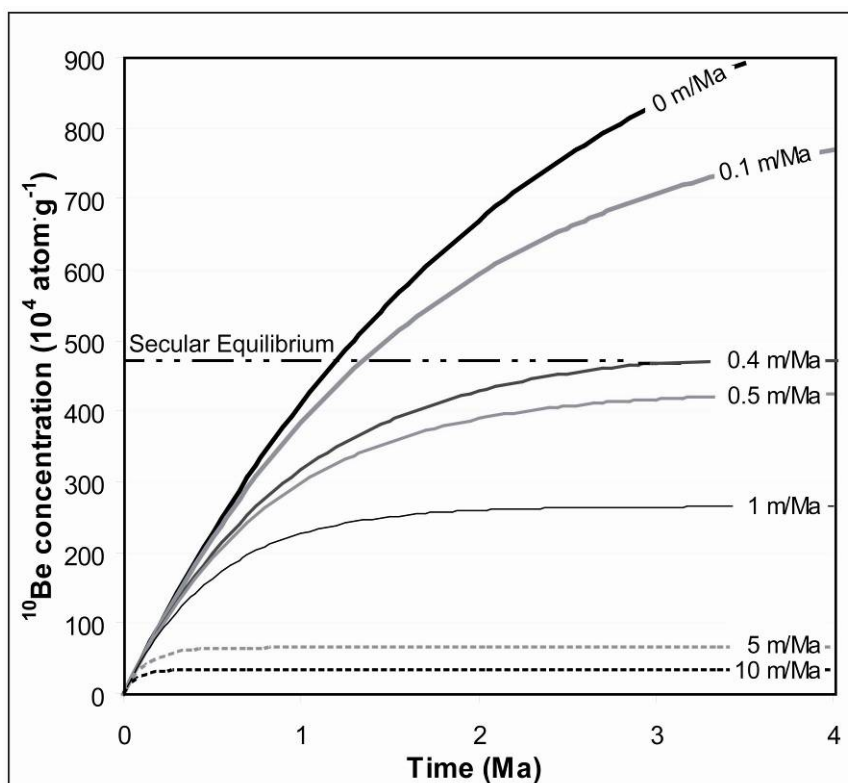


Figure 4.10 Plot illustrates the effect of erosion on the secular equilibrium concentration using a ^{10}Be concentration normalized for SLHL production rate of $5.1 \text{ atom g}^{-1} \text{ a}^{-1}$. The secular equilibrium dashed line marks the concentration of the highest ^{10}Be till sample prior to burial as suggested by the $^{26}\text{Al}/^{10}\text{Be}$ ratio. Such a large TCN concentration precludes erosion rates greater than 0.4 m/Ma .

Table 4.1 Sample location and TCN data. Uncertainties reflect 1- σ analytical uncertainties in the AMS analyses. ^9Be carrier is from a shielded beryl, prepared by J. Klein, U. Penn.. ^{10}Be chemical blanks run with these samples ranged from 6.0×10^4 to 9.8×10^4 ^{10}Be atoms. AMS was completed at Lawrence Livermore National Lab (LLNL). ^{10}Be and ^{26}Al concentrations were normalized to a sea level high-latitude (SLHL) surface production rate of $5.1 \text{ atom} \cdot \text{g}^{-1}$ (Gosse and Stone, 2001) to eliminate any effect of higher production rates with altitude. The post-glacial cosmogenic nuclide concentration is calculated by subtracting the lowest measured ^{10}Be concentration from each of the measured ^{10}Be concentrations of the other samples. Erosion thickness (cm) is calculated by using Equation 4.1, 4.2 and SLHL normalized ^{10}Be abundance, in conjunction with Eq. 4.3 for the effects of muogenic TCN production.. The uncertainty in the erosion $\text{thick}_{\text{non-int}}$ (unmixed) and $\text{thick}_{\text{int}}$ (integrated or mixed) are the sum of the ^{10}Be measurement uncertainty and the till density uncertainty. See Appendix 7 for the derivation of erosion calculation.

Table 4.1

	field ID	cnef ID	nuc.	site specific data			cosmogenic concentrations					ratio		erosion			
				lat deg	alt. km	prod rate ² atom g ⁻¹ a ⁻¹	measured 10 ⁴ atom g ⁻¹	meas err 10 ⁴ atom g ⁻¹	prec %	norm SLHL ³ 10 ⁴ atom g ⁻¹	wo post-glac 10 ⁴ atom g ⁻¹	²⁶ Al/ ¹⁰ Be	unc %	thick _{non-int} cm	error cm	thick _{int} cm	error cm
cold-based ice deposit	Baffin 21808	1510	¹⁰ Be ²⁶ Al	71.99	1.04	12.6 74.7	256.3 749.9	5.9 19.0	2% 3%	103.9 304.0	102.3 296.9	2.93	3%	---	---	---	---
	Baffin 21681	1509	¹⁰ Be ²⁶ Al	71.81	0.59	8.6 50.9	142.7 180.8	3.3 7.4	2% 4%	85.0 107.7	83.5 100.6	1.29	5%	110	6	409	25
	Baffin 21679	1508	¹⁰ Be ²⁶ Al	71.91	1.02	12.4 73.7	188.3 486.0	4.4 12.3	2% 3%	77.4 199.7	75.8 192.6	2.58	3%	117	6	416	25
	Baffin 21684	1514	¹⁰ Be ²⁶ Al	71.63	0.73	9.7 57.5	78.2 329.1	2.0 30.5	3% 9%	41.2 173.4	39.7 166.3	4.21	10%	162	9	460	28
	Baffin 21830	1511	¹⁰ Be ²⁶ Al	71.25	0.69	9.4 55.6	70.8 305.4	1.9 9.3	3% 3%	38.5 166.3	37.0 159.2	4.32	4%	169	9	466	28
	Baffin 21858	1528	¹⁰ Be ²⁶ Al	71.37	0.70	9.5 56.3	48.1 196.9	1.1 10.1	2% 5%	25.9 105.9	24.3 98.8	4.09	6%	197	10	494	30
	Baffin 21606	1507	¹⁰ Be ²⁶ Al	71.90	0.67	9.2 54.8	36.6 53.4	0.9 1.8	3% 3%	20.2 29.5	18.7 22.4	1.46	4%	217	12	513	31
	Baffin 21700	1517	¹⁰ Be ²⁶ Al	71.90	0.62	8.8 52.6	19.7 64.5	0.5 64.5	3% 10%	11.4 37.2	9.8 30.1	3.32	10%	262	14	557	33
intermediate	Baffin 21686	1515	¹⁰ Be	71.50	0.77	10.0	13.0	0.4	3%	6.6	5.1	nd	nd	307	20	601	36
	Baffin 21838	1520	¹⁰ Be ²⁶ Al	71.69	0.90	11.2 66.6	10.3 39.9	0.4 1.9	3% 5%	4.7 18.2	3.1 11.1	3.88	6%	339	22	632	38
	Baffin 21836	1519	¹⁰ Be	71.69	0.88	11.1	7.5	0.2	3%	3.4	1.9	nd	nd	371	22	664	40
	Baffin 21834	1518	¹⁰ Be ²⁶ Al	71.80	0.87	10.9 64.7	7.0 27.8	0.3 2.1	4% 7%	3.3 13.0	1.7 5.9	3.97	8%	377	26	670	40
warm-based ice deposit	Baffin 21803	1523	¹⁰ Be ²⁶ Al	71.73	0.16	5.8 34.7	5.8 34.6	0.3 8.6	6% 24%	5.5 30.2	3.9 23.1	6.00	25%				
	Baffin 21604	1522	¹⁰ Be	71.94	0.29	6.6	5.9	0.2	3%	4.5	3.0	nd	nd				
	Baffin 21833	1527	¹⁰ Be ²⁶ Al	71.85	0.29	6.6 39.0	5.0 26.2	0.2 2.7	5% 10%	3.9 20.4	2.3 13.3	5.24	12%				
	Baffin 21831	1526	¹⁰ Be ²⁶ Al	71.84	0.23	6.2 37.0	3.8 25.7	0.2 3.1	5% 12%	3.1 21.1	1.5 14.0	6.84	13%				
	Baffin 21820	1525	¹⁰ Be ²⁶ Al	71.55	0.70	9.5 56.3	4.6 27.7	0.2 2.6	5% 9%	2.5 14.9	0.9 7.8	6.05	10%	411	31	704	42
	Baffin 21871	1521	¹⁰ Be ²⁶ Al	71.47	0.28	6.5 38.7	2.1 10.7	0.2 2.1	8% 20%	1.7 8.4	0.1 1.3	5.01	21%				
	Baffin 21818	1524	¹⁰ Be ²⁶ Al	71.09	0.18	6.0 35.6	1.8 8.3	0.1 1.7	7% 21%	1.6 7.1	0 0	4.55	22%				

CHAPTER 5

IMPLICATIONS AND CONCLUSIONS

5.1 IMPLICATIONS OF DIFFERENTIAL GLACIAL EROSION

Chapters 3 and 4 address the role of cold-based and warm-based overriding ice during the last and previous glaciations and the effect of differential erosion on Arctic and sub-Arctic landscapes and have implications for those three themes introduced in Chapter 1. These themes were:

- (1) the influence of erosion on orogenic processes (e.g., Zeitler et al. 2001; Beaumont et al., 2001; Tomkin and Braun, 2003),
- (2) the increased sediment flux during the Quaternary reflecting or promoting climate variability (e.g., Molnar and England, 1990; Raymo and Ruddiman, 1992; Montgomery et al., 2001), and
- (3) glacial erosion perturbing stable landscapes to create relief (e.g. Brozovic et al. 1997; Small and Anderson, 1998; Whipple et al., 1999; Tomkin and Braun, 2002).

5.1.1 ESTIMATE OF EROSION IN WARM-BASED GLACIAL ZONES

There are several remaining methods to estimate the amount of bedrock erosion due to glaciation beside those described in Chapters 3 and 4. A first-order approach to

estimating the maximum amount of bedrock eroded by glaciers in northeastern Canada is to assume that the existing relief (depth of the channels) was due entirely to glacier erosion over the past 2.5 Ma, and no glacial erosion occurred on the intervening summits. (U-Th)/He results from Labrador indicate that high-elevation plateau is mainly a palimpsest Mesozoic surface with antecedent drainage network influenced by rift flank uplift during the opening of the Labrador Sea (Centeno, 2005). Centeno's (2005) results demonstrate that there has been less than 1 km of exhumation of the valleys since Cretaceous time and forms an upper bound for possible erosion due to Quaternary glacial erosion.

An estimate of the erosion in fiords is the maximum depth below modern sea level and forms a lower bound of the amount of erosion possible due to Quaternary glacial erosion. Most of the fiords on Baffin Island and the Labrador Peninsula are 200 to 400 m below sea level and bedrock depths can reach 500 m below sea level (Dowdeswell and Andrews, 1985; Rogerson et al., 1986; Bell, 1987). The number of glaciations during the Quaternary is highly speculative, but ranges from 25 to 50 glaciations based on oxygen isotope records derived from benthic foraminifera (Hays et al., 1976; Wright, 2001). This range produces 10-20 m of erosion in the zones of highest basal ice velocity in these areas. However, during the waning period of the last and presumably earlier glacial cycles, fluvial base level may have also been lowered due to the lock-up of water in remnant continental ice sheets on land. Evidence for decreased elevation of base level during deglaciation is the presence of emerged deglacial-aged, stream-fed deltas up to 80 m above modern sea level (Miller et al., 2002) that have been uplifted from Holocene isostatic rebound. Thus, the 500 m depth of incision can be considered a maximum value

of glacial erosion. Notably, the fluvial component of bedrock erosion inferred from these raised deltas could be minimal because many of these deltas were fed by transport-limited, glacially fed streams and were incapable of effectively eroding their channels.

Another way of constraining erosion due to Quaternary glaciations is to measure the quantity of Quaternary-aged glacial sediment. The thickness of rock removed by glacial erosion due to glaciation in North America has been the subject of significant debate and various estimates are shown in Table 5.1. Flint (1847, 1971) calculated that subglacial erosion had been insignificant based on the relatively small volume of morainal sediment around the former margins of the Laurentide Ice Sheet (LIS). White (1972) argued that much of the glacial sediment was deposited in the ocean, not in paleo-ice marginal moraines. White (1972) estimated that Canadian Precambrian rocks were exhumed by up to a kilometer of glacial erosion based on his rough estimates of Quaternary-aged sediment volume in the oceans. Working in smaller field areas in North America, Ambrose (1964), Gravenor (1975), Sugden (1976), Rutter (1980), and Kaszycki and Shilts (1980) concluded that there is only evidence for tens of meters of glacial erosion during the Quaternary period. Laine (1980) and Bell and Laine (1985) argued that the oceans are the main repository for glacial sediment as White (1972) suggested, but that White (1972) overestimated the sediment volume. Bell and Laine (1985) re-estimated the amount of marine sediment volume from then-new seismic technologies and concluded that the average depth of erosion by the Pleistocene LIS was closer to 120 m and that an additional ca. 20 m could be attributed to chemical erosion. This estimate yields an erosion rate of 2.8 – 5.6 m erosion/glaciation, assuming 25 or 50 glaciation during the Quaternary period (See Table 5.1).

To test the glacial erosion expression relating basal sliding speed and erosion against previously published estimates of LIS erosion, I ran five UMISM simulations of ice cover that produced reasonable southerly ice margin extents and basal ice sliding distances normalized by the duration of ice cover over North America over a 100-ka glacial cycle. From the average of those five simulations, those areas that experienced basal sliding had an average basal sliding speed of 80 km/ka. This average value, when multiplied against the glacial erosion coefficient (K_g) derived in Chapter 3 determines an erosion rate of $0.0004 \text{ m}\cdot\text{a}^{-1}$ over the warm-based Laurentide region, assuming a linear relationship between sliding speed and erosion. Over 100 ka of the glacial cycle, this erosion rate equals 4 m of erosion. For 25 – 50 glaciations of the Quaternary period, the estimate of average total thickness of glacial erosion is 100 – 200 m, which lies in the range of the thickness of total Laurentide erosion given in Table 5.1. This estimate (4 m/glaciation) is similar to the erosion thickness determined by Bell and Laine (1985) from Quaternary-aged sediment volumes and the erosion thickness determined by Balco (2004) from atmospheric ^{10}Be depth profile erosion. However, the K_g in Chapter 3 is tuned to erosion-resistant bedrock and is a minimum estimate of the glacial erosion coefficient. The previously published glacial erosion coefficient (K_g) of 10^{-4} (Humphrey and Raymond, 1994) provides an estimate of ca. 800 m of erosion/glacial cycle for the modeled sliding velocity, which is not supported by the marine sediment volume calculation (Bell and Laine, 1985).

If there is a linear relationship between glacial erosion and sliding velocity as assumed in Chapter 3, then it is difficult to envision a realistic scenario in which cold-based, non-erosive ice contributes zero erosion and the glacial erosion coefficient can be

as low as 10^{-4} . Table 5.1 show the values of K_g that correspond to a range of erosion rates for a given normalized sliding speed modeled for the Torngat Mountain valleys. Assuming an estimates of glacial erosion on the order of 3 m/glaciation for warm-based areas, Table 5.1 shows values of K_g that correspond to a range of normalized sliding distances for that given erosion rate.

5.1.2 ESTIMATE OF EROSION IN COLD-BASED GLACIAL ZONES

Bell and Laine (1985) divided the total volume of Quaternary-aged sediment by the total area covered by the Laurentide Ice Sheet. This method assumes that all the total Laurentide area is overlain by erosive ice does not consider portions of the Laurentide-covered landscape that have not been eroded significantly. The model simulations used to determine the average sliding distance beneath the LIS show that the portion of land covered by warm-based ice was only ca. 75% the total basal area during the LGM (Fig. 5.1). If the Bell and Laine (1985) estimate of glacial erosion accounted for the cold-based zones of the Laurentide Ice Sheet contributing no portion of that Quaternary-aged sediment, the thickness of material removed increases to 175 m of erosion, or 3.5 – 7 m of erosion/glaciation. This range of erosion is on the same order as the range of calculated thicknesses of material eroded based on warm-based and intermediate till TCN concentrations in Chapter 4 over the entire Quaternary period.

5.1.3 INTERPRETATION SUMMARY

Based on the published values of glacial erosion for the LIS-eroded region and the modeled average sliding speeds, the glacial erosion coefficient in Chapter 3 produces 4 m of glacial erosion per glaciation and is consistent with Bell and Laine's (1985) estimate of erosion. Bell and Laine's (1985) estimate was revised to exclude their overestimation of the erosion in cold-based ice zones to 3.5 – 7 m erosion/glaciation and is consistent with calculations of thicknesses of glacial erosion calculated in Chapter 4. If 3.5 – 7 m of regolith or bedrock during a single glaciation and great depths of overlying soils and regolith protect rock from weathering, then glaciations enhance weathering during interglacials. Removing this thickness of regolith over a large, LIS-sized area has implications for a fluctuating climate producing a greater amount of erosion and sedimentation than a non-fluctuating climate (Peizhen et al., 2001). This is also seen in the sediment record where Quaternary sedimentation rates increased the most in southerly areas formerly covered by warm-based ice (Peizhen et al., 2001).

Geodynamic models used to address the influence of glacial erosion on orogenic processes or valley morphology (MacGregor, 2000; Tomkin and Braun, 2003) that use a simple linear relationship to describe glacial erosion with a glacial erosion coefficient as high as 10^{-4} could be overestimating glacial erosion in some lithologies. Overestimating the high-elevation glacial erosion could act to decrease the local relief, whereas cold-based zones juxtaposed with warm-based zones in alpine settings can act to generate relief. Relief generation also initiates a feedback effect where ice could accumulate and

persist at higher elevations and induce more glacial erosion in valleys owing to thicker valley ice (Montgomery, 2002).

5.2 CONCLUSIONS

5.2.1 CLIMATE-INDUCED GLOBAL VARIABILITY OF TCN PRODUCTION RATES

LGM climate-induced atmospheric conditions cause temporal and spatial variability in TCN production rates. Two conditions were found to have caused LGM production rates to be as much as 10% greater than the present-day. Changes in atmospheric pressure near large glaciers due to katabatic winds will increase production rates up to 10%. Changes in the altitudinal distribution of atmospheric mass due to cooling will have increasing influence with greater elevation up to 7%. Changes in the synoptic atmospheric pressure distribution due to cooling and the increased volume of ice masses lead to worldwide effects that vary spatially owing to complex atmospheric dynamics.

The magnitude of the time-integrated changes in production rates is proportional to the amount of the total exposure duration that experienced glacial conditions, but is less than the total production rate decrease at the LGM. Re-scaling previously published production rates for ^{10}Be to account for the climate effect on TCN production has a minimal effect (-2%) on the mean production rate, but slightly improve the standard deviation of the production rates.

TCN in nunatak bedrock would be affected significantly by the climate effect on production rates due to persistent glacial atmospheric conditions, but were not resolvable

in the coarsely sampled topographic grid of the climate simulation. The production rates used in chapters 3 and 4 were not corrected for climate effects described in Chapter 2 because of the topographic scale, but may have experienced greater production during late-glacial and Holocene exposure.

5.2.2 RELIEF GENERATION IN THE TORNGAT MOUNTAINS

To interpret TCN data from glacial landscapes of polythermal ice, double-nuclide ratios must be used to differentiate exposure, burial, and erosion signals. These ratios in Torngat bedrock samples reveal that the exposure plus ice cover history retained on some summit surfaces probably spans more than 800 ka despite complete ice cover and subsequent deglaciation as recently as 11 ka.

Glacier bed erosion in the Torngat Mountains is inferred to depend on the basal thermal regime of the ice-substrate interface. Our results show that even areas that were completely covered by polythermal ice sheets or ice caps, differential rates of glacial erosion will tend to complement valley deepening with wet-based, erosive ice overriding valleys and cold-based, non-erosive ice atop felsenmeer-covered interfluvial plateaus. TCN data suggest > 2.5 m of erosion per single glacial-interglacial cycle occurred within Torngat Mountain valleys. On summit plateaus, the longer-term (over several glacial-interglacial cycles) erosion rates are < 1.4 m/Ma. Therefore, in the Torngat Mountains, glacial erosion may have generated > 62-125 m of relief over ~25 to 50 glacial cycles of the Quaternary period. Relief generating due to cold-based ice protection at the summits has not been documented prior to this work.

A thermodynamic ice sheet model with a basal water calculation is used to calculate the sliding distance normalized by the duration of ice cover for the region. An empirical glacial erosion rule for the Torngat Mountains correlates TCN-derived erosion rates for terrain once overridden by polythermal glacier ice with modeled average ice basal sliding speeds. Erosion rates vary linearly with average sliding speed by a glacial erosion coefficient of 5×10^{-7} – orders of magnitude lower than previously published values.

5.2.3 GLACIAL EROSION AND SEDIMENT DISPERSION FROM DETRITAL TCN

I described a new method to identify paleo-glacier ice polythermal conditions from the measurement of TCN in till. In areas that were classified as warm-based or cold-based (end member) zones based on sedimentology, geomorphology, and the presence of exotic erratics, concentrations of ^{10}Be and ^{26}Al in till samples reflected the degree and depth of glacial erosion. Samples from zones classified as previously covered by cold-based, non-erosive ice had high TCN concentrations, while samples from zones classified as previously covered by warm-based ice had low TCN concentrations. In most instances, the TCN concentrations in samples classified as warm-based tills was equal to the post-glacial exposure with the related Holocene snow cover and erosion uncertainties and indicate negligible presence of the inherited TCN preserved in the tills classified as cold-based.

The $^{26}\text{Al}/^{10}\text{Be}$ ratio further distinguished tills with more complicated exposure histories from cases with simple exposures that lack any inheritance of pre-glacial TCN.

The samples classified as warm-based have are consistent with a single, uncomplicated exposure history since deglaciation. Samples classified as cold-based tills have a complex and long exposure history despite recent deglaciation. In the most extreme case, this ratio in short-distance tills represented a minimum of 800 ka of exposure followed by one of more burial episodes, presumably by cold-based ice, for a minimum of 3 million years, suggesting that recently deglaciated surfaces near modern ice caps may have been covered since the Pliocene. In four localities that resembled intermediate cases, i.e. cold-based conditions but with exotic clasts in the till, the ^{10}Be and $^{26}\text{Al}/^{10}\text{Be}$ reveal that the surface experienced a combination of cold-based ice burial and glacial erosion, but the minimal burial duration was shorter than the minimal burial durations for the cold-based ice end members.

An ice sheet simulation of bed conditions reflected the same pattern of cold-based and warm-based end-members, despite conflicting resolution of the model grid and outcrop scales. The northeast corner of the Ice Bound Lakes region experienced persistent frozen bed conditions with negligible basal transport potential in the model and is consistent with the highest TCN concentrations. High TCN concentrations in these zones are consistent with little interaction with the cold-based ice cap and any far-traveled ice was funneled through the constricted valleys and fiords. The tills with low TCN concentrations have experienced one or more cycles of basal freezing of previously thawed basal water in the model. One of the warm-based tills with low TCN concentrations were sampled from high elevations, but were farther from the coast and farther from the modeled terminal ice margin position. In some areas beneath an ice

sheet, even high elevation sites can experience basal sliding depending on the thickness and velocity of the ice.

5.2.4 CONCLUSIONS SUMMARY

This section summarized the research presented in chapters 2, 3, and 4. The highlights of the research are as follows: First, the effect of glaciations on the TCN production rate is up to 10% different at the LGM, but much less than 10% different for exposures that average the in situ production rates between present-day and glacial conditions. Second, the protection beneath non-erosive, cold-based ice cover enables the use of a long-term record of differential preservation of pre-glacial TCN. Third, this TCN inventory must be used in conjunction with multiple nuclide ratios and field evidence and is the basis for the techniques used to determine spatial variation of glacial erosion in Chapters 3 and 4. Fourth, UMISM modeled bed characteristic matched the spatial variation in TCN and when coupled with TCN-derived erosion rates, calibrated a glacial erosion-sliding speed relationship that varied linearly with a coefficient of 5×10^{-7} . Fifth, regions classified as cold-based or warm-based paleo-ice cover zones based on sedimentology (clast angularity, matrix characteristics), clast provenance (abundance of exotic lithologies), and geomorphology contained matching TCN abundances in till matrices.

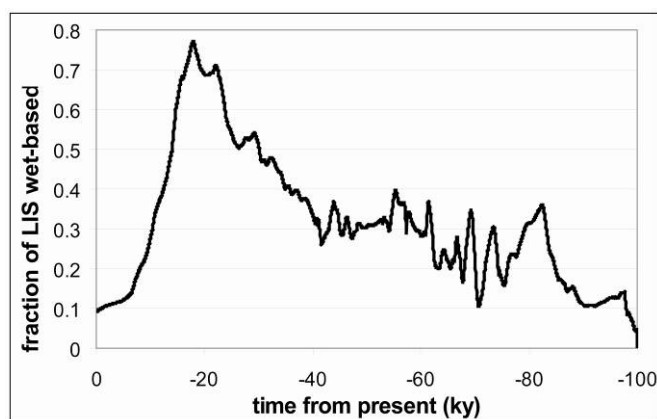


Figure 5.1 The average of five simulations of the LIS shows that only ~75% of the LIS ice was warm-based over the 100 ka glacial cycle.

(a)

Investigator	Erosion/glaciation m in 25-50 glaciations	Total erosion m
Flint, 1971	0.5 - 1	25
White, 1972	20 - 40	1000
Sugden, 1976, 1978	0.4 - 3.6	20-90
Laine, 1980	1.1 - 3.8	55-95
Bell and Laine, 1985: erosion in cold-based zones	2.8 - 5.6	140
Balco, 2004	4	100-200
Bell and Laine, 1985: no erosion in cold-based zones	3.7 - 7.5	187

(b)

	sliding velocity km/ka	Erosion/glaciation m in 50 glaciations	K_g	
$\epsilon_g = K_g \cdot u_s$ in Chapter 3	adjusted m erosion/ 50 glaciations for 80 km/ka sliding velocity	80	3	2×10^{-6}
		80	4	3×10^{-6}
		80	10	6×10^{-6}
		80	20	1×10^{-5}
		80	40	3×10^{-5}
		80	80	5×10^{-5}
		80	400	1×10^{-4}
	adjusted average sliding velocity for 3 m erosion/ 50 glaciations	0.7	3	1×10^{-4}
		2	3	8×10^{-5}
		5	3	3×10^{-5}
		10	3	2×10^{-5}
		20	3	8×10^{-6}
		50	3	3×10^{-6}
100	3	2×10^{-6}		

Table 5.1 a. The thickness of erosion determined by various investigators working in North America. The bold Bell and Laine (1985) erosion rate is adjusted to represent only the erosive portion of the LIS. **b.** Erosion rates calculated for given thicknesses of substrate eroded during a glaciation against the average sliding speeds and their associated glacial erosion coefficients. Glacial erosion coefficients as high as 10^{-4} would require very low average sliding speeds, while average sliding speeds of 80 km/ka like those modeled in the Torngat Mountain valleys would require extreme erosion each glaciation.

APPENDIX 1

ESPL COPYRIGHT RELEASE LETTER

APPENDIX 2

TERRESTRIAL IN SITU COSMOGENIC NUCLIDE (TCN) SYSTEMATICS

A2.1 HISTORY

The first development of TCN methods for solving geological problems (Davis and Schaefer, 1955) arose long after Grosse (1934) suggested that “cosmogenic radioelements” could be produced at the surface of the Earth (Gosse and Phillips, 2001). Two innovations that allowed TCN to be employed throughout the world came from the models of production rates at any latitude and elevation (Lal, 1958) and development of Accelerator Mass Spectrometry (AMS) (Klein et al., 1982) that permitted measurement of extremely low concentrations of cosmogenic isotopic ratios.

Refinement of the method continues today as the applications of the technique require more and more precision and address new and innovative subjects. The Cosmogenic Nuclide Extraction Facility (CNEF) at Dalhousie University, Halifax, NS, was the first Canadian laboratory to extract the cosmogenic radionuclides from rock and sediment samples. AMS measurements are contracted to Lawrence Livermore National Labs (LLNL) in Livermore, California.

A2.2 FUNDAMENTAL TECHNIQUE

Galactic cosmic radiation (GCR) is composed of highly energetic particles (1-100 GeV) that originate within the Milky Way, but outside our solar system (Gosse and Phillips, 2001). The nucleons (mostly protons) spiral through interplanetary and terrestrial magnetic fields and produce a cascade of secondary particles principally consisting of neutrons and a smaller number of π^{\pm} and K^{\pm} mesons. Most cosmogenic nuclide production results from neutron spallation reactions where high-energy neutrons break up target nuclei. Energy is lost due to successive reactions until the neutrons are no longer capable of causing spallation reactions. Their remaining energy is dissipated through the transfer of momentum to the shattered particles. Another pathway for cosmogenic isotopes is short-lived (10^{-6} s = $t_{1/2}$) muons. Secondary particles can cause spallation of terrestrial in situ elements (e.g. an Oxygen atom or a Silicon atom) to leave a lighter residual nucleus (e.g. ^{10}Be or ^{26}Al) (Gosse and Phillips, 2001).

The concentration of a TCN is affected by the decay of the nuclide. In the case of ^{10}Be , the half-life is 1.5 Ma (Yiou and Raisbeck, 1972, Hofmann et al., 1987, Holden, 1990, Middleton et al., 1993 in Gosse and Phillips, 2001) though in recent work, researchers use the value 1.3 Ma (Partridge et al., 2003; Balco, 2005). The production of TCN from spallation reactions decreases exponentially with depth below the surface of an exposed landform. TCN production is largely concentrated in the upper ~3 m of the Earth's surface (Gosse and Phillips, 2001). Near the surface, close to 98% of the ^{10}Be and ^{26}Al produced is from spallation reactions involving fast neutrons (Stone, 2000). Fast neutrons are mostly attenuated within depths of 1 to 3 m in bedrock and alluvium. Muons are lighter particles and less interactive with mass and are able to penetrate to far greater depths (tens of meters), thus playing a larger role in producing ^{10}Be and ^{26}Al

below the ground surface. (Fig. A2.1). Spallation production can be calculated using the following equation from Gosse and Phillips (2001):

$$P = P_o e^{-z\rho/\Lambda} \quad (\text{Eq. A2.1})$$

where P is the production rate (atoms $\text{g}^{-1} \text{y}^{-1}$) at a certain depth, P_o is the production rate at the surface (atoms $\text{g}^{-1} \text{y}^{-1}$), z is the depth of the sample (cm), ρ is the bulk density of the rock or sediment (g cm^{-3}), and Λ is the mass attenuation length (g cm^{-2}). The average production rate through a depth (z_2 to z_1 , where $z_2 > z_1$) of sample can be calculated by the equation:

$$P_{z_2 \text{ to } z_1} = P_o \frac{\Lambda}{\rho(z_2 - z_1)} e^{-(z_2 - z_1)\rho/\Lambda} - 1. \quad (\text{Eq. A2.2})$$

The number atoms of *in situ* cosmogenic radionuclides can be described by the equation:

$$N = \frac{P}{\lambda + \frac{\rho\varepsilon}{\Lambda}} \left(1 - e^{-(\lambda + \rho\varepsilon/\Lambda)t}\right) + N_o e^{-\lambda t} \quad (\text{Eq. A2.3})$$

where N is the number of produced cosmogenic atoms (atom g^{-1}), λ is the decay constant (year^{-1}), ε is the steady erosion rate ($\text{grams cm}^{-2} \text{y}^{-1}$ (transformed to cm years^{-1} via ρ : density in g cm^{-3})), and t is the exposure duration (y) (Kurz and Brook, 1994).

The number of cosmogenically produced atoms, N , is measured indirectly. The decay constants, λ , and attenuation lengths, Λ , can be independently determined and are well known. Currently used values for production rate, P , are a function of altitude, latitude and time that are associated with the attenuation of galactic cosmic rays by the atmosphere (altitude) and geomagnetic variation (latitude and time). The production rates

have considerable uncertainties, although recent work decreases the uncertainty for specific radioisotopes.

However, the system is still underdetermined with two unknown variables, t and ε . Consequently, the system is modeled to assume zero erosion for a minimum exposure age and to assume a sufficiently high exposure age to reach a steady-state erosion rate. These assumptions reduce equation (A2.3) to equation (A2.4) for time and (A2.5) for erosion:

$$N = \frac{P}{\lambda} (1 - e^{-\lambda t}) + N_o e^{-\lambda t} \quad (\text{Eq. A2.4})$$

$$N = \frac{P}{\lambda + \frac{\rho\varepsilon}{\Lambda}} \quad (\text{Eq. A2.5})$$

The formulas above describe minimum exposure age and maximum (steady-state) erosion rates (Gosse and Phillips, 2001).

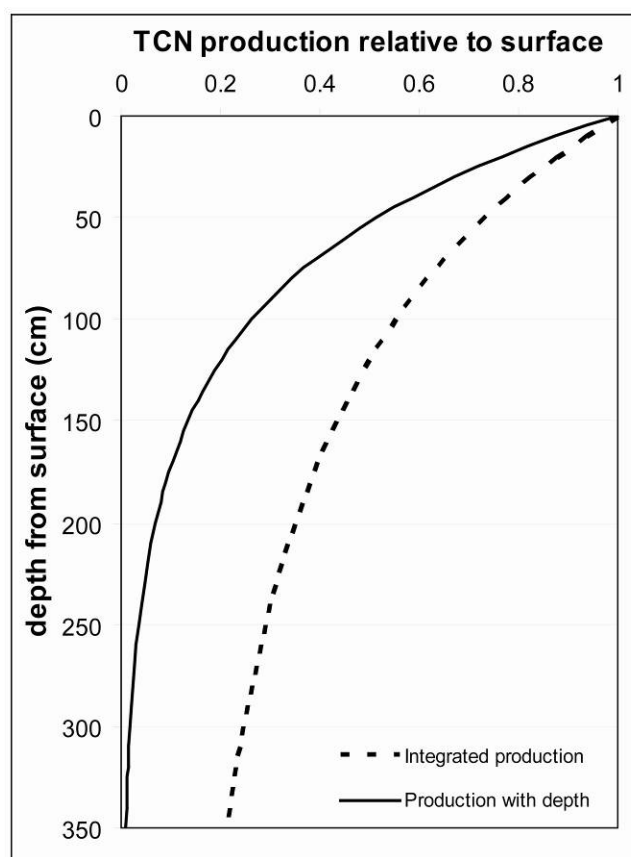


Figure A2.1 TCN spallation production with depth below the surface (solid line) and the integrated production for a mixed till layer or an amalgamated bedrock of sediment sample (dashed).

APPENDIX 3

SUMMARY OF ASSUMPTIONS IN CHAPTER 3 CALCULATIONS

A3.1 FOR APPARENT AGE CALCULATIONS:

1. TCN production rates, attenuation lengths, and decay constants have not changed enough over the period of TCN accumulation, exposure, and burial to significantly affect the results of this work.
2. Samples have experienced negligible erosion or burial.

A3.2 FOR EROSION CALCULATIONS:

1. TCN concentrations within the summit surface bedrock have attained a steady state for a particular constant erosion rate over that time.
2. Glacial erosion scales linearly with basal ice sliding velocity such that the basal ice sliding distance normalized by the duration of ice cover is roughly equivalent to the average basal ice sliding velocity.

Calculation of maximum erosion rate in Table 3.1 for bedrock on high summits following Lal (1991):

$$\varepsilon = \left(\frac{P}{N} - \lambda \right) \left(\frac{\Lambda}{\rho} \right) \quad (\text{Eq. A3.1})$$

where: ε = erosion rate (cm a^{-1})
 P = surface production rate ($\text{atom g}^{-1} \text{ a}^{-1}$)
 N = nuclide concentration (atom g^{-1})
 λ = decay constant (a^{-1})
 Λ = apparent mass attenuation length (g cm^{-2})
 ρ = bulk density (g cm^{-3}).

Lab ID	field ID	site specific data				
		Lat deg.	Long deg.	Altitude km	corrections	
					shield	depth
270 Be	LAB-00-26A	58.92233	-63.56573	1.547	0.0%	3.4%
1308 Be	LAB-02-NACH-225	59.03467	-64.12500	1.460	0.0%	1.3%
219 Be	LAB-00-01A ¹	58.68750	-63.94900	1.453	0.0%	3.4%
220 Be	LAB-00-01B ¹	58.68750	-63.94900	1.453	0.0%	0.9%
221 Be	LAB-00-02A ¹	58.69000	-63.94900	1.355	0.0%	1.7%
1304 Be						
1304 Al	LAB-02-NACH-221	59.29167	-64.56633	1.257	0.0%	2.6%
197 Be	KAU-99-01 ¹	57.88167	-62.05000	1.245	0.0%	4.2%
312 Be						
312 Al	LAB-00-09A ¹	58.70438	-63.78763	1.200	0.0%	0.9%
237 Be	LAB-00-08A	58.69487	-63.78117	1.173	0.0%	1.3%
339 Be	LAB-00-10A	58.69903	-63.78763	1.172	0.0%	1.3%
309 Be	LAB-00-08B	58.69487	-63.78117	1.170	0.0%	1.7%
223 Be	LAB-00-04A ¹	58.69550	-63.93767	1.169	0.0%	1.7%
224 Be	LAB-00-04B ¹	58.69550	-63.93767	1.169	0.0%	1.7%
225 Be	LAB-00-04C ¹	58.69550	-63.93767	1.169	0.0%	1.7%
366 Be	LAB-00-33A	59.48300	-63.90297	1.162	0.0%	3.5%
268 Be						
268 Al	LAB-00-22A ¹	58.60195	-63.72302	1.090	0.0%	1.3%
1306 Be	LAB-02-NACH-223	59.24917	-64.42833	1.086	0.0%	1.7%
1309 Be	LAB-02-NACH-226	58.88300	-64.13367	1.041	0.0%	1.7%
201 Be	LAB-99-06A-1 ¹	59.46500	-64.65833	1.000	0.0%	1.7%
1050 Be	LAB-95-11 ¹	59.61000	-64.68333	0.960	0.0%	2.0%
206 Be	LAB-99-19 ¹	59.31500	-64.62267	0.870	0.0%	1.7%
1291 Be	LAB-02-NACH-202	58.98430	-64.68143	0.822	0.0%	2.6%
1292 Be	LAB-02-NACH-203	58.98463	-64.68017	0.803	0.0%	2.6%
271 Be						
271 Al	LAB-00-38B	58.50007	-65.10992	0.741	0.0%	2.6%
330 Be	LAB-00-27B	59.05467	-63.27532	0.639	0.0%	1.7%
331 Be	LAB-00-27A	59.05467	-63.27532	0.639	0.0%	1.8%
255 Be						
255 Al	LAB-00-25B ¹	58.70320	-63.62263	0.776	0.0%	2.6%
269 Be						
269 Al	LAB-00-23A ¹	58.59525	-64.21200	0.740	0.0%	1.7%
328 Be	LAB-00-24D	58.61167	-64.10370	0.316	0.0%	3.4%
1331 Be	LAB-02-STK-228	58.82778	-63.53392	0.312	2.0%	3.0%
1332 Be	LAB-02-STK-229	58.84583	-63.53463	0.311	2.0%	2.0%
336 Be	LAB-00-29B	58.88367	-63.64400	1.289	0.0%	1.7%
1305 Be						
1305 Al	LAB-02-NACH-222	59.25917	-64.42833	1.086	0.0%	1.7%
196 Be	MTH-99-01 ¹	56.92167	-61.46167	0.908	0.0%	1.7%
250 Be	LAB-00-16B	58.70667	-63.71667	0.859	0.0%	1.7%
198 Be	KAU-99-02A ¹	57.87167	-62.06000	0.850	0.3%	1.7%
240 Be	LAB-00-20A ¹	58.61633	-63.63682	0.838	0.0%	1.3%
1290 Be	LAB-02-NACH-201	58.98430	-64.68143	0.822	0.0%	1.7%
267 Be						
267 Al	Lab-00-15A	58.70190	-63.71473	0.809	0.0%	2.0%
1293 Be	LAB-02-NACH-204	58.98463	-64.68017	0.803	0.0%	1.7%
205 Be	LAB-99-23-1A ¹	59.31333	-64.65000	0.766	1.1%	1.7%
324 Be	LAB-00-14B	58.69717	-63.61432	0.748	0.0%	1.3%
325 Be	LAB-00-14A	58.69717	-63.61432	0.736	0.0%	1.7%
55b Al	LAB-97-24A ¹	59.32000	-64.84683	0.730	0.0%	2.0%
266 Be	LAB-00-11B	58.69635	-63.75142	0.715	0.0%	0.9%
313 Be						
313 Al	LAB-00-17A ¹	58.63973	-63.59698	0.713	0.0%	1.7%
329 Be	LAB-00-27C	59.05905	-63.26483	0.530	0.0%	1.7%
338 Be	LAB-00-24C	58.61167	-64.10370	0.316	0.1%	2.6%
326 Be	LAB-00-28A	59.00252	-63.37618	0.191	0.2%	1.7%

Table A3.1 Site characteristics and sample correction data for cosmogenic data presented in Chapter 3. ¹Samples were originally reported in Marquette et al., (2004).

APPENDIX 4

TERRESTRIAL IN SITU COSMOGENIC NUCLIDE CHEMISTRY

A4.1 INTRODUCTION

The methodology presented in this appendix is based on the lab procedures outlined in Gosse (2001) “Dal-CNEF Laboratory Procedures.” The Be and Al isolation is a five-step process. These processes are physical pre-treatment, chemical pre-treatment, chemical isolation, oxide preparation, and AMS measurement.

A4.2 PHYSICAL PRE-TREATMENT

Physical preparation of the samples included crushing, milling and sieving in order to reduce bulk field samples, rocks or mixed sand fractions into well-sorted sand fractions. All Torngat Mountain rock samples underwent crushing and milling. Each crushed sample was poured into the mill slowly to ensure that there was minimal sample loss to dust while pulverizing. The initial spacing between the disks was approximately 2 mm to crush the granule-sized clasts and was incrementally decreased until it was < 0.5 mm wide. Samples were sieved between passes through the disk mill using the >500

μm , 500-355 μm , and 355-250 μm sieves and sieved finally using a RoTap™ sieve shaker for 10 minutes.

After separating the grain sizes in a RoTap™ sieve shaker, fractions with a grain size of 355-500 μm were used for the chemical pre-treatment. This size was considered the optimal grain size for the Torngat Mountain and Baffin Island samples. Between samples, the sieves were cleaned using wire brushes and a brush and dental pick to remove any leftover grains. Fractions with a 250-355 μm grain size were also used in conjunction with the 355-500 μm grain size for the Baffin Island samples because the light mineral separates were typically small and larger amounts of sample were required in order to maintain ~20 g for final chemistry. In the case of the Baffin Island till samples, crushing and milling of the size fraction greater than 500 μm was not done so that those fractions could be saved.

All of the Baffin Island till samples were gravelly-medium to coarse sands and had to be sieved through a > 0.5 cm mesh to isolate the larger clasts. Clasts larger than 1 cm in diameter were removed from the sample and archived in a labeled Ziplock™ bag.

A4.3 CHEMICAL PRE-TREATMENT

Chemical pre-treatment was performed in the Cosmogenic Nuclide Extraction Facility (CNEF) at Dalhousie University. Up to 600 g of the 250-355 μm and 355-500 μm grain sizes of sample were mixed with a highly oxidizing aqua regia solution (mixture of 3HCl: 1HNO₃) and heated at 200°C for at least 2 hours. Aqua regia weakens, dissolves and breaks up many of the Fe-bearing non-quartz minerals. Some of the lighter

minerals, such as mica, floated off as the samples were rinsed. From this stage on, only ultra-pure (18 M Ω) water was used to minimize the introduction of Be and B that can be present in tap water. The samples were then etched with a concentrated reagent-grade hydrofluoric acid (HF) at 200°C for 30 minutes. HF etching dissolved many of the unwanted silicate mineral grains and stripped off the outer layer from each quartz grain, removing any meteoric (vs. terrestrial in situ) cosmogenic ^{10}Be .

Following HF etching, samples underwent several ultrasonic acid leaching cycles to purify the samples in a modified form of the Kohl and Nishiizumi (1992) technique. The cycles started with high acid ratio (eg. 240 ml HF: 80 ml HNO₃: 3900 ml H₂O). Less acid was added with successive cycles as the sample became quartz-enriched and smaller. These cycles were repeated until most of the non-quartz minerals were removed and a >95% quartz concentrate remained. If the samples retained a significant portion of feldspars and other minerals softer than quartz, 25-gram aliquots of the samples were placed in abrasion chambers for 20 to 40 minutes. The principle of abrasion is the break up of minerals that are softer than quartz by pumping high pressure (40 psi) air into a small chamber where grains abrade other grains. Abrasion was always followed by rinsing with ultrapure water to remove the grains smaller than ~150 μm . This fine fraction of minerals that broke in the abrasion chamber was removed by swirling the container with a water-and-sample slurry to keep the small grains in suspension and slowly decant them.

Remaining magnetic minerals such as pyroxene, hornblende, magnetic shale and other opaque minerals that do not dissolve in dilute HF were removed using a Lithium bar magnet or in some cases, the Frantz™ Magnetic Separating device. This device

further separates the Fe-bearing minerals from the quartz and other non-magnetic minerals and was used for minerals with minor magnetic properties or for samples with a large magnetic mineral fraction. In some Torngat Mountain garnetiferous gneisses, the magnetic garnet fraction was almost 10% of the total sample size.

It is important to ensure the sample has few non-quartz minerals because (1) the ^{10}Be and ^{26}Al production rates for other minerals are not necessarily the same as for quartz and (2) non-quartz minerals have greater Al concentrations. High Al concentrations are unwanted because of complications in the following cation column chemistry step. To ensure that samples had less than 100 ppm of aluminum, Al tests were conducted on 1 g samples that was dissolved in HF and then re-dissolved in 0.5 N HCl. A Quant-EM™ Al test strip kit was then used to calculate the Al concentration in those 5 g of quartz. Those samples with Al concentrations less than 100 ppm were ready for the next phase. Those samples with higher concentrations underwent further chemical pre-treatment that was sample dependent and included some combination of HF etching, ultrasonic leaching or abrasion before being Al-tested again. If the total concentration of Al is very low in the quartz, <1.0 mg, then the statistical count from the accelerator is worsened. In the case of low Al ppm, an aluminum carrier of known concentration (1000 ppm) is added in order to maintain 1 mg of total Al. There is a trade-off adding Al carrier to samples that could contain low ^{26}Al because the greater the native ^{27}Al , the lower the $^{26}\text{Al}/^{27}\text{Al}$ ratio. $^{26}\text{Al}/^{27}\text{Al}$ ratios lower than 10^{-15} are difficult to measure precisely with the AMS.

A4.3.1 QUARTZ DISSOLUTION

Approximately 0.3 ml of 1015 ppm Be carrier was added to each quartz sample (up to 40 g). The carrier is mostly ^9Be with a known amount of ^{10}Be that is used to give the AMS a larger target for analysis. The carrier mass must be measured to 4 decimal places. A geochemical blank was also prepared to which only carrier was added without any quartz for each sample. Samples and blanks were dissolved in 5 ml HF, 2 ml HClO_4 , and 5 ml aqua regia for each 5 g of quartz in the sample. If dissolution took longer than ~48 hours, additional HF was added. Adding acid above the normal suggested volumes was done sparingly in order to minimize the possible addition of B or Be. The samples were then allowed to fume with HNO_3 to remove the SiF_4 . Successive evaporations and re-dissolutions with concentrated HClO_4 acid (HClO_4 with water boiling temperature (T_b) = 200°C) and HNO_3 (HNO_3 with water: T_b = 120°C) aimed to eliminate the fluoride (HF with water: T_b = 120°C) almost entirely. Addition of perchloric acid, although dangerous, strips the F^- and reduces the possibility of the formation of BeF_4 , which is a difficult complex to break. Fluoride that is not fumed off in this process causes problems in column chemistry. Fe, Ti, Al, Be, alkalis and other metals present should now have been in the form of chloride salts (Be as BeClO_4 and Al as $\text{Al}_2(\text{ClO}_4)_3$) required to pass through the anion columns. Aliquots of the samples were extracted to analyze for the native Al concentration. If samples contained less than 50 ppm native Al, an Al carrier was added to the sample to increase the future Al-oxide mass (Fig. A4.1).

A4.3.2 ION CHROMATOGRAPHY

Ion chromatography purified the samples even more. This purification step was necessary because the cosmogenic nuclide component is low even in completely pure samples. It is necessary to purify the sample solution as well as possible in order to prevent the dilution of Al or Be by other elements for the best possible AMS precision. Samples were re-dissolved in 9 N HCl. At this stage, the sample solutions were usually bright or dull yellow probably due to Fe (as FeCl_3). At this point in the procedure, some of the Torngat Mountain samples had a suspended white precipitate that clouded the solution. This precipitate was probably TiO_2 . Be and Al should not have precipitated with the Ti at a pH this high, so the samples were centrifuged and the precipitate was removed before passing the samples through the anion columns.

Samples were transferred into an anion exchange column that contained microscopic spheres of styrene resin with high exchange capacities allowing unwanted elements to adhere to the 200-400 μm mesh AG1-X8 BIORAD™ resin while the purer sample passed through the column unfettered. Anions in the sample solutions were either adsorbed onto or substituted into the resin spheres. By controlling the pH of the columns, it was possible to control which anions the resin collected (Fig. A4.2). In 9N HCl, Fe(III) forms a range of anionic Cl^- complexes: $[\text{FeCl}_4]^-$, $[\text{FeCl}_5]^{2-}$, and $[\text{FeCl}_6]^{3-}$, which bind tightly to the anion exchange resin (Stone et al., 2003). These Cl^- complexes can form a brown band at the top of the resin column. Al and Be do not form strong Cl^- complexes and elute from the column with the HCl. Titanium is more problematic; some Ti in the form of $[\text{Ti(IV)Cl}_6]^{2-}$ will bind, but a sizeable fraction always drains through in the form

of cationic or neutral species, ending up with the Al and Be (Stone et al., 2003). BeCl_2 and AlCl_3 passed through the columns at 9N HCl and were collected as eluant for the following steps. NH_4OH was added to the elute from the anion column to separate unwanted elements that precipitate as hydroxides from other elements (Fig. A4.3). In the 6.5-9.5 pH range, $\text{Be}(\text{OH})_2$ and $\text{Al}(\text{OH})_3$ are insoluble. The un-precipitated portion was decanted and the precipitate was rinsed with ultrapure water twice and dissolved in concentrated HCl acid, dried and re-dissolved in 0.5 N HCl.

Samples were then placed in pH-controlled cation columns to separate Be and Al from all remaining elements by ion chromatography (Fig. A4.4). The unwanted cation supernates were collected and set aside and Be and Al eluants were concentrated and collected separately.

A4.4 OXIDE PREPARATION

The Be eluant underwent further dissolution and evaporations and precipitation using ultrapure ammonia gas (Fig. A4.5). These processes converted the BeCl to BeOH that were then baked in ACE™ glass quartz vials at 850°C leaving a BeO powder (approximately 1 mg) that was packed into special target holders 1:1 BeO : Niobium powder and then sent to LLNL for AMS analysis (Fig. A4.6). The process for the Al eluants are similar but the AlCl_3 is converted to $\text{Al}(\text{OH})_3$ with 1:1 $\text{NH}_4\text{OH}:\text{H}_2\text{O}$ and the $\text{Al}(\text{OH})_3$ with baked in quartz vials at 950°C (Fig. A4.7-A4.8). Several of the quartz vials baked at 950°C to oxidize the Al_2O_3 samples broke and were not submitted for AMS because the of unknown concentration of Al in the quartz vial. ACE™ quartz vials are

only rated to temperatures less than 250°C. Quartz vials seem to withstand temperatures greater 850°C if the bottom of the quartz vial is in contact with only a small portion Alumina-holder. The baked Al₂O₃ powder from the vials (approximately 1 mg) was crushed and packed into special target holders with silver powder (1:1 Al₂O₃ : silver powder to send to LLNL for AMS (Fig. A4.9).

A4.5 AMS AND DATA REDUCTION

AMS measures the isotopic ratio of stable and cosmogenic Be and Al isotopes. The ¹⁰Be/⁹Be ratios of the samples and blanks were measured with acceptable precisions. The amount of ¹⁰Be was calculated using the following equation:

$$N = (R_{\text{cos/nat}}) \left(\frac{m_c}{\rho_c \cdot c_c} \right) \left(\frac{A}{W_{\text{cos}}} \right) / m_{\text{qtz}} \quad (\text{Eq. A4.1})$$

where N is the number of produced cosmogenic atoms per gram of quartz (atom g⁻¹), R_[cos/nat] is the ratio of cosmogenic nuclide to native nuclide measured by AMS, m_c is the mass of carrier used (g), ρ_c is the density of the carrier (g·ml⁻¹) and c_c is the concentration of the carrier (g·ml⁻¹), A is Avogadro's number (6.022x10²³ atom·mole⁻¹), W_{cos} is the atomic weight of the cosmogenic isotope (g·mole⁻¹) and m_{qtz} is the mass of quartz (g).

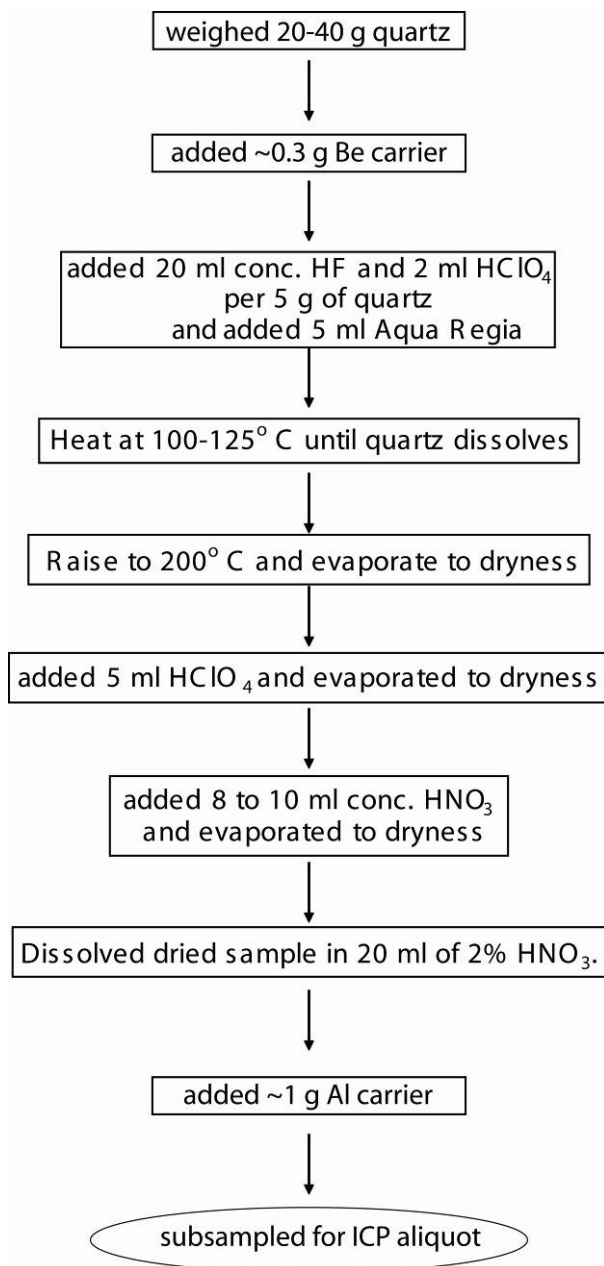


Figure A4.1 Generic procedure for quartz dissolution and ICP-AES subsampling.

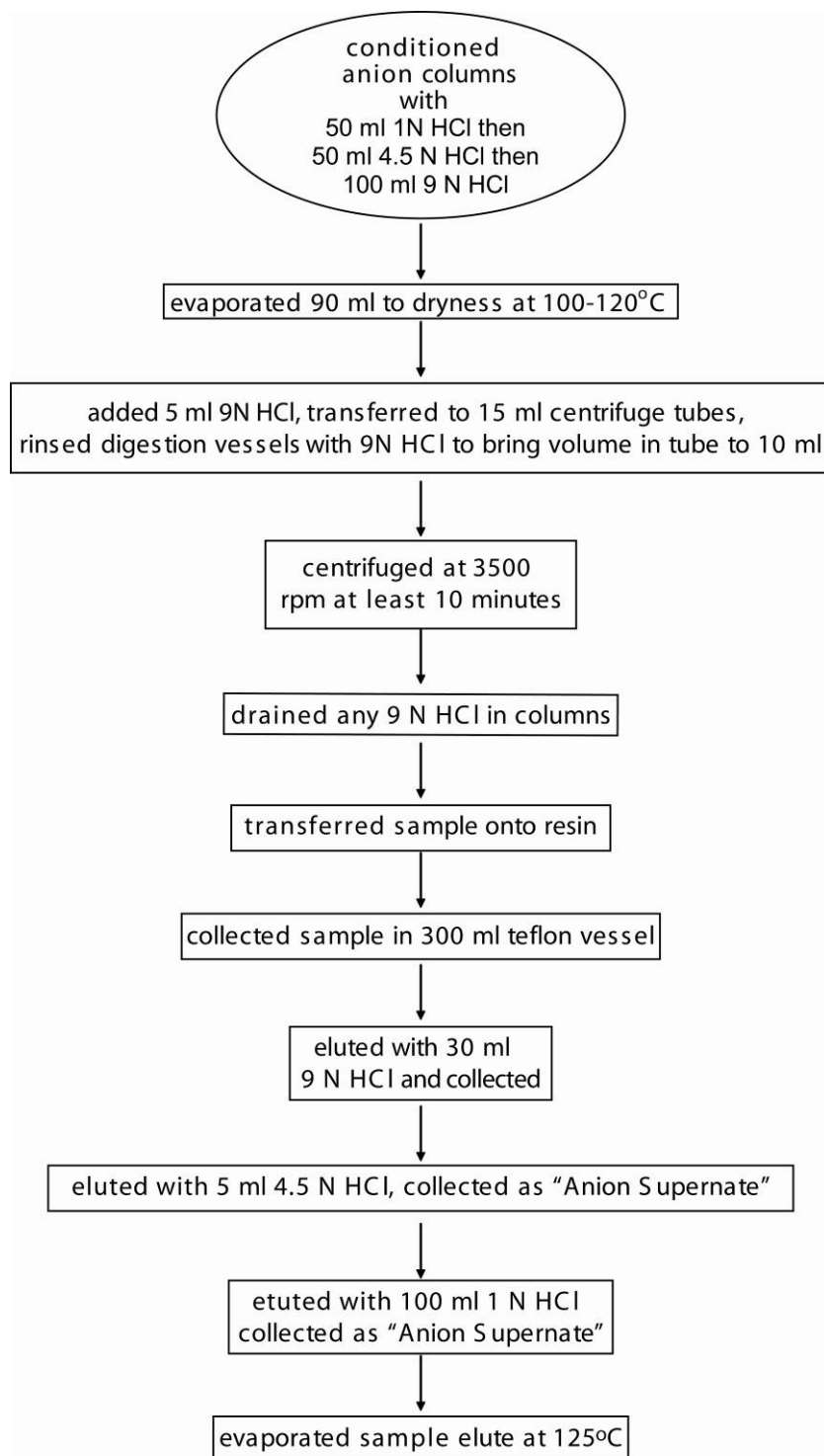


Figure A4.2 Generic procedure for anion column chemistry.

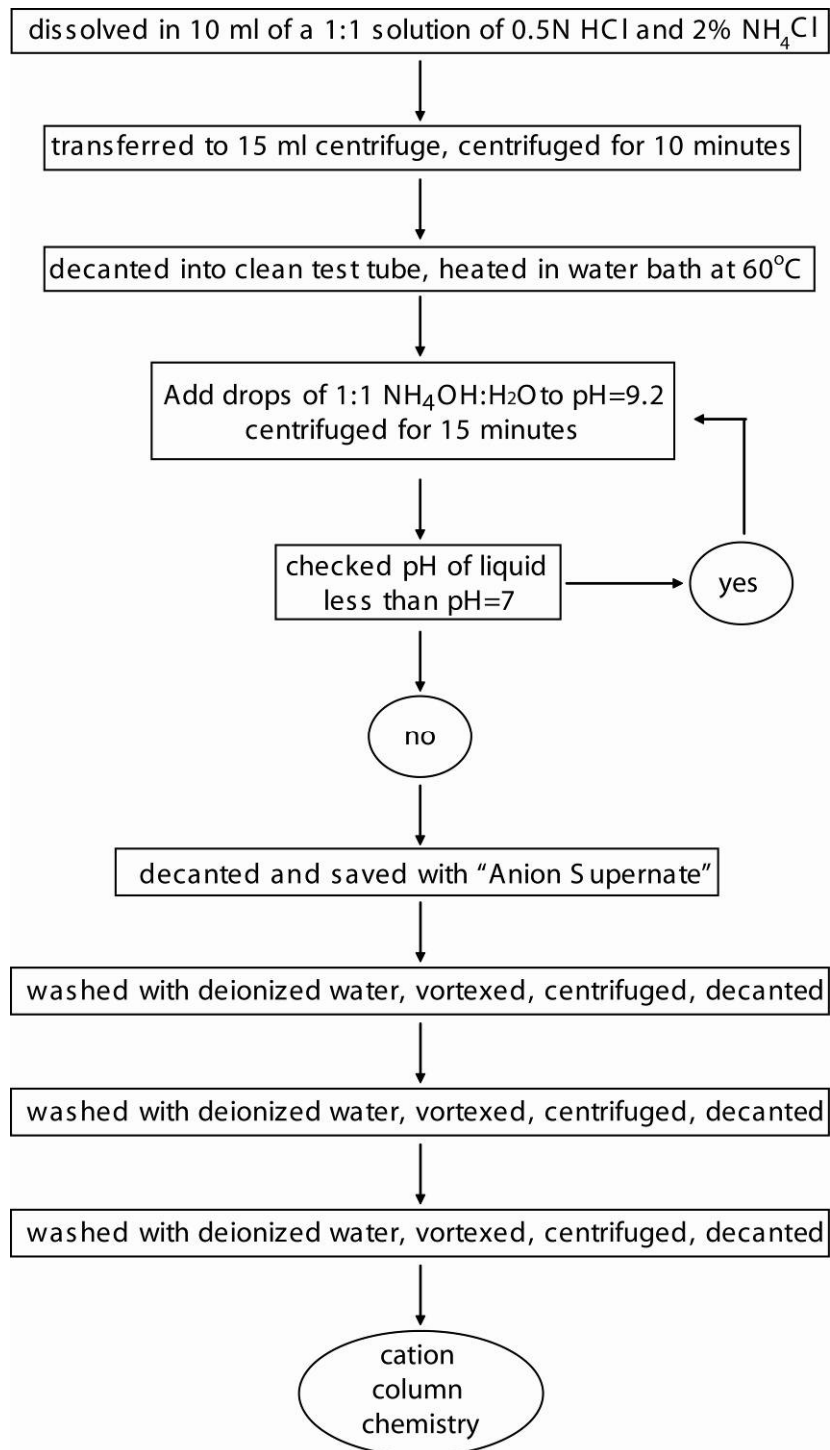


Figure A4.3 Generic procedure for controlled precipitate chemistry.

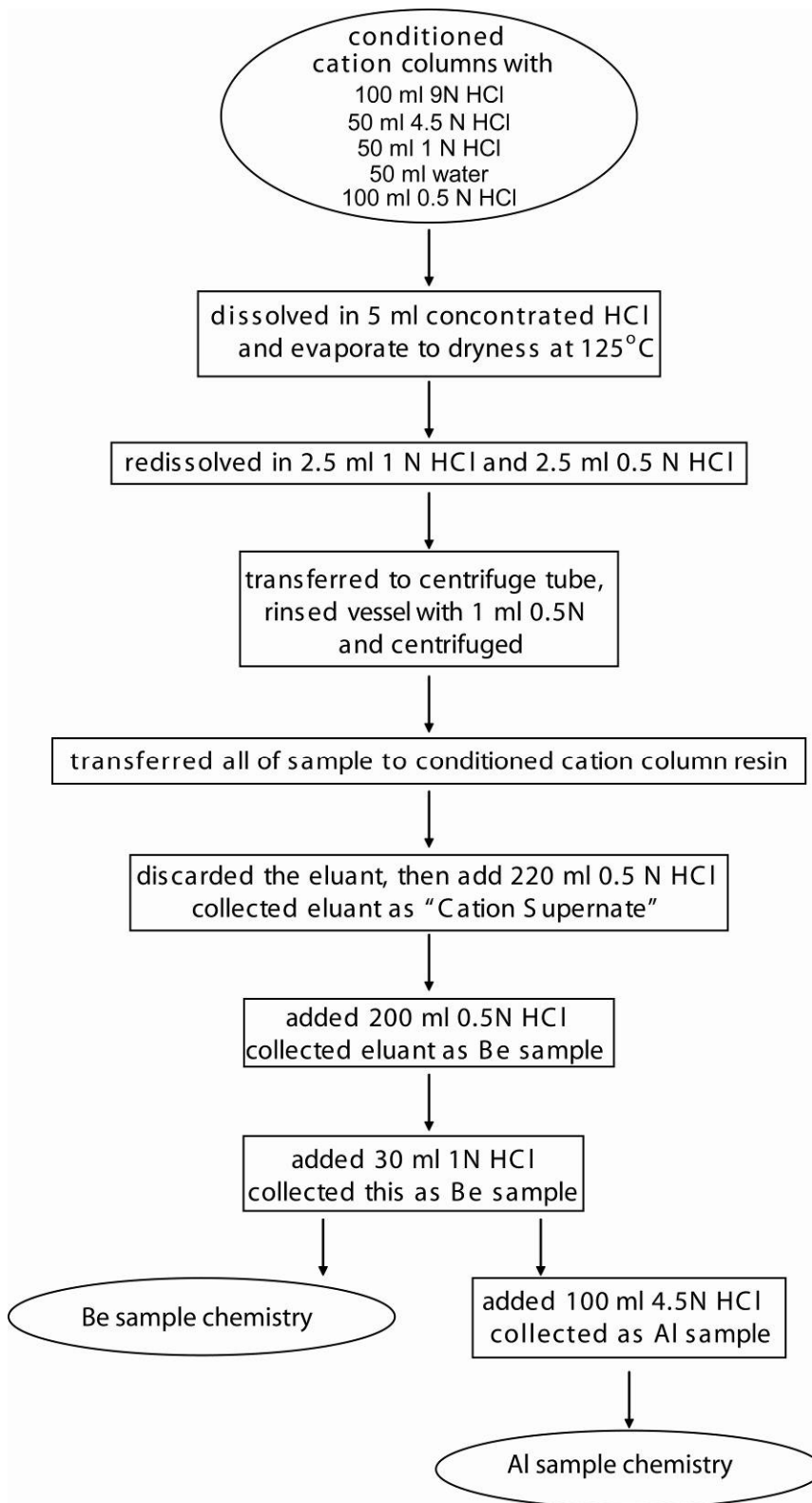


Figure A4.4 Generic procedure for cation column chemistry.

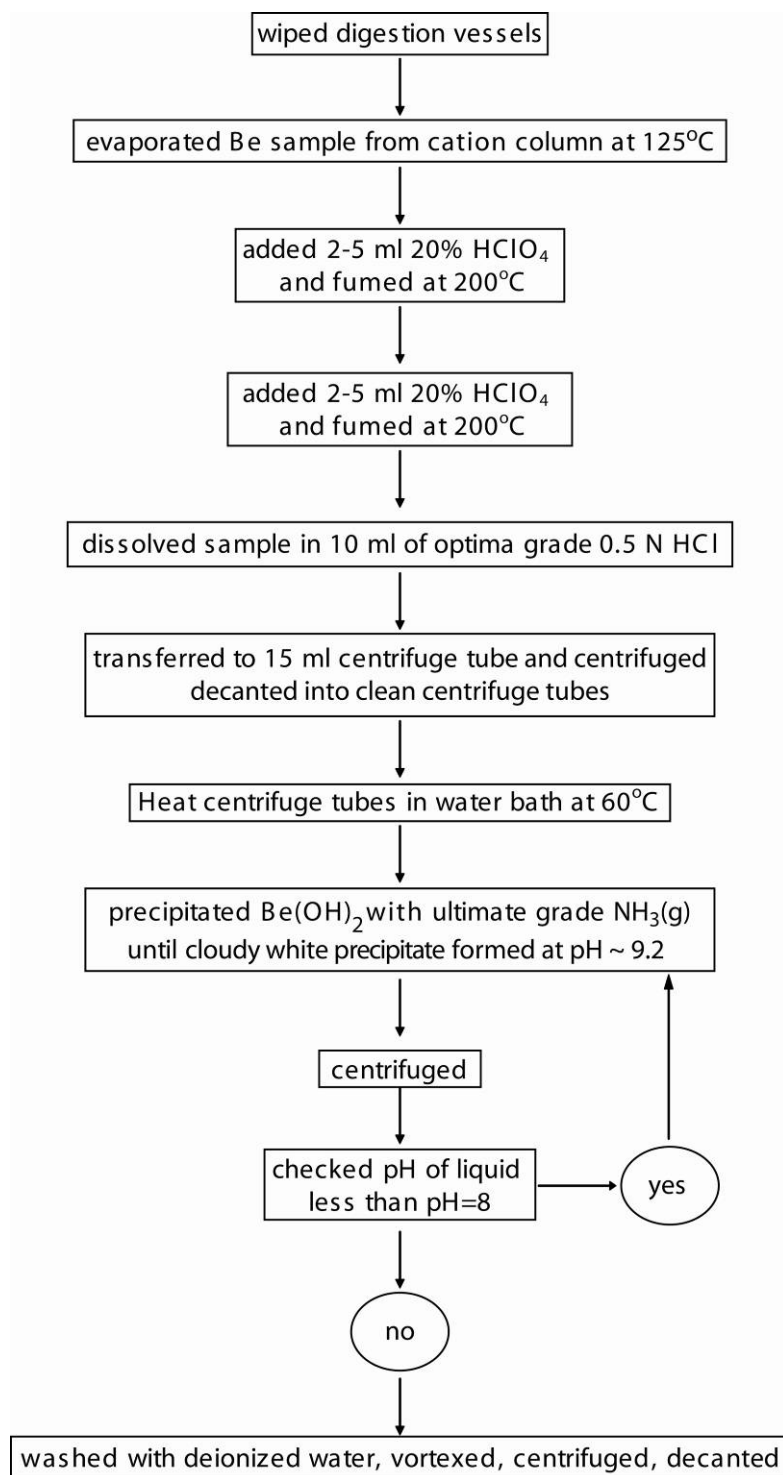


Figure A4.5 Generic procedure for Be sample chemistry.

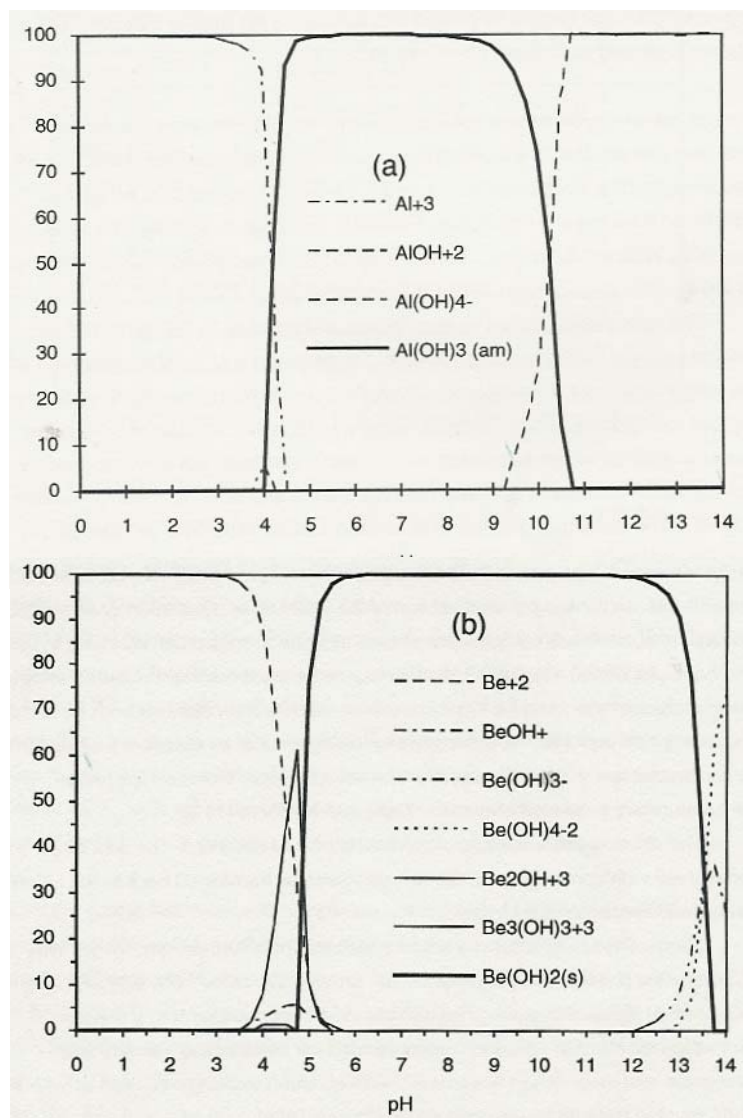


Figure A4.6 Speciation with pH diagram for **a.** Al and **b.** Be (from Ochs and Ivy-Ochs, 1996).

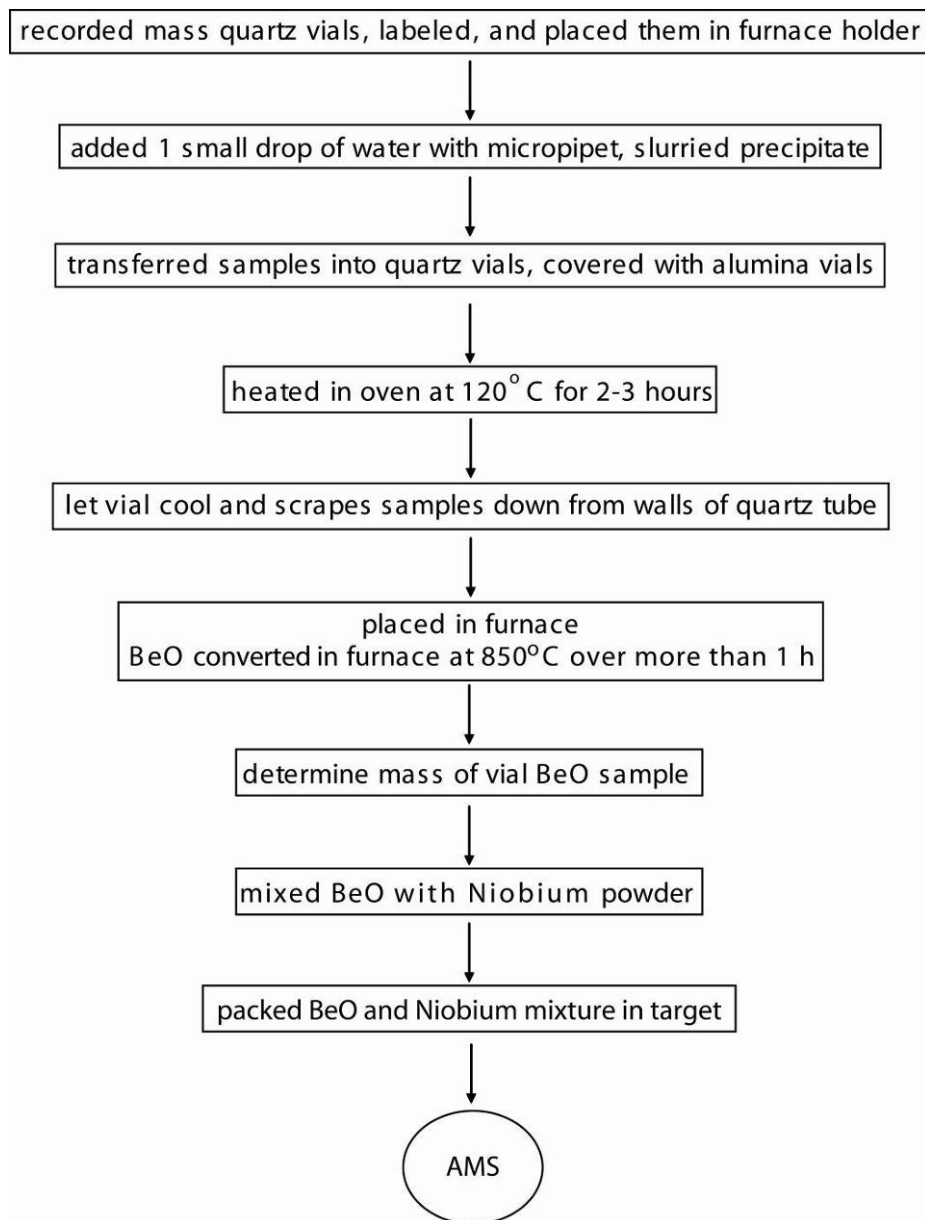


Figure A4.7 Generic procedure for Be oxide preparation.

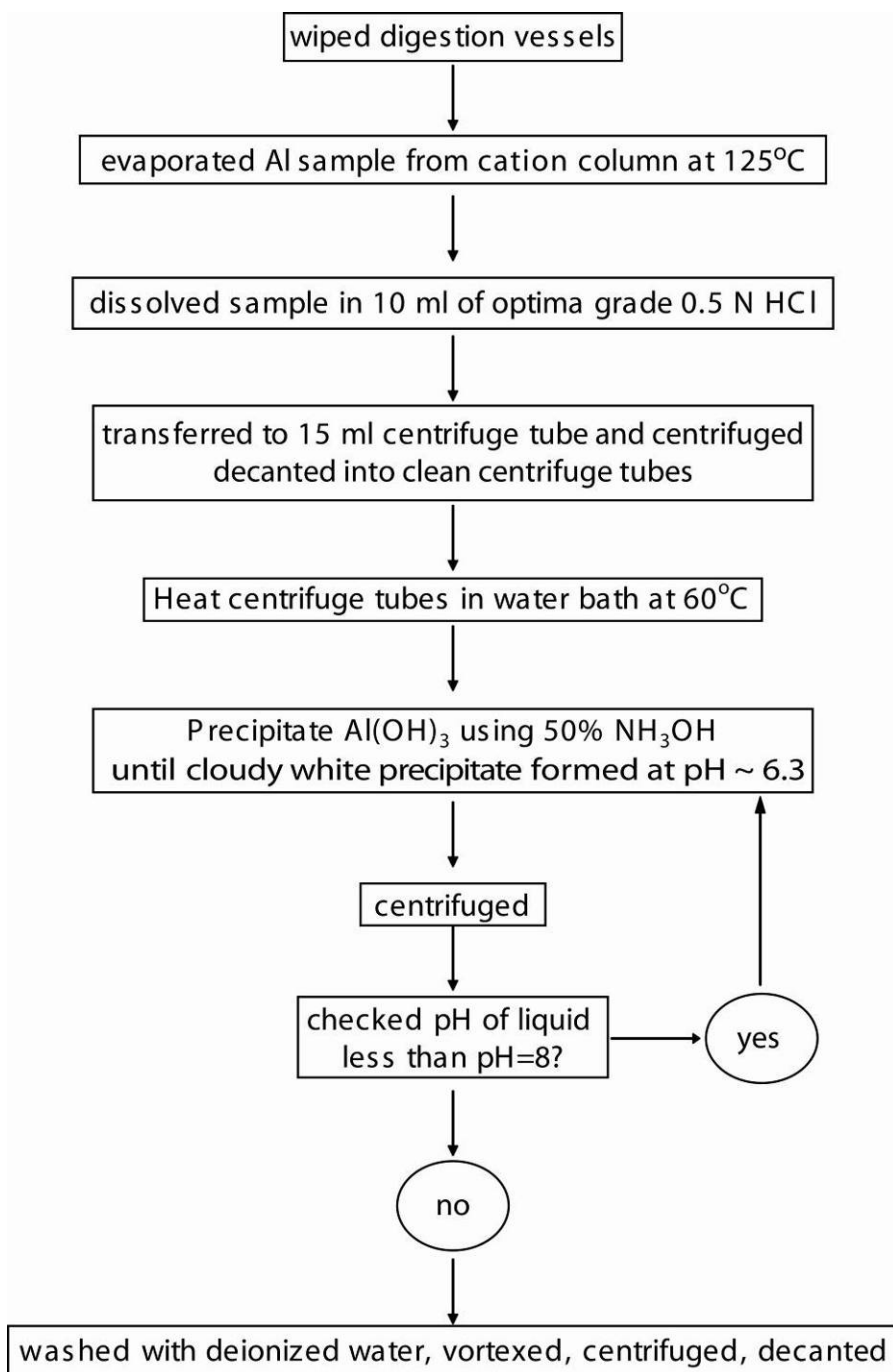


Figure A4.8 Generic procedure for Al sample chemistry.

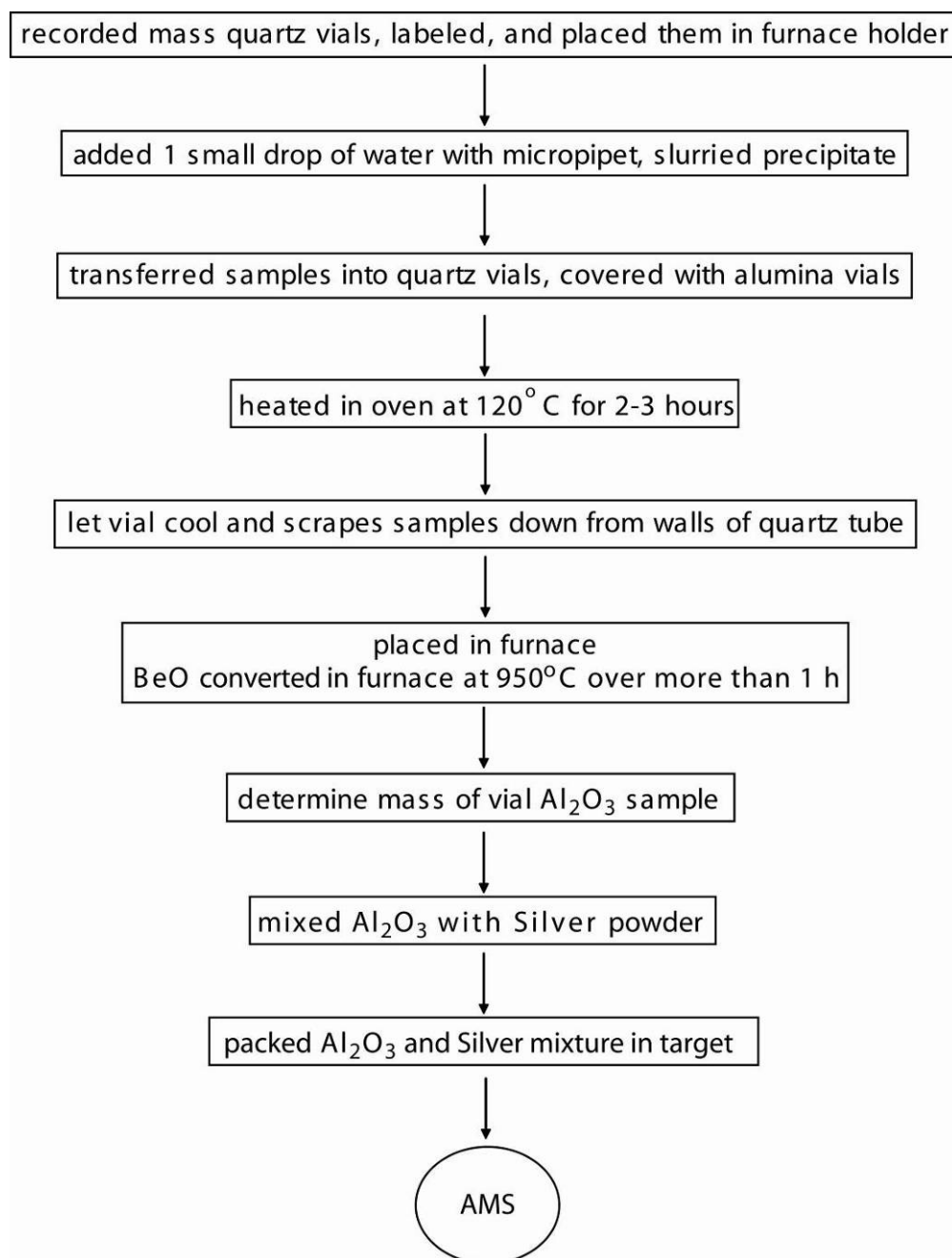


Figure A4.9 Generic procedure for Al oxide preparation.

Table A4.1 Chemical data for Labrador samples.

Sample name	CNEF#	Qtz mass (g)	mass carrier soln (g)	$^{10}\text{Be}/^9\text{Be}$ Corr. for Bckgrd & Boron	$^{10}\text{Be}/^9\text{Be}$ Error	AMS Precision (%)	Notes
Blank	1151	---	0.5531	5.11E-15	1.87E-15	37%	---
LAB-02-NACH-201	1290	40.0088	0.6617	9.70E-14	8.45E-15	9%	mountain north of basecamp: bedrock
LAB-02-NACH-202	1291	40.0463	0.5548	1.22E-13	3.51E-15	3%	mountain north of basecamp: erratic
LAB-02-NACH-203	1292	40.0216	0.5545	3.42E-13	9.22E-15	3%	mountain north of basecamp: erratic
LAB-02-NACH-204	1293	40.0196	0.5585	1.14E-13	3.47E-15	3%	mountain north of basecamp: bedrock
LAB-02-TRNS-210	1294	40.1296	0.5642	4.63E-13	1.42E-14	3%	southeast of basecamp: summit
LAB-02-TRNS-211	1295	40.0998	0.5615	2.77E-13	7.94E-15	3%	southeast of basecamp: summit
LAB-02-TRNS-212	1296	40.1698	0.5543	1.08E-13	4.66E-15	4%	southeast of basecamp
Blank	1152	---	0.5505	6.51E-15	1.41E-15	22%	---
LAB-02-TRNS-215	1300	40.7359	0.5500	9.84E-14	4.46E-15	5%	southeast of basecamp
LAB-02-TRNS-216	1301	40.1536	0.5618	1.77E-13	5.14E-15	3%	southeast of basecamp: moraine boulder
LAB-02-NACH-221	1304	40.1553	0.5596	2.62E-12	5.40E-14	2%	Jacques Rousseau peak
LAB-02-NACH-222	1305	40.8708	0.5501	2.68E-13	7.38E-15	3%	erratic on J.R. summit hilltop
LAB-02-NACH-223	1306	39.9051	0.5930	1.25E-12	2.42E-14	2%	hill summit ESE of Jacques Rousseau peak
LAB-02-NACH-225	1308	40.0806	0.5640	1.55E-12	2.66E-14	2%	Inuit Mountain, highest bedrock but fels. is higher
LAB-02-NACH-226	1309	40.1150	0.5686	1.09E-12	3.10E-14	3%	w. of palmer rv. valley, s. of Nackvak: tor summit
Blank	1153	---	0.5545	6.24E-15	8.95E-16	14%	---
LAB-02-TRNS-213	1297	40.0910	0.5560	1.04E-13	3.97E-15	4%	southeast of basecamp
LAB-02-KOROC-230	1310	36.1961	0.5975	5.68E-14	2.63E-15	5%	postdates the 890 m lake level
LAB-02-ARROW-233	1313	40.1775	0.5689	7.79E-14	4.30E-15	6%	Qaht2 moraine, second inland from lake
LAB-02-ARROW-234	1314	40.0427	0.5581	8.00E-14	3.69E-15	5%	Qaht2 moraine, second inland from lake
LAB-02-LAKE-217	1328	40.1520	0.5571	4.45E-13	1.13E-14	3%	highest lake level, sample should date the lake
LAB-02-LAKE-218	1329	40.0000	0.5630	4.45E-13	1.14E-14	3%	highest lake level, sample should date the lake
LAB-02-STK-228	1331	20.0707	0.3131	8.19E-14	2.48E-15	3%	Stecker River drainage divide
LAB-02-STK-229	1332	20.0314	0.3090	9.14E-14	4.79E-15	5%	Stecker River Drainage Divide
LAB-02-KOROC-231	1311	40.0274	0.3056	1.34E-13	2.99E-15	2%	postdates the 890 m lake level
LAB-02-TRNS-214	1298	20.0460	0.3014	8.91E-14	2.46E-15	3%	southeast of basecamp

Table A4.2 Baffin Island till sample Be chemistry data

Sample name	CNEF#	Qtz mass (g)	mass carrier soln (g)	¹⁰ Be/ ⁹ Be Corr. for Bckgrd & Boron	¹⁰ Be/ ⁹ Be Error	AMS Precision (%)	Notes
Blank	1500	---	0.3094	4.10E-15	5.53E-16	13%	---
Baffin 21686	1515	20.5954	0.3123	6.45E-14	2.21E-15	3%	cold-based till
Baffin 21606	1507	40.3959	0.3020	7.51E-13	1.88E-14	3%	cold-based till
Baffin 21700	1517	30.0375	0.3073	2.96E-13	7.49E-15	3%	cold-based till
Baffin 21838	1520	20.1652	0.3194	9.98E-14	3.46E-15	3%	cold-based till
Blank	1501	---	0.3060	4.89E-15	5.90E-16	12%	---
Baffin 21679	1508	20.0308	0.3109	1.86E-12	4.34E-14	2%	cold-based till
Baffin 21681	1509	20.4050	0.3055	1.46E-12	3.37E-14	2%	cold-based till
Baffin 21808	1510	20.0132	0.3000	2.62E-12	6.05E-14	2%	cold-based till
Baffin 21830	1511	20.0666	0.3031	7.19E-13	1.89E-14	3%	cold-based till
Baffin 21834	1518	20.2124	0.3020	7.18E-14	2.75E-15	4%	cold-based till
Baffin 21836	1519	20.2700	0.3031	7.66E-14	2.24E-15	3%	cold-based till
Blank	1502	---	0.3057	4.94E-15	5.02E-16	10%	---
Baffin 21871	1521	20.6060	0.3030	2.22E-14	1.72E-15	8%	warm-based till
Baffin 21803	1523	20.1995	0.3021	6.45E-14	4.08E-15	6%	warm-based till
Baffin 21818	1524	20.0886	0.3082	1.83E-14	1.33E-15	7%	warm-based till
Baffin 21820	1525	20.4350	0.3012	4.77E-14	2.22E-15	5%	warm-based till
Baffin 21833	1527	20.2254	0.3052	5.09E-14	2.52E-15	5%	warm-based till
Blank	1503	---	0.3076	3.03E-15	4.45E-16	15%	---
Baffin 21604	1522	20.0103	0.3000	5.99E-14	2.02E-15	3%	warm-based till
Baffin 21831	1526	20.0183	0.3128	3.69E-14	1.89E-15	5%	warm-based till
Baffin 21858	1528	20.0261	0.3088	4.79E-13	1.11E-14	2%	cold-based till
Baffin 21684	1514	11.5770	0.3006	4.62E-13	1.21E-14	3%	cold-based till

Table A4.3 Baffin Island till sample Al-chemistry data. CNEF # with a * refers to samples originally run with a different quartz mass.

Sample name	CNEF#	Qtz mass (g)	mass carrier soln (g)	²⁶ Al/ ²⁷ Al Corr. for Bckgrd & Boron	²⁶ Al/ ²⁷ Al Error	AMS Precision (%)	Notes
Baffin 21686	1515	20.5954	0.0000	no current	---	---	cold-based till
Baffin 21606	1507	40.3959	0.0000	1.21E-12	4.16E-14	3%	cold-based till
Baffin 21700	1517*	20.0329	1.0143	4.85E-13	4.91E-14	10%	cold-based till
Baffin 21838	1520*	20.0568	0.0000	2.59E-13	1.23E-14	5%	cold-based till
Blank	1501	---	0.5004	5.57E-14	5.57E-14	100%	---
Baffin 21679	1508	20.0308	0.0000	4.56E-12	1.16E-13	3%	cold-based till
Baffin 21681	1509	20.4050	0.0000	7.90E-13	3.21E-14	4%	cold-based till
Baffin 21808	1510	20.0132	0.0000	1.34E-11	3.40E-13	3%	cold-based till
Baffin 21830	1511	20.0666	0.0000	3.20E-12	9.75E-14	3%	cold-based till
Baffin 21834	1518	20.2124	0.0000	1.96E-13	1.45E-14	7%	cold-based till
Baffin 21836	1519	20.2700	---	---	---	---	cold-based till
Blank	1538*	---	1.0036	8.20E-15	5.80E-15	71%	---
Baffin 21871	1521*	20.0642	0.0000	8.78E-14	1.72E-14	20%	warm-based till
Baffin 21803	1523*	20.0150	---	---	---	---	warm-based till
Baffin 21818	1524*	20.0318	0.0000	3.62E-14	7.57E-15	21%	warm-based till
Baffin 21820	1525*	20.0494	0.0000	1.42E-13	1.31E-14	9%	warm-based till
Baffin 21833	1527*	20.0188	0.0000	2.44E-13	2.53E-14	10%	warm-based till
Blank	1620*	---	1.0036	6.20E-15	6.20E-15	100%	---
Baffin 21604	1522	20.0103	---	---	---	---	warm-based till
Baffin 21831	1526*	20.0450	0.0000	2.56E-13	3.04E-14	12%	warm-based till
Baffin 21858	1528*	20.0166	0.4199	1.46E-12	7.51E-14	5%	cold-based till
Baffin 21684	1514*	11.5770	0.4023	1.94E-12	1.80E-13	9%	cold-based till

APPENDIX 5

ICE SHEET MODELING WITH UMISM

A5.1 INTRODUCTION

The model used to investigate the dynamic and spatially variable subglacial characteristics in Chapters 3 and 4 is called UMISM: the University of Maine Ice Sheet Model. Since the original two-dimensional map-plane model with a finite element method to solve the continuity equation for ice deformation appeared, UMISM has grown in sophistication to include temperature profiles (Fastook 1990, 1992, 1993). Eventually, UMISM was applied to glaciological problems in Fastook (1996); Fastook and Grosswald (1998); Fastook and Holmlund (1994); Fastook et al. (1995) and Fastook (1998). I ran the model in its January 2004 form on a Linux platform. The model was programmed in FORTRAN. Portions of the code that were originally described in Fastook and Chapman (1989) are still in the ice sheet model version that was run in 2004.

This section represents a synopsis of the fundamental building blocks of the existing ice sheet model and the basal water portion that allows us to answer those questions addressed in Chapters 3 and 4 that bear on the spatial variation of the basal water, velocity, and the presence of ice over the Torngat Mountains and Baffin Island during the last 100 ka. This appendix was written based on descriptions of UMISM found in Fastook et al. (2002), Johnson and Fastook (2003) and Johnson (2002).

For a glacier that is cold-based or frozen to its bed, ice flow is due to internal deformation of the ice (Paterson, 1994), which can be modeled more simply than glaciers that have an additional sliding component to basal velocity. For an ice sheet that has a mobile layer of water at its base, the computation and modeling becomes more difficult. As with many modeling endeavors, tradeoffs exist between functionality, computational speed, and accuracy.

The model uses a series of boundary conditions such as temperature, sea level, geothermal heat flux, and topography to control the initial conditions for the glacier bed as well as bounds on the flux of heat from the base of the ice (geothermal heat flux) and the surface of the ice (temperature). The boundary conditions form the foundation on which the computations are made to calculate isostatic effects, the distribution of heat, velocity, and basal water (Fig A5.1). The calculations are based fundamentally on the conservation of mass, energy and momentum. Within a dynamic ice sheet, these calculations can be described by very complicated multivariate 2-D non-linear differential equations. The domain on which the calculations are performed is often irregular and complex. Attempts to solve the equations can include using simplifying assumptions, such as a glacier in equilibrium with the climate, using iterative schemes, and making certain limiting assumptions. UMISM uses as standard numerical technique called finite-element method (FEM) to solve the conservation equations in a time-dependant situation. FEM has several advantages for use in an ice sheet model. The gridding within the domain on which the conservation equations are solved can be very irregular, and the boundary conditions can be easily specified along this irregular boundary (Fastook et al., 2002). The following sections describe the FEM calculations

that must be made based on given boundary conditions, the interdependence of these calculations, and the robustness of techniques for the purposes described in Chapters 3 and 4.

A5.2 BOUNDARY CONDITIONS

A5.2.1 CLIMATE

UMISM is a time-dependant ice sheet model, and as such, it can model ice sheets not in balance with the climate. In fact, changes in climates actually drive the evolution of the ice sheet model. The 100 ka paleoclimate was controlled by the $\delta^{18}\text{O}$ curve from the GRIP (GREENland Ice sheet Project) ice core from central Greenland, transformed to a temperature record (Johnsen et al., 1995)(Fig. A5.2). The mean annual temperature for each node varies by standard meteorological altitudinal and latitudinal lapse rate values (Fortuin and Oerlemans, 1990). Accumulation is calculated from temperature and surface slope. This climatology scheme for the model was developed and first published in Fastook and Prentice (1994).

The first priority in adjusting the model to match known regional ice configurations was to match known ice margins and basic flow patterns by adjusting parameters that are considered unknowns for the region. Adjusting the climate is done by adjusting the amplitude and offset of this climate record. The “climate knob” can be adjusted to change the distribution of precipitation. This distribution can be seen in the mass balance diagram in Fig. A5.3.

Although this technique has been employed successfully to recreate known paleo-ice margins, I attempted to use climate data from MM5 modeling output (Bromwich et al., 2004) for the last glaciation that incorporates the Laurentide Ice Sheet as a boundary condition with that model. This scheme included a linear fit between the NOAA-CIRES Climate Diagnostic Center NCEP Reanalysis climate dataset for present-day conditions (available online at: <http://www.cdc.noaa.gov/>) and MM5 simulated climate for the LGM climate. This method is circular but as there is no built-in General Circulation Model (GCM) in UMISM, it is probably the best compromise. However, this scheme for adjusting climate did not produce large-enough Laurentide ice and stopped-far short of the known LGM extents on both the southern and eastern margin of North America. The linear interpolation between LGM and NCEP II may have been a lingering problem in this attempt to better constrain the unknown climate.

A5.2.2 SEA LEVEL

The sea level record is derived from a northern hemisphere model simulation, including both the Laurentide Ice Sheet and the Scandinavian Ice Sheet all in one grid. The model calculated its own sea level equivalent locked up in continental ice. Because the model simulation does not include any sea level equivalent from Antarctic or South American ice, the sea level record is a lower bound and reaches a maximum of 100 m below current sea level (Fig. A5.4).

In our inset model simulations for the Torngat Peninsula and Baffin Island, a more rigorous technique would be to use local sea level curves. However, changing the

sea level had very little effect on the Torngat Peninsula or Baffin Island ice configuration and always produced an ice cap that extended to the continental shelf. In the Torngat region, unlike in southern Atlantic Canada, the deglaciation was probably not closely linked to sea level change and instead driven by climate forcing. In the Baffin Island simulation, the effect of changing the sea level curve and ice calving factor, even unrealistically, could not produce ice configuration that stopped before the edge of the shelf as is suggested by work conducted to the southeast of the 37G area (Briner et al., 2005).

A5.2.3 GEOTHERMAL HEAT FLUX

Geothermal heat flux is heat that is being transferred to the base of the ice sheet due to heat flowing from the Earth's crust. This heat source is incorporated into the temperature equation as a boundary condition. Geothermal heat flux varies widely within North America; northern hemisphere values are known to vary by as much as a factor of two (Hooke, 1998). However, the area investigated in this thesis in Chapter 3 potentially had a low geothermal heat flux due to a thick Proterozoic crustal root (Funck et al., 2001). In cold-based glaciers, this can be the greatest source of heat at the base of the ice. Johnson and Fastook (2001) conducted a sensitivity test to determine the effect of variation of geothermal heat flux has on ice configuration. Changing the geothermal heat flux by a factor of 40 resulted in less than a 7% change in ice volume or thickness of the LIS (Johnson, 2002).

A5.2.4 TOPOGRAPHY

The bed topography is from a gridded inset ETOPO2 2-minute DEM (Fig. A6.6). Land topography is from the GLOBE Project, an independently peer-reviewed global digital elevation model (DEM), at a latitude-longitude grid spacing of 30 arc-seconds (30"), provided by the National Geophysical Data Center. Coarser resolution topography based on sampling of GTOPO 30, a 30-arc second DEM forms the ice flux boundary conditions for the inset model (Fig. A5.5). A finer resolution is not supported by physics because of the assumptions in the shallow ice approximation and our estimates of realistic LGM ice thicknesses. The finest model resolution contained ~30,000 nodes on which it calculated those features of the ice sheet below.

A5.3 COMPUTATIONS

A5.3.1 ISOSTASY

This sinking of the Earth's crust due to a load placed on it is referred to as isostatic depression. Based on the principle of buoyancy, or density-driven adjustments, the amount of depression is one third of the thickness in ice. So, for central North America, depression is one third of 3500 m (a good estimate for the maximum Laurentide thickness). When the load is removed, the crust rebounds. Isostatic rebound and depression are not reached instantaneously, and there are various methods for considering

the time lag. Because feedback mechanisms controlling ice dynamics and accumulation depend directly on the depression of the bedrock, the ice dynamics and isostasy are critically linked and thus cannot be calculated separately in the model. A simple and effective method from Oerlemans (1980) used in UMISM considers the density differences, the thickness of the ice, and a characteristic relaxation time to calculate the new elevation of the bed. In practice, more rigorous formulations that consider the bending of a rigid elastic plate (Hughes, 1987) are computationally time consuming and for all runs conducted in Chapter 3 and 4 the simpler approach based on the simpler scheme is used.

A5.3.2 TEMPERATURE CALCULATIONS

The boundary conditions required for a solution to the equation are surface temperature (from climate) and the heat at the base (geothermal heat flux plus frictional heating). The frictional heating is dependant on sliding velocity that is dependant on the presence of water. Thus, the presence of water is inherently dependant on the heat calculation because without heat, ice will not melt. The temperature distribution in the ice sheet is based on a 1-D, vertical heat-flow equation that depends on ice density, specific heat of ice, the vertical diffusion of heat, the vertical advection of heat from accumulation and ablation, as well as internal heat generation. Because this 1-D calculation is solved at each node, the effect of horizontal advection and diffusion is neglected and the temperature distribution, which is a reasonable computational trade-off

for areas thought to be always covered by slow-moving, cold-based ice but becomes less rigorous in fiords and other areas with greater ice velocities.

Temperature dependence also exists in the flow parameters based on creep activation energies that change with temperature (Mellor and Testa, 1969 in Fastook et al., 2002). Some researchers have used a flow enhancement factor to simulate basal softening of ice and basal water (c.f. Hulbe, 1998, Naslund et al. 2003). A flow enhancement factor was not used in the simulations in Chapters 3 and 4 because the basal water model gives a better parameterization of the actual physical properties of ice and was a more rigorous treatment of the physics of basal sliding, basal flow and melt generation. Flow enhancement factors are also more appropriate for modeling areas with fast flowing ice riding on a deep-seated deformable bed, such as in the West Antarctic ice streams (Cuffey and Alley, 1996).

A5.3.3 SLIDING VELOCITY

Basal sliding is the mechanism responsible for the flow of ice beyond that due to internal deformation. For sliding to take place, there must be liquid water at the bed of the ice sheet. While the role of basal water remains largely unanswered, the common feature of the most general formulations of the basal sliding velocity is dependence on the presence of the water layer despite a lack of a fundamental formulation for faster flow. Sliding relations are numerous, but in most sliding laws as well as the sliding law used in UMISM (Johnson, 2002), basal sliding is a function of a constant multiplied by the basal shear (or driving) stress raised to a power, and a function depending on the thickness of

basal water raised to a power (effective pressure: Alley, 1989a; Alley 1989b). In Johnson and Fastook (2003), the exponents were considered variable parameters and were adjusted to fit the LIS to sea level equivalent of the ice sheet model. The sea level equivalent LIS volume arising from sliding law exponents of 1 and 2/3 provides the best sea level lowering of 125 m and 116 m, respectively. Larger exponents of 2 and 3 failed to produce today's nearly ice-free conditions during the present-day climate.

A5.3.4 BASAL WATER

The temperature distribution model and the determination of sliding velocity have a large and linked impact on the water model employed by Johnson and Fastook (2002). The basal water model is based on a conservation equation that relates the change in basal water layer thickness with time to the flux of the water, or the velocity of that water layer, plus whatever water contribution is from the temperature model, either basal melting or basal water freeze-on. The velocity of water at the base of the ice comes from the Manning equation (Schetz and Fuhs, 1996). The Manning equation is also used to describe the flow of water through pipes, so it immediately seems pertinent to the study of pressurized water conduits moving beneath glacier ice, but is less applicable when one considers the coarse resolution of the model. The applicability of the water model at this coarse scale is secondary to reproducing natural systems. Testing the water model against natural systems also allows calibration of fitting parameters to the sliding law.

Water pressure has been the focus of several glaciological studies of glacier dynamics and glacial erosion recently (Rothlisberger and Iken, 1981; Anderson et al.,

2004). Water pressure, although not specifically output from the model, is implicitly linked to the basal water scheme and so is tied to the velocity and heat calculations that determine the ice dynamics.

A5.4 SENSITIVITY ANALYSES

A5.4.1 INTRODUCTION

To investigate the sliding formulation and the importance of external boundary conditions, a series of sensitivity tests were conducted and reported in Huybrechts et al. (1995, 1996) and Johnson and Fastook (2002).

A5.4.2 EISMINT

One of the most important tests of the ice sheet model was participation in EISMINT (European Ice Sheet Modelling INiTiavite). This initiative established a comparison with other ice sheet models and produced similar results in agreement with other existing ice sheet models, and arguably, that they are all reproducing realistic ice dynamics. The results appear in Huybrechts et al. (1995, 1996). EISMINT considered ice sheet model applications to the Greenland and Antarctic ice sheets including thermo-mechanical coupling, grounding line treatments, and ice shelf models. Considering that Antarctica and Greenland Ice Sheets are the only extant terrestrial analogs for the

Laurentide Ice Sheet, these tests are important for assessing the results of UMISM to address the ice dynamics of the LIS, though there is no modern analog for the southern margin of the Laurentide Ice Sheet.

A5.4.3 COMPARISON WITH REAL EXAMPLES

Comparing model results with real data is also a sort of sensitivity study because it is important to see how much adjustment of a given parameter can reproduce known ice features. This kind of comparison also lends credit to the model's applicability for systems that no longer exist and thus cannot be checked. Johnson's (2002) comparison of predicted lakes based on the inventory of Siegert et al. (1996) with modeled lake locations from closed basins at the pressure-melting point beneath the Antarctic Ice Sheet shows a clear pattern of agreement. Another important test of the basal water component of UMISM is the reproduction of the pattern and magnitude of velocities of ice streams that flow into the Ross Ice Shelf, Antarctica. The overall shape of each of the Ross Ice Streams was remarkably similar to what has been measured by InSAR, including the upstream areas and tributaries. The model produces a very strong match in the pattern and amplitude Ice Stream D, Ice Stream E, Ice Stream B velocities or stagnation for Ice Stream C.

Especially pertinent to the applications of UMISM in this thesis, Johnson and Fastook (2002) demonstrated the crucial role the water model plays in UMISM in controlling ice sheet configuration. Johnson and Fastook (2003) experimented by adjusting the water model to determine the effect on the volume and configuration of the

northern hemisphere ice sheets over the last glacial cycle. As a check on the volume, global sea level data was used to match the equivalent ice volume. Simulations neglecting sliding altogether provide the worst results, grossly overestimating the contribution to sea level change, failing to terminate the glaciation properly, and producing ice sheets 1 km thicker (4.5 km) than those that were thought to have existed during the LGM (Johnson, 2002). Northern hemispheric ice sheets modeled without a relation between basal water and sliding velocity produces sea level change of 140 m during the LGM, whereas when the model related sliding to water depth, northern hemispheric ice sheets contributed 110 m sea level equivalent. 110 m sea level equivalent is closer to published estimates of global sea level changes from northern hemispheric ice build-up (125 m: Shackleton, 1987).

A5.5 DIFFICULTIES

Johnson (2002) noted several problems in the water model. The biggest problems that might affect the results in Chapters 3 and 4 are as follows:

- (1) There is a difference in time scales between the water model and the ice sheet model.
- (2) The lack of horizontal advection in the temperature model overestimates the heat flux.
- (3) As mentioned above, there are also different spatial scales between the ice sheet and the basal water system. The scale problem also affects attempt to link

bedrock TCN records of sub-glacial thermal regimes and the coarse resolution required by the shallow ice approximation in the ice sheet model.

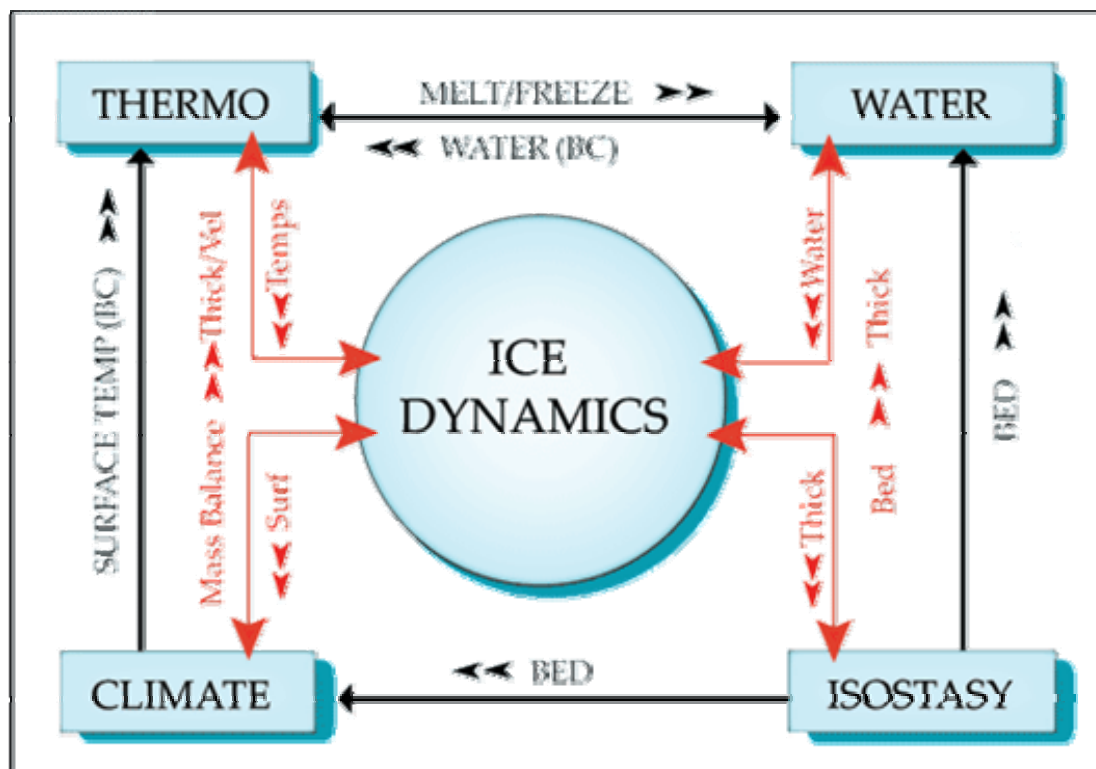


Figure A5.1 The major components of the ice sheet model. The major internal components of the ice sheet model are; ice flow, ice sliding, Isostasy, temperature distribution, and basal water flow. The figure also shows that each component exists within the boundary conditions. Figure taken from <http://www.ume.maine.edu/iceage/Research/Contrib/html/contrib15.html>.

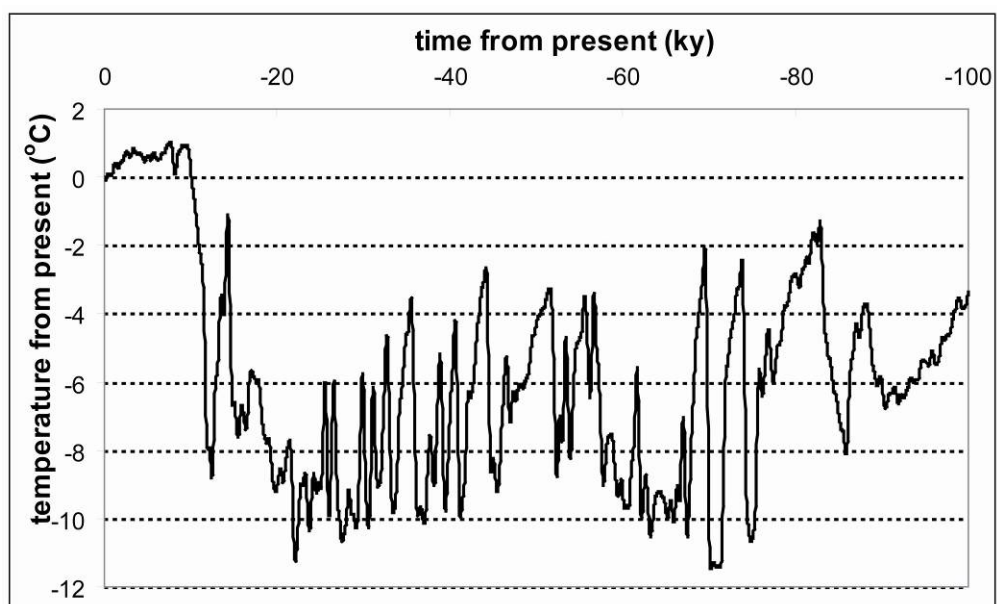


Figure A5.2 Temperatures used for the initial temperature input from Johnsen et al. (1995). GRIP core results calibrated in terms of change from present temperature. Zero years is present day.

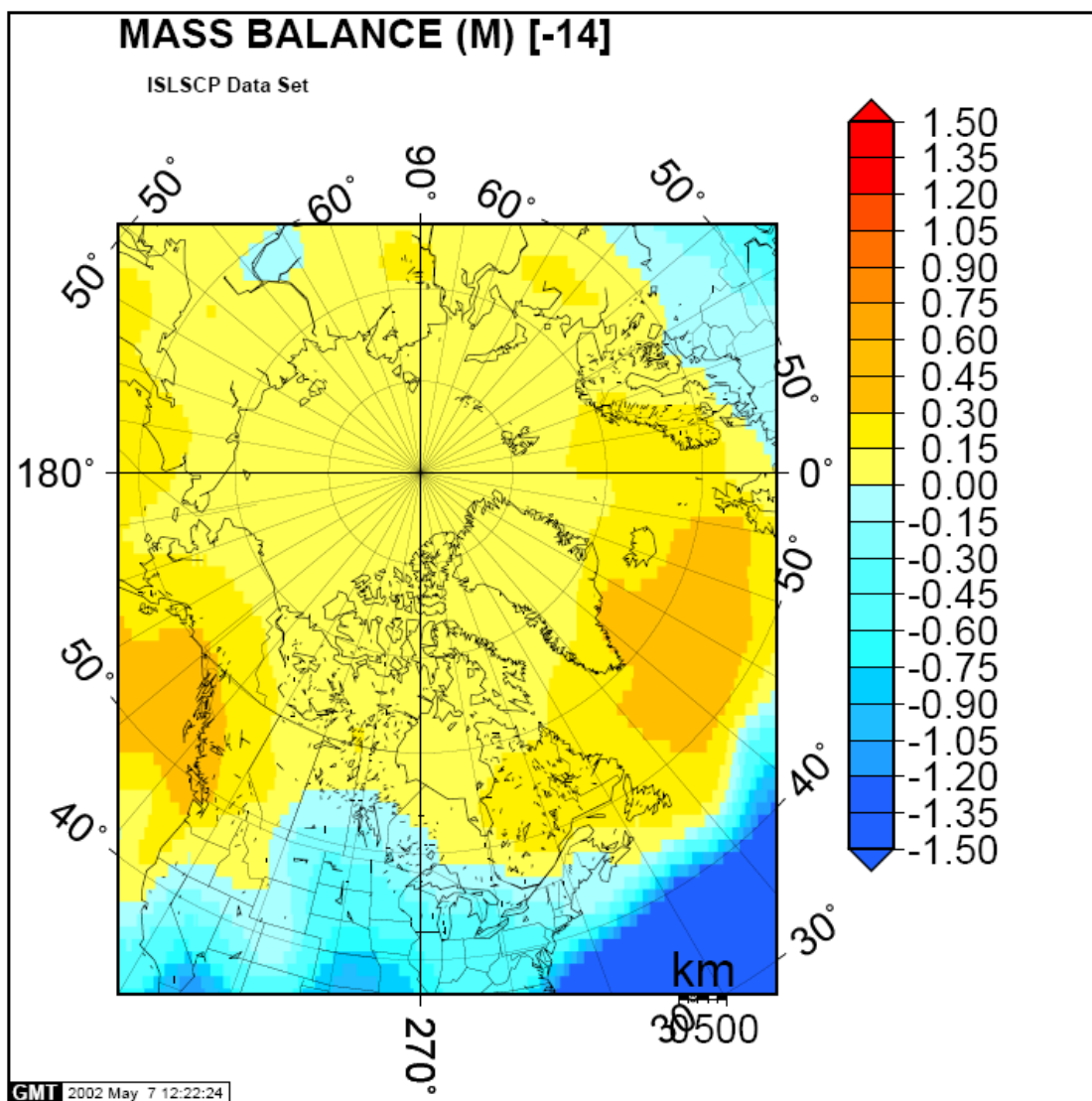


Figure A5.3 Net mass balance for climate “knob” setting 14, figure from Fastook et al. (2002).

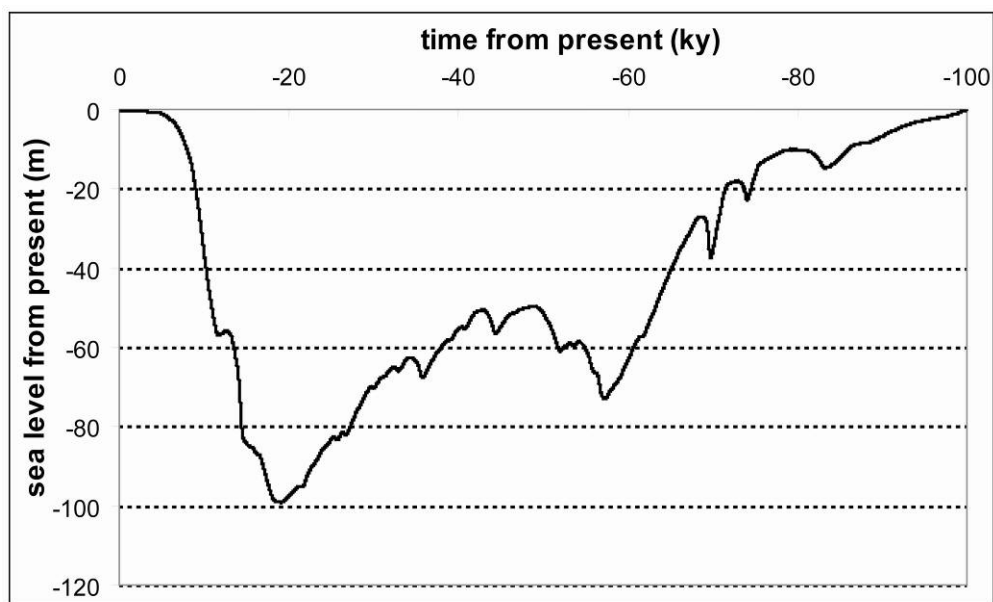


Figure A5.4 Sea level used for the sea level input derived from a model run for the Northern Hemisphere. This dataset does not include the sea level contribution due to Antarctic or South American ice cover. The pattern, but not the amplitude of this diagram, matches the SPECMAP sea level compilation.

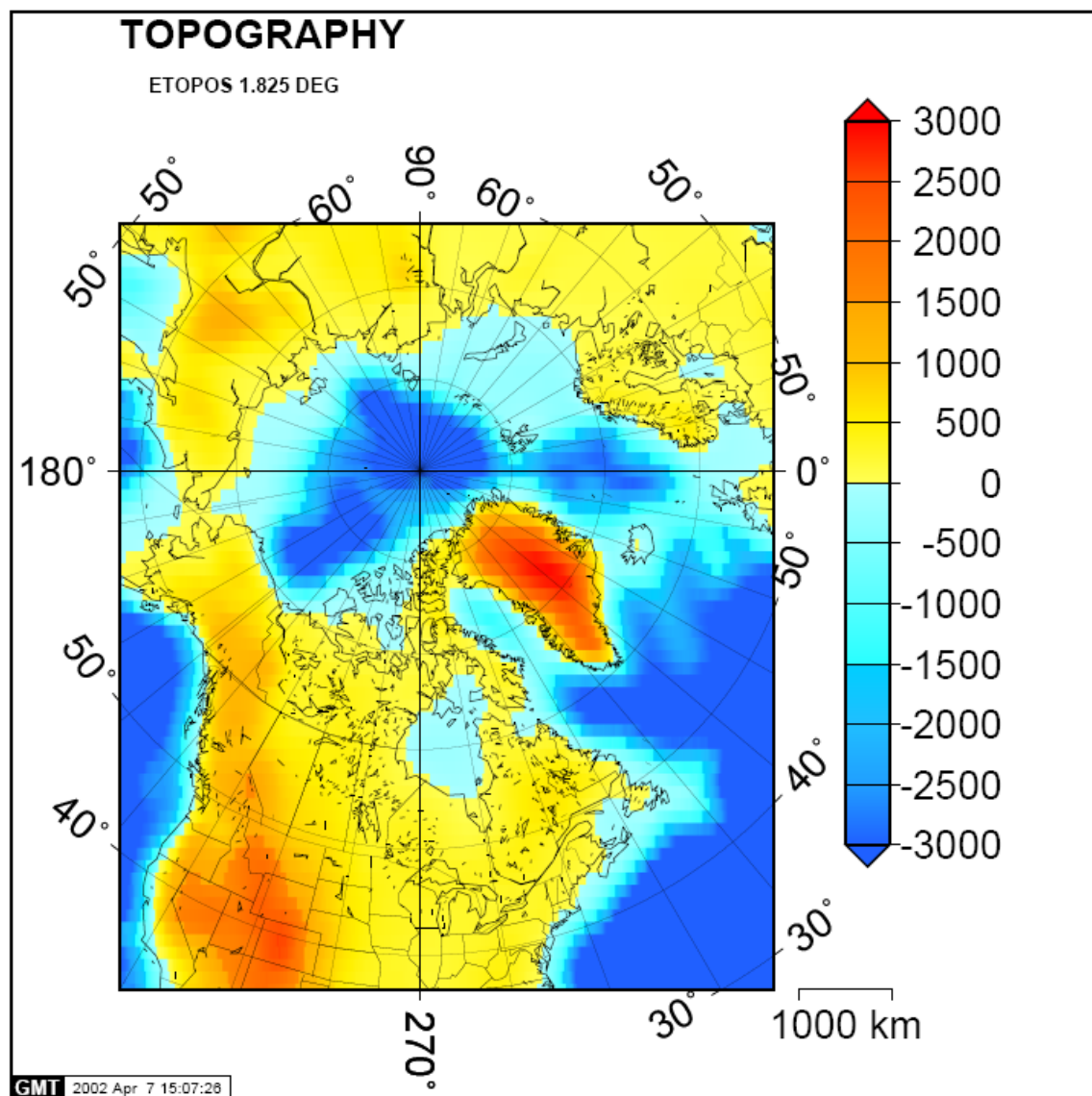


Figure A5.5 Gridded ETOPO 30 dataset used for the North America ice simulation was coarsely sampled by UMISM (1.8 deg. by 1.8 deg.). Figure is from Fastook et al. (2002).

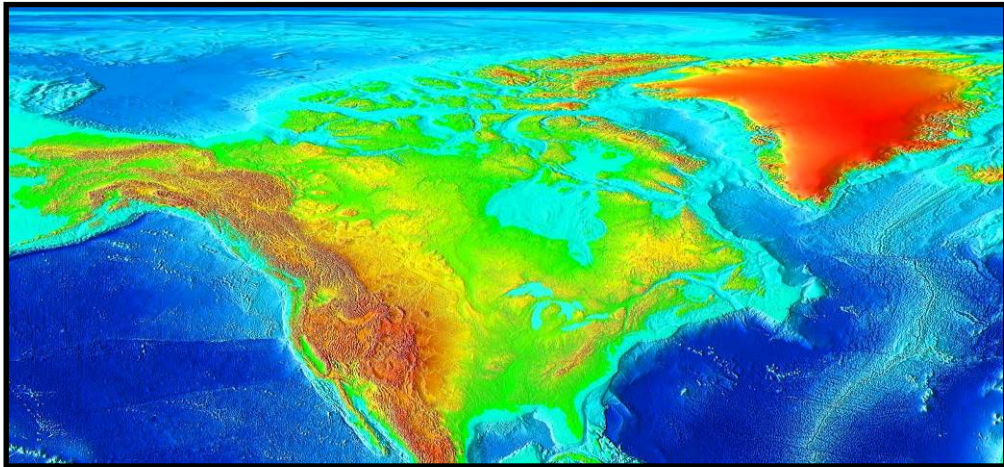


Figure A5.6 Bed topography ETOPO2 gridded elevation dataset from the National Geophysical Data Center (<http://www.ngdc.noaa.gov/>).

APPENDIX 6

USISM INSTRUCTIONS AND PARAMETER TABLES

A6.1 INTRODUCTION

Using UMISM consists of three main parts: selecting the boundary conditions (e.g. bed selection), running the ice sheet model and post-processing of output data. Throughout the instructions, executable files are designated by a “.e” or “.x” suffix and user input tags that distinguish the separate runs are designated by a wildcard asterisk “*”. After each run of the ice sheet model, a “console.*” file is saved that contains the input parameters for each run. The each individual simulation was run a number of times (between 5-20 times for all the inset and bounding models) with different parameters. The parameters of each simulation were assessed based on the match with known ice margin positions during the last deglaciation. These positions were based on maps compiled by Dyke et al. (2003) for the Laurentide Ice Sheet and Baffin Island and on maps compiled by Gray et al. (2002) for deglaciation of the Torngat Peninsula and Ungava Bay. The console.* files that were used to simulate the bounding and inset ice dynamics are given in Tables A6.1 – A6.2.

A6.2 BED SELECTION

1. read2n.e – selected the input area within the etopo5 dataset
 - a. designated the number of columns and rows
 - b. input the limits of the highest and lowest elevations within the etopo5 dataset
2. send the file out3a.data to the mapq directory
3. unpack.e * * – wrote the file to binary form

or

1. extract1.x – selected the input area within the etopo2 dataset
 - a. designated the number of elements needed to sample the dataset
2. sent the file *.data to the mapq directory
3. unpack.e * * – wrote the file to binary form

A6.3 ICE SHEET MODEL

1. map5.e * * – ran the ice sheet model for the given boundary condition files from the mapq directory
 - a. saw default setting list and checked which parameters needed to be changed since the last run or saw message that boundary condition files were not found
 - b. chose a climate scenario from the climate menu
 - c. chose to adjust the model parameters

- i. chose to graph data and parameters (e.g. thickness, velocity, bed melting, fraction of velocity due to sliding, bed depression, volume in sea level equivalence) through the model run
- ii. toggled the water model on
- iii. toggled the temperature calculation to full
- iv. toggled the Isostasy calculation to simple
- v. set the flow law constant
- vi. changed other dataset parameters
 1. set initial time
 2. set the time-step and output interval
 3. decided whether to change/changed the pole position
 4. modified flow enhancement factor
 5. adjusted the climate curve
 6. set the model to run on high-resolution datasets (if applicable)
- vii. quit adjusting parameters
- d. ran the model with adjusted parameters
- e. quit the program

A6.4 POST-PROCESSING

1. Ran pack1.e * *
 - a. Extracted timesteps to visualize

2. Ran `genmake.e * *` to make a GMT (Generic Mapping Tools)TM-ready script
3. Adjusted the GMTTM script
4. Ran the GMTTM script (`generic-erosion.gmt` or `generic.gmt`)

Table A6.1. Console.* file parameter selections for map5.e runs for Torngat Peninsula.

console.namer_pole_12	console.tornbaffhi_res6	console.torn_ice_cap4	console.torn_ice_cap6
17	17	17	17
0	0	0	0
1	1	1	1
h	h	h	h
h	h	h	h
o	h	a	a
t	a	c	c
c	v	e	e
e	i	-100000.	-100000.
-100000.	10. 100. 1000. 1	k	k
c	o	1.2 0.	1.2 0.
t	l	c	c
200 10 500.	c	5	5
c	e	1	1
d	-100000.	c	c
-999.	k	1	1
31	1.2 0.	14.	14.
c	c	c	c
l	a	y	y
-9.	0.5	10. 100. 1000. 1	10. 100. 1000. 1
a	c	o	o
r	6	w	w
m	c	8	8
s	5	c	c
-	1	t	t
-400.	c	4000 200 20.	16000 200 5.
c	l	q	q
v	14.25	1	1
-10.	c	v	v
10.	t	i	i
s	8000 200 10.	1	1
9	q	1	1
c	1	c	c
v	3	e	e
-1.	1	-20000.	-20000.
0.1	c	c	c
c	e	t	t
y	-20000.	1000 200 20.	4000 200 5.
8	c	b	b
a	t	y	y
r	2000 200 10.	0	0
m	b	y	y
c	y	y	y
o	0	0	0
1900. -1700.	y	q	q
q	y	1	1
1	0	-9	-9
1	q		
-9	1		
	-9		

Table A6.2. Console.* file parameter selections for map5.e runs for Baffin Island.

console.namer_pole_12	console.tornbaffhi_res_6	console.etopo37G_92	console.etopo37G_94
17	17	17	17
0	0	0	0
1	1	1	1
h	h	h	h
h	h	h	h
o	h	a	a
t	a	c	c
c	v	e	e
e	i	-100000.	-100000.
-100000.	10. 100. 1000. 1	k	k
c	o	1.2 0.	1.2 0.
t	l	c	c
200 10 500.	c	5	5
c	e	1	1
d	-100000.	c	c
-999.	k	l	l
31	1.2 0.	14.	14.
c	c	c	c
l	a	y	y
-9.	0.5	10. 100. 1000. 1	10. 100. 1000. 1
a	c	o	o
r	6	w	w
m	c	8	8
s	5	c	c
-	l	t	t
-400.	c	4000 200 20.	16000 200 5.
c	l	q	q
v	14.25	l	l
-10.	c	v	v
10.	t	i	i
s	8000 200 10.		
9	q	1	1
c	l	l	l
v	3	c	c
-1.	l	e	e
0.1	c	-20000.	-20000.
c	e	c	c
y	-20000.	t	t
8	c	1000 200 20.	4000 200 5.
a	t	b	b
r	2000 200 10.	y	y
m	b	0	0
c	y	y	y
o	0	y	y
1900. -1700.	y	0	0
q	y	q	q
l	0	l	l
l	q	-9	-9
-9	l		
	-9		

APPENDIX 7

DERIVATION OF DEPTH CALCULATIONS USED IN CHAPTER 4

Production with depth (z):

$$P_z = P_o e^{-z\rho/\Lambda} \quad (\text{Eq. A7.1})$$

where P_o is surface production of TCN, P_z is TCN production at depth, z. Bulk density is ρ . The mass attenuation length is Λ .

Solve for z:

$$\frac{P_z}{P_o} = e^{-z\rho/\Lambda} \quad (\text{Eq. A7.2})$$

$$\ln \frac{P_z}{P_o} = \frac{-z\rho}{\Lambda} \quad (\text{Eq. A7.3})$$

$$-z = \frac{\Lambda}{\rho} \ln \frac{P_z}{P_o} \quad (\text{Eq. A7.4})$$

substitute $\frac{P_z}{P_o}$ for $\frac{N_{meas} - N_{post}}{N_{max}}$

where N_{meas} is the measured TCN concentration, N_{post} is the post-glacial contribution to the measured concentration, and N_{max} is the maximum measured concentration.

The z in this equation is the lower bounds for the erosion depth calculation assuming negligible glacial comminution of the inherited TCN depth profile.

Production over a depth ($z_2 > z_1 \geq 0$).

$$P_{z_2 \text{ to } z_1} = \int_{z_1}^{z_2} P_o e^{-z\rho/\Lambda} dz = \frac{-P_o \Lambda}{\rho} e^{-z\rho/\Lambda} \Big|_{z_1}^{z_2} \quad (\text{Eq. A7.5})$$

$$= \frac{-P_o \Lambda}{\rho} e^{\frac{-z_2 \rho}{\Lambda}} - \frac{-P_o \Lambda}{\rho} e^{\frac{-z_1 \rho}{\Lambda}} \quad (\text{Eq. A7.6})$$

$$= \frac{-P_o \Lambda}{\rho} \left(e^{\frac{-z_1 \rho}{\Lambda}} - e^{\frac{-z_2 \rho}{\Lambda}} \right) \quad (\text{Eq. A7.7})$$

set $z_1=0$, the surface.

$$P_{z_2 \text{ to } z_1} = \int_{z_1}^{z_2} P_o e^{-z\rho/\Lambda} dz = \frac{-P_o \Lambda}{\rho} e^{\frac{-z\rho}{\Lambda}} \Big|_0^{z_2} \quad (\text{Eq. A7.8})$$

$$= \frac{-P_o \Lambda}{\rho} e^{\frac{-z_2 \rho}{\Lambda}} - \frac{-P_o \Lambda}{\rho} \quad (\text{Eq. A7.9})$$

$$= \frac{-P_o \Lambda}{\rho} \left(1 - e^{\frac{-z_2 \rho}{\Lambda}} \right) \quad (\text{Eq. A7.10})$$

solving for z_2 :

$$\frac{\rho}{P_o \Lambda} P_{z_2 \text{ to } 0} = 1 - e^{-z_2 \rho / \Lambda} \quad (\text{Eq. A7.11})$$

$$1 - \frac{\rho}{P_o \Lambda} P_{z_2 \text{ to } 0} = e^{-z_2 \rho / \Lambda} \quad (\text{Eq. A7.12})$$

$$\ln \left(1 - \frac{\rho}{P_o \Lambda} P_{z_2 \text{ to } 0} \right) = -\frac{z_2 \rho}{\Lambda} \quad (\text{Eq. A7.13})$$

$$z_2 = -\frac{\Lambda}{\rho} \ln \left(1 - \frac{\rho}{P_o \Lambda} P_{z_2 \text{ to } 0} \right) \quad (\text{Eq. A7.14})$$

substitute $\frac{P_{z_2 \text{ to } 0}}{P_o}$ for $\frac{N_{meas} - N_{post}}{N_{max}}$ to solve for z_2 .

The z_2 in this equation is the upper bounds for the erosion depth calculation assuming complete glacial mixing of the production profile from the surface to the depth of erosion.

APPENDIX 8





DALHOUSIE
University

Faculty of
Graduate Studies

STUDENT CONTRIBUTION TO MANUSCRIPTS IN THESIS

NAME: Jane Kathryn Willenbring Staiger	STUDENT ID #: B00163136
DEPARTMENT: Earth Sciences	PROGRAMME: Ph.D.
PHONE: 902-494-1211	E-MAIL: jane.staiger@dal.ca


MANUSCRIPT AUTHORS:	Staiger, J.K.W. , Gosse, J.C., Toracinta, R. Oglesby, R., Fastook, J., and Johnson, J.
MANUSCRIPT TITLE:	Atmospheric scaling of cosmogenic nuclide production: the climate effect
JOURNAL:	<i>submitted to</i> Journal of Geophysical Research – Solid Earth
STUDENT CONTRIBUTION:	J. Staiger performed the calculations involved in the conversion of the surface pressures to scaling factors, compiled the worldwide production rates, re-scaled the production rates, drafted the figures and wrote the manuscript. The co-authors, J. Fastook and J. Johnson provided the UMISM output of global LGM ice configuration to R. Toracinta and B. Oglesby. Co-authors, R. Toracinta and B. Oglesby provided output of surface pressures from the CCM3 global circulation model. Co-author, J. Gosse revised and clarified the writing and brought the idea of atmospheric compression and its potential effect on production rates to J. Staiger's attention.
SUPERVISOR SIGNATURE:	

MANUSCRIPT AUTHORS:	Staiger, Jane W. , Gosse, John C., Johnson, Jesse V., Fastook, James, Gray, James T., Stockli, Daniel F., Stockli, Lisa, Finkel, Robert.
MANUSCRIPT TITLE:	Relief generation by polythermal glacier ice
JOURNAL:	<i>in press</i> Earth Surface Processes and Landforms
STUDENT CONTRIBUTION:	J. Staiger collected new samples, extracted the samples for Be-10 and Al-26 analyses, ran UMISM, drafted the figures, and wrote the manuscript. Co-authors, J. Fastook and J. Johnson provided the ice sheet model that was used to simulate ice cover over the Torngat Mountains. Co-authors, J. Gray, J. Gosse and D. Stockli assisted sample collection in the field. Co-authors, L. Stockli and B. Finkel provided laboratory assistance and accelerator mass spectrometry (AMS) analyses, respectively. Co-author, J. Gosse, revised the writing and provided use of the CNEF laboratory.
SUPERVISOR SIGNATURE:	


 Faculty of
Graduate Studies

STUDENT CONTRIBUTION TO MANUSCRIPTS IN THESIS

NAME: Jane Kathryn Willenbring Staiger	STUDENT ID #: B00163136
DEPARTMENT: Earth Sciences	PROGRAMME: Ph.D.
PHONE: 902-494-1211	E-MAIL: jane.staiger@dal.ca

MANUSCRIPT AUTHORS:	Staiger, Jane W. , Gosse, John C., Little, Edward C., Utting, D., Johnson, Jesse V., Fastook, James, Finkel, Robert.
MANUSCRIPT TITLE:	Glacial erosion and sediment dispersion from detrital cosmogenic nuclide analyses
JOURNAL:	<i>to be submitted to Geological Society of America Bulletin</i>
STUDENT CONTRIBUTION:	J. Staiger assisted sample collection in the field, performed the physical and chemical processing of all samples, ran ice sheet simulations with UMISM, drafted the figures and wrote the manuscript. Co-authors, T. Little and D. Utting provided till samples and helped chose the subset of till samples to analyze. Co-authors, J. Johnson and J. Fastook provided the ice sheet model. Co-author, R. Finkel provided AMS analyses of the TCN samples. Co-author, J. Gosse revised and clarified the writing and brought the challenge of making measurements of multiple TCN in till for glacial erosion to J. Staiger's attention.
SUPERVISOR SIGNATURE:	

REFERENCES

- Ackert, R. P., Singer, B. S., Guillou, H., Kaplan, M. R., Kurz, M. D. 2003, Long-term cosmogenic ^3He production rates from $^{40}\text{Ar}/^{39}\text{Ar}$ and K-Ar dated Patagonian lava flows at 47°S, *Earth and Planetary Science Letters* **210**: 119-136.
- Ahnert, F. 1994. Equilibrium, scale and inheritance in geomorphology. *Geomorphology* **11**: 125-140.
- Alley, R. 1989a. Water-pressure coupling of sliding and bed deformation: I. Water system. *Journal of Glaciology* **35**(119):108–118.
- Alley, R. 1989b. Water-pressure coupling of sliding and bed deformation: II. Velocity-depth profiles. *Journal of Glaciology* **35**(119):119–129.
- Alley, R. B., Lawson D. E., Larson G. J., Evenson E. B., Baker G. S. 2003. Stabilizing feedbacks in glacier-bed erosion. *Nature* **424**(6950): 758-760.
- Anderson, R. S., Anderson, S. P., MacGregor, K. R., O'Neel, S., Riihimaki, C. A., Waddington, E. D., Loso, M. G. 2004. Strong feedbacks between hydrology and sliding of a small alpine glacier. *JGR-Earth Surface* **109**: F03005, doi:10.1029/2004JF000120.

- Andrews, J. T. 1963. End moraines and late-glacial chronology in the northern Nain-Okak section of the Labrador coast. *Geografiska Annaler* **45**(2-3): 158-171.
- Andrews, J. T. 1972. Glacier power, mass balances, velocities, and erosion potential. *Zeitschrift für Geomorphologie Supplementband* **13**: 1-17.
- Andrews, J.T., Kirby, M.E., Aksu, A., Barber, D.C., Meese, D. 1998. Late Quaternary detrital carbonate (DC-) layers in Baffin Bay marine sediments (67 degrees-74 degrees N); correlation with Heinrich events in the North Atlantic. *Quaternary Science Reviews* **17**(12): 1125-1137.
- Atkins C. B., Barrett P. J., Hicock S. R. 2002. Cold-based glaciers erode and deposit: Evidence from the Allan Hills, Antarctica. *Geology* **30**(7): 659–662.
- Atkinson, B. K., Meredith, P. G., 1987. The theory of subcritical crack growth with applications to minerals and rocks. In: Atkinson, B. K. (Ed.), *Fracture Mechanics of Rock*. Academic Press Inc. Ltd., San Diego, 111–166.
- Augustinus, P.C. 1992. The influence of rock mass strength on glacial valley cross-valley profile morphometry: A case study from the Southern Alps, New Zealand. *Earth Surface Processes and Landforms* **17**: 39-51.

- Balco, G. 2004. *The sedimentary record of subglacial erosion beneath the Laurentide Ice Sheet*. Unpublished Ph.D. thesis, University of Washington. 153 pp.
- Balco, G., Patterson C. J., Stone, J. O. 2003. The fate of preglacial regolith beneath the Laurentide Ice Sheet; XVI INQUA congress; shaping the earth; a Quaternary perspective. *Congress of the International Union for Quaternary Research* **16**: 189.
- Balkwill, H. R., McMillan, N. J., MacLean B., Williams G. L., Srivastava S. P. 1990. Geology of the Labrador Shelf, Baffin Bay, and Davis Strait. in *Geology of the Continental Margin of Eastern Canada*. Keen MJ, Williams GL (eds). The Geology of North America **I-1**: 295-348.
- Bell, J. S. 1989. Labrador Sea = Mer du Labrador. Dartmouth, N.S. East Coast Basin atlas series, Atlantic Geoscience Centre. 112 leaves.
- Bell, T. 1987. Quaternary geomorphology, glacial history and relative sea level change in outer Nachvak Fiord, northern Labrador. M.Sc. thesis, Memorial University of Newfoundland, St. John's Newfoundland.
- Bell, M., Laine, E. 1985. Erosion of the Laurentide region of North America by glacial and glaci-fluvial processes. *Quaternary Research* **23**, 154–174.

- Bierman, P. R., Larsen, P., Clapp, E., Clark, D. 1996. Refining estimates of ^{10}Be and ^{26}Al production rates. *Radiocarbon* **38**: 149.
- Bierman, P. R., Marsella, K. A., Patterson, C., Davis, P. T., Caffee, M. 1999. Mid-Pleistocene cosmogenic minimum-age limits for pre-Wisconsin glacial surfaces in southwestern Minnesota and southern Baffin Island: a multiple nuclide approach. *Geomorphology* **27**: 25–39.
- Bockheim, J. G. 1979. Properties and relative ages of soils of southwestern Cumberland Peninsula, Baffin Island, N.W.T., Canada. *Arctic and Alpine Research* **11**: 289-304.
- Bockheim, J. G., Tarnocai, C.. 1998. Recognition of cryoturbation for classifying permafrost-affected soils. *Geoderma* **81**: 281–293.
- Bonan, G.B. 1998. The land surface climatology of the NCAR land surface model (LSM1.0) coupled to the NCAR Community Climate Model (CCM3), *Journal of Climatology* **11**: 1307-1326.
- Bonney, T. G. 1871. On the formation of cirques and their bearing upon theories attributing the excavation of alpine valleys mainly to the action of glaciers, *Quarterly Journal of Geological Society* **27**: 312-324.

- Boulton, G. S. 1972. The role of thermal regime in glacial sedimentation. *IN*: Price, R. J. and Sugden, D. E. (eds), *Polar Geomorphology*, 1–19. Special Publication No. 4, Institute of British Geographers, London.
- Boulton, G. S., 1979. Processes of glacier erosion on different substrata. *Journal of Glaciology* **23**: 15–38.
- Bougamont, M., Tulaczyk, S. 2003. Glacial erosion beneath ice streams and ice-stream tributaries: constraints on temporal and spatial distribution of erosion from numerical simulations of a West Antarctic Ice Stream. *Boreas* **32**:178-190.
- Braun, J., Zwartz, D., Tomkin, J. 1999. A new surface processes model combining glacial and fluvial erosion. *Annals of Glaciology* **28**: 282–290.
- Briegleb, B. P., Bromwich, D. H. 1998a. Polar radiation budgets of the NCAR CCM3. *Journal of Climatology* **11**: 1246-1269.
- Briegleb, B. P., Bromwich, D. H. 1998b. Polar climate simulation of the NCAR CCM3. *Journal of Climatology* **11**: 1270-1286.
- Briner, J., Swanson, T. 1998: Using inherited cosmogenic ^{36}Cl to constrain glacial erosion rates of the Cordilleran ice sheet. *Geology* **26**(1): 3-6.

- Briner, J. P., Miller, G. H., Davis, P. T., Bierman, P. R., Caffee, M. 2003: Last Glacial Maximum ice sheet dynamics in Arctic Canada inferred from young erratics perched on ancient tors. *Quaternary Science Reviews* **22**: 437-444.
- Briner, J. P., Miller, G. H., Davis, P. T., Finkel, R. C. 2005. Cosmogenic exposure dating in arctic glacial landscapes: implications for the glacial history of northeastern Baffin Island, Arctic Canada. *Canadian Journal of Earth Sciences* **42**: 67-84.
- Briner, J. P., Kaufman, D. S., Manley, W. F., Finkel, R. C., Caffee, M. W. 2005. Cosmogenic exposure dating of late Pleistocene moraine stabilization in Alaska. *Geological Society of America Bulletin* **117**: 1108-1120.
- Brook, E. J., Nesje, A., Lehman, S. J., Raisbeck, G. M., Yiou, F. 1996. Cosmogenic nuclide exposure ages along a vertical transect in western Norway - implications for the height of the Fennoscandian ice sheet. *Geology* **24**(3): 207-210.
- Bryson, R. A., Wendland, W. M., Ives, J. D., Andrews, J. T. 1969. Radiocarbon isochrones on the disintegration of the Laurentide Ice Sheet. *Arctic and Alpine Research* **1**: 1-14.
- Centeno, J. P. 2005. Exhumation of the Torngat Mountains, northern Labrador, Canada. M.Sc. thesis, University of Kansas, Lawrence, Kansas.

- Cerling, T. E., Craig, H. 1994. Geomorphology and in situ cosmogenic isotopes. *Annual Reviews of Earth and Planetary Science* **22**: 273-317.
- Chalmers, J. A. 2000. Offshore evidence for Neogene uplift in central West Greenland. *Global and Planetary Change* **24**: 311-318.
- Clark, D. H., Bierman, P., Gillespie, A. R. 1996. ^{10}Be and ^{26}Al production rates and a revised glacial chronology for the Sierra Nevada. *Radiocarbon* **38**: 152.
- Clark, P. U., 1987. Subglacial sediment dispersal and till composition. *Journal of Geology* **95**: 527-541.
- Clark, P. U. 1988. Glacial geology of the Torngat Mountains, Labrador. *Canadian Journal of Earth Sciences* **25**: 1184-1198.
- Clark, P. U. 1991. Landscapes of glacial erosion, Torngat Mountains, Northern Labrador - Ungava. *The Canadian Geographer* **35**: 208-213.
- Clark, P. U., Brook, E. J., Raisbeck, G. M., Yiou, F., Clark, J. 2003. Cosmogenic ^{10}Be ages of the Saglek Moraines, Torngat Mountains, Labrador. *Geology* **31**: 617-620.
- Colgan, P. M., Bierman, P. R., Mickelson, D. M., Caffee, M. 2002. Variation in glacial erosion near the southern margin of the Laurentide Ice Sheet, south-central

Wisconsin, USA: Implications for cosmogenic dating of glacial terrains.
Geological Society of America Bulletin **114**(12): 1581–1591.

Cooke, H. C. 1929. Studies of the physiography of the Canadian Shield: I, Mature valleys of the Labrador Peninsula. *Transactions of the Royal Society of Canada* **23**(24): 91-120.

Cotter, J. F. P. 1984. The minimum age of the Woodfordian deglaciation of northeastern Pennsylvania and Northwestern New Jersey, Ph.D. thesis, Lehigh University, Bethlehem.

Cotter, J. F. P., Ridge, J. C. Evenson, E. B. Sevon, W. Sirkin, D. L., Stuckenrath, R. 1986. The Wisconsinan history of the Great Valley, Pennsylvania and New Jersey, and the age of the "terminal moraine", *Bulletin - New York State Museum*, (1976) **455**: 22-49.

Cowan, E. A., Powell, R. D., 1991, Ice-proximal sediment accumulation rates in a temperate glacial fjord, southeastern Alaska, in Anderson, J.B., and Ashley, G.M., eds., *Glacial marine sedimentation; paleoclimatic significance: Geological Society of America Special Paper* **261**: 61–74.

Cuffey, K., Alley, R. 1996. Is erosion by deforming subglacial sediments significant? (Toward till continuity). *Annals of Glaciology* **22**: 17–24.

Cuffey, K. M., Conway, H., Gades, A. M., Hallet, B., Lorrain, R., Severinghaus, J. P.

2000. Entrainment at cold glacier beds. *Geology* **28**(4): 351-354.

Davis, R. J., Schaefer, O. A., 1955. Chlorine-36 in nature. *Annals New York Academy of Science* **62**: 105-122.

Davis, P. T., Bierman, P. R., Marsella, K. A., Caffee, M. W., Southton, J. R., 1999,

Cosmogenic analysis of glacial terrains in the eastern Canadian Arctic: A test for inherited nuclides and the effectiveness of glacial erosion: *Annals of Glaciology* **28**: 181–188.

Davis, P. T., Briner, J. P., Miller, G. H., Coulthard, R. D., Bierman, P., Finkel, R. W.

2002. Huge >54,000 yr old glaciomarine delta on northern Baffin Island overlain by boulders with <20,000 yr old cosmogenic exposure ages: implications for non-erosive cold-based ice on Baffin Island during the LGM. *Geological Society of America Annual Meeting* (October 27-30, 2002) Denver Colorado.

Daly, R. A. 1902. The Geology of the northeast coast of Labrador. *Bulletin of the*

Museum of Comparative Zoology at Harvard College **38**(5): 203-270.

- Desilets, D., Zreda M. 2001. On scaling cosmogenic nuclide production rates for altitude and latitude using cosmic-ray measurements. *Earth and Planetary Science Letters* **193**: 213-225.
- Desilets, D., Zreda, M. 2003. Spatial and temporal distribution of secondary cosmic-ray nucleon intensities and applications to in situ cosmogenic dating. *Earth and Planetary Science Letters* **206**: 21-42.
- Dowdeswell, E.K., and Andrews, J.T., 1985, The fiords of Baffin Island—Description and classification, *in* Andrews, J.T., ed., Quaternary environments: Eastern Canadian Arctic, Baffin Bay, and western Greenland: Boston, Allen and Unwin, p. 93–123.
- Dreimanis, A. and Vagners, U. J. 1969. Lithologic relation of till to bedrock, in Wright, H. E., Jr., ed. Quaternary Geology and Climate: Washington, National Academy of Sciences, p. 93-98.
- Dunai, T. J. 2000. Scaling factors for production rates of in situ produced cosmogenic nuclides: A critical reevaluation. *Earth and Planetary Science Letters* **176**: 157-169.

- Dunai, T. J. 2001. Influence of secular variation of the geomagnetic field on production rates of in situ produced cosmogenic nuclides. *Earth and Planetary Science Letters* **193**(1-2): 197-212.
- Dunai, T. J., Lopez, G. A. G., Juez-Larre, J. 2005. Oligocene-Miocene age of aridity in the Atacama Desert revealed by exposure dating of erosion-sensitive landforms. *Geology* **33**(4): 321 - 324.
- Dyke, A. S. 1978. Indications of neoglaciation on Somerset Island, District of Franklin. *Paper - Geological Survey of Canada* **78-1B**: 215-217.
- Dyke, A. S. 1993. Landscapes of cold-centred late Wisconsin ice caps, arctic Canada. *Progress in Physical Geography* **17** (2): 223-247.
- Dyke, A. S. 1999. Last glacial maximum and deglaciation Devon Island, arctic Canada: Support for an Inuitian Ice Sheet. *Quaternary Science Reviews* **18**: 393–420.
- Dyke, A. S., Hopper, J. M. G. 2001: Deglaciation of northwest Baffin Island, Nunavut, Geological Survey of Canada, A-Series Map 1999A, scale 1:500,000.
- Dyke, A. S., Morris, T. F. 1988. Canadian Landform examples .7. drumlin fields, dispersal trains, and ice streams in arctic Canada. *Canadian Geographer* **32** (1): 86-90.

- Dyke, A. S., Prest, V. K. 1987. Late Wisconsin and Holocene history of the Laurentide Ice Sheet. *Géographie physique et Quaternaire*, **41**: 237–263.
- Dyke, A. S., Andrews, J. T., Clark, P. U., England, J. H., Miller, G. H., Shaw, J., Veillette, J. J. 2002. The Laurentide and Innuitian Ice Sheets during the Last Glacial Maximum. *Quaternary Science Reviews* **21**: 9–31.
- Dyke, A. S., Moore, A., Robertson, L. 2003: Deglaciation of North America. Geological Survey of Canada, Open File 1574. Thirty-two maps at 1:7,000,000 scale with accompanying digital chronological database and one poster (in two sheets) with full map series.
- Elverhøi, A., Hooke, R. L., Solheim, A. 1998. Late Cenozoic erosion and sediment yield from the Svalbard-Barents Sea region: implications for understanding erosion of glacierized basins. *Quaternary Science Reviews* **17**: 209–241.
- Endt, P. M., Van der Leun, C., 1973. Energy levels of $A=21-44$ A- nuclei. *Nuclear Physics A* **214**: 1-625.
- England, J. 1987. Glaciation and the evolution of the Canadian high arctic landscape. *Geology* **15**: 419-424.

England, J. 1996. Glacier dynamics and paleoclimatic change during the last glaciation of eastern Ellesmere Island, Canada. *Canadian Journal of Earth Sciences* **33**: 779–799.

England, J. 1998. Support of the Innuitian Ice Sheet in the Canadian High Arctic during the Last Glacial Maximum. *Journal of Quaternary Science* **13**: 275–280.

England, J. 1999. Coalescent Greenland and Innuitian ice during the Last Glacial Maximum: Revisiting the Quaternary of the Canadian High Arctic. *Quaternary Science Reviews* **18**: 421–456.

Environment Canada. 1991. Canadian Climate Normals. 1961-1990. http://climate.weatheroffice.ec.gc.ca//climate_normals_1990.

Fabel D., Stroeven, A. P., Harbor, J., Kleman J., Elmore, D., Fink, D. 2002. Landscape preservation under Fennoscandian ice sheets determined from in situ produced ^{10}Be and ^{26}Al . *Earth and Planetary Science Letters* **201**: 397-406.

Fabel, D., Harbor, J., Dahms, D., James, A., Elmore, D., Horn, L., Daley, K., Steele, C. 2004. Spatial patterns of glacial erosion at a valley scale derived from terrestrial cosmogenic ^{10}Be and ^{26}Al concentrations in rock. *Annals of the Association of American Geographers* **94**(2): 241-255.

- Fahn, C. 1975. Glaciers of northern Labrador. in *Mountain glaciers of the Northern Hemisphere*. Field WO (eds). Hanover, N.H., U.S. Army Cold Regions Research and Engineering Lab **2**: 673–682.
- Falconer, G., Ives, J. D., Løken, O. H., Andrews, J. T. 1965: Major end moraines in eastern and central arctic Canada. *Geographic Bulletin* **7**(2): 137-153.
- Fastook, J. 1984. West Antarctica, the sea-level controlled marine instability: Past and future. In Hansen, J. and Takahashi, T., editors, *Climate Process and Climate Sensitivity*, pages 275–287. Geophysical Monograph 29, American Geophysical Union, Washington, D.C.
- Fastook, J. 1987. Use of a new finite element continuity model to study the transient behavior of Ice Stream C and causes of its present low velocity. *Journal of Geophysical Research* **92**(B9): 8941–8949.
- Fastook, J. 1990. A map-plane finite-element program for ice sheet reconstruction: A steady-state calibration with Antarctica and a reconstruction of the Laurentide Ice Sheet for 18,000 BP. In Brown, H. U., editor, *Computer Assisted Analysis and Modeling on the IBM 3090*, pages 48–80. IBM Scientific and Technical Computing Dept., White Plains, N.Y.

- Fastook, J. 1992. A map-plane finite-element program for ice sheet reconstruction. In Billingley, K. R., Brown, H. U., and Derohanes, E., eds, *Computer Assisted Analysis and Modeling on the IBM 3090*, Volume 1: 45–80. The Baldwin Press, The University of Georgia, Athens, Georgia.
- Fastook J. L. 1994. Modelling the Ice Age: the finite element method in glaciology. *Computational Science and Engineering* **1**(1): 55-67.
- Fastook, J., Chapman, J. 1989. A map plane finite-element model: Three modeling experiments. *Journal of Glaciology* **35**(119):48–52.
- Fastook, J., Grosswald, M. 1998. Quaternary glaciation of Lake Baikal and adjacent highlands: modelling experiments. In Horie, S., editor, *International Project on Paleolimnology and Late Cenozoic Climate*. No. 11. IPPCCE, Innsbruck, Austria.
- Fastook, J., Holmlund, P. 1994. A glaciological model of the Younger Dryas event in Scandinavia. *Journal of Glaciology* **40**(134):125–131.
- Fastook, J., Hughes, T. 1982a. A numerical model for reconstruction and disintegration of the Late Wisconsin glaciation in the Gulf of Maine. In Larson, G. and Stone, B., editors, *Late Wisconsinan Glaciation of New England*, pages 229–242. Kendall/Hunt Publishing Company, Dubuque, Iowa.

- Fastook, J., Hughes, T. 1982b. When ice sheets collapse. *Perspectives in Computing* **2**(1): 4–15.
- Fastook, J., Hughes, T. 1988. A geomorphic method for reconstructing paleo ice sheets part II: Glaciology. In Kite, J., Lowell, T., and Thompson, W., editors, Contributions to the Quaternary geology of Northern Maine and adjacent Canada. *Maine Geological Survey Bulletin* **37**: 19–34.
- Fastook, J., Prentice, M. 1994. A finite-element model of Antarctica: Sensitivity test for meteorological mass balance relationship. *Journal of Glaciology* **40**(134): 167–175.
- .
- Fastook, J., Schmidt, W. 1982. Finite element analysis of calving from ice fronts. *Annals of Glaciology* **3**: 103–106.
- Fastook, J. L., Johnson, J. V., Hughes, T. 2002. University of Maine Ice Sheet Model (UMISM). University of Maine. Online at <http://tulip.umcs.maine.edu/~shamis/umism/umism.html>. 178 pp.
- Fastook, J., Brecher, H., Hughes, T. 1995. Derived bedrock elevations, strain rates, and stresses from measured surface elevations and velocities: Jakobshavn Glacier, Greenland. *Journal of Glaciology* **41**(137):161–173.

- Flint, R. *Glacial Geology and the Pleistocene Epoch* (J. Wiley and Sons, New York, 1971).
- Funck, T., Loudon, K. E., Wardle, R. J., Hall, J., Hobro, J. W., Salisbury, M. H., Muzzati, A. M. 2000. Three-dimensional structure of the Torngat Orogen (NE Canada) from active seismic tomography. *Journal of Geophysical Research* **105**(B10): 23 403-23 420.
- Garwood, E. J. 1910. Features of alpine scenery due to glacial protection, *Geographical Journal* **36**: 310-339.
- Gellatly, A. F., Whalley, W. B., Gordon, J. E., Hansom, J. D. 1988. Thermal regime and geomorphology of plateau ice caps of northern Norway: observations and implications. *Geology* **16**: 983-986.
- Gilpin, R. R. 1979. A model of the "liquid-like" layer between ice and a substrate with applications to wire regelation and particle migration. *Journal of Colloid and Interfacial Science* **68**: 235-251.
- Gosse, J. C. 2001. Dal-CNEF Laboratory Procedures. 28 pp.
- Gosse, J., Klein, J., 1996. Production rate of in situ cosmogenic ^{10}Be in quartz at high altitude and mid-latitude. *Radiocarbon* 38 (1), 154-155.

- Gosse, J. C., Phillips, F. M. 2001. Terrestrial in situ cosmogenic nuclides: theory and application (Reviews). *Quaternary Science Reviews* **20**: 1475-1560.
- Gosse, J. C., Stone, J. O. 2001. Terrestrial cosmogenic nuclide methods passing milestones of paleo-altimetry. *EOS* **82** (7): 82, 86, 89.
- Gosse, J. C., Grant, D. R., Evenson, E. B., Klein, J., Lawn, B., Middleton, R. 1993. Significance of altitudinal weathering zones in Atlantic Canada, inferred from in situ produced cosmogenic radionuclides. *Abstracts with Programs - Geological Society of America* **25**(6): 394.
- Gradstein, F. M., Srivastava, S. P. 1980. Aspects of Cenozoic stratigraphy and paleoceanography of the Labrador Sea and Baffin Bay. *Palaeogeography, Palaeoclimatology, Palaeoecology* **30**: 261-295.
- Granger, D. E., Muzikar, P. F. 2001. Dating sediment burial with in situ-produced cosmogenic nuclides: theory, techniques, and limitations. *Earth and Planetary Science Letters* **188**(1-2): 269-281.
- Granger, D. E., Smith, A. L., 2000. Dating buried sediments using radioactive decay and muogenic production of ^{26}Al and ^{10}Be . *Nuclear Instruments and Methods in Physics Research B* **172**(1-4): 822-826.

Gravenor, C. P. 1975. Erosion by continental ice sheets. *American Journal of Science* **275**: 595–604.

Hack, J. J., Kiehl, J. T., Hurrell J. W. 1998. The hydrologic and thermodynamic characteristics of the NCAR CCM3. *Journal of Climate* **11**: 1179-1206.

Hall, A., Sugden, D. 1987. Limited modification of mid-latitude landscapes by ice sheets: the case of northwest Scotland. *Earth Surface Processes and Landforms* **12**: 531–542.

Hall, J., Loudon, K. E., Funck, T., Deemer S. 2002. Geophysical characteristics of the continental crust along the Lithoprobe Eastern Canadian Shield Onshore-Offshore Transect (ECSOOT): a review. *Canadian Journal of Earth Sciences* **39**: 569-587.

Hallet, B. 1979. A theoretical model of glacial abrasion. *Journal of Glaciology* **23**(89): 39-50.

Hallet, B. 1996. Glacial quarrying; a simple theoretical model. *Annals of Glaciology* **22**: 1-8.

Hallet, B., Hunter L., Bogen J. 1996. Rates of erosion and sediment evacuation by glaciers; a review of field data and their implications; impact of glaciations on

basin evolution; data and models from the Norwegian margin and adjacent areas. *Global and Planetary Change* **12**(1-4): 213-235.

Harbor, J. M. 1995. Development of glacial-valley cross sections under conditions of spatially variable resistance to erosion; glacial geomorphology; process and form development. *Geomorphology* **14**(2): 99-107.

Harbor, J. M., 1992. Numerical modeling of the development of U-shaped valleys by glacial erosion. *Geological Society of America Bulletin* **104**: 1364–1375.

Hay, W. W. 1998. Detrital sediment fluxes from continents to oceans. *Chemical Geology* **145**(3-4): 287-323.

Hilchey, A. 2004. Holocene Deglacial Geologic History of the Ravn River Valley, Northern Baffin Island, Nunavut. Honours thesis, Dalhousie University, Halifax. 99 pp.

Hodgson, D. A., Haselton, G. M. 1974. Reconnaissance glacial geology, northeastern Baffin Island; Geological Survey of Canada Paper: 74-20.

Hofmann, H. J., Beer, J., Bonani, G., von Gunten, H. R., Raman, S., Suter, M., Walker, R.L., Wölfi, W., Zimmermann, D. 1987. ^{10}Be : Half-life and AMS-standards. *Nuclear Instruments and Methods in Physics Research B* **29**: 32-36.

Holden, N. E. 1990. Total half-lives for selected nuclides. *Pure and Applied Chemistry* **62**(5): 941-958.

Hooke, R. L. 1991. Positive feedbacks associated with erosion of glacial cirques and overdeepenings. *Geological Society of America Bulletin* **103**: 1104-1108.

Hooke, R. L. 1998. Principles of Glacier Mechanics. Prentice Hall, Upper Saddle River, New Jersey.

Hooyer, T. S., Iverson, N. R. 2000. Diffusive mixing between shearing granular layers: constraints on bed deformation from till contacts. *Journal of Glaciology* **46**: 641–651.

Hostetler, S. W., Bartlein, P. J., Clark, P. U., Small, E. E., Solomon, A. M. 2000. Simulated influences of Lake Agassiz on the climate of central North America 11,000 years ago. *Nature* **405**: 334–337.

Hovius, N. 2000, Macro scale process systems of mountain belt erosion, in, *Geomorphology and Global Tectonics*. Summerfield M (eds). New York, John Wiley and Sons: 77- 105.

Hughes, T. 1987. Ice dynamics and deglaciation models when ice sheets collapsed. In Ruddiman, W. and Wright, H., editors, North America and adjacent oceans during

the last deglaciation: The Geology of North America, K-3, pages 183–220.
Geological Society of America, Boulder, Colorado.

Hulbe, C. L. 1998. Heat Balance of West Antarctic Ice Streams, Investigated with a
Numerical Model of Coupled Ice Sheet, Ice Stream, and Ice Shelf Flow.
University of Chicago. Ph.D. Thesis.

Hulton, N. R., Purves, R. S. McColloch, R. D. Sugden, D. E., Bentley, M. J. 2002. The
Last Glacial Maximum and deglaciation of southern South America. *Quaternary
Science Reviews* **21**: 233-241.

Humphrey, N. F., Raymond, C. F. 1994. Hydrology, erosion and sediment production in
a surging glacier; the Variegated Glacier surge, 1982-83. *Journal of Glaciology*
40(136): 539-552.

Hurrell, J. W., Hack, J. J. Boville, B. A. Williamson, D. L., Kiehl, J. T. 1998. The
dynamical simulation of the NCAR Community Climate Model Version 3
(CCM3). *Journal of Climatology* **11**: 1207-1236.

Huybrechts, P., Payne, T., Abe-Ouchi, A., Calov, R., Fastook, J., Greve, R., Hindmarsh,
R., Hoydal, O., Johannesson, T., MacAyeal, D., Marsiat, I., Ritz, C., Verbitsky,
M., Waddington, E., Warner, R. 1995. The EISMINT benchmarks for testing ice-

sheet models. In *Annals of Glaciology* Volume 23, Chamonix, France.
IGS/EISMINT International Conference on Ice Sheet Modelling.

Huybrechts, P., Payne, T., Abe-Ouchi, A., Calov, R., Fabre, A., Fastook, J., Greve, R., Hindmarsh, R., Hoydal, O., Johannesson, T., MacAyeal, D., Marsiat, I., Ritz, C., Verbitsky, M., Waddington, E., Warner, R. 1996. The EISMINT benchmarks for testing ice-sheet models. *Annals of Glaciology* **23**:1–12.

Issler, D. R. 1987. The thermal and subsidence history of the Labrador Margin. Ph. D. thesis, Dalhousie University, Halifax, Nova Scotia, Canada: 235 pp.

Ives, J. D. 1958. Mountain-top detritus and the extent of the last glaciation in northeastern Labrador-Ungava. *The Canadian Geographer* **12**: 25-31.

Ives, J. D. 1978. The maximum extent of the Laurentide Ice Sheet along the east coast of North America during the last glaciation. *Arctic* **31**(1): 24-53.

Ivy-Ochs, S. 1996. The dating of rock surfaces using in situ produced ^{10}Be , ^{26}Al and ^{36}Cl , with example from Antarctica and the Swiss Alps. Dissertation ETH No. 11763 .
196 pp.

Japsen, P., Chalmers, J. A. 2000. Neogene uplift and tectonics around the North Atlantic: overview. *Global and Planetary Change* **24**: 165-173.

Jennings, A. E., Tedesco, K. A., Andrews, J. T., Kirby, M. E. 1996: Shelf erosion and glacial ice proximity in the Labrador Sea during and after Heinrich events (H-3 or H-4 to H-0) as shown in foraminifera; in Andrews et al. eds., Late Quaternary Paleooceanography of the North Atlantic Margins: *Geological Society of America Special Publication 111*: 29-49.

Johnsen, S., Dahl-Jensen, D., Dansgaard, W., Gunderup, N. 1995. Greenland paleotemperatures derived from GRIP bore hole temperature and ice core isotope profiles. *Tellus 47B*: 624-629.

Johnson, J. V., Fastook, J. L. 2002. Northern Hemisphere glaciation and its sensitivity to basal melt water. *Quaternary International 95-96*: 87-98.

Johnson, J. V. 2002. A basal water model for ice sheets. Ph.D. dissertation U. of Maine, Orono. 187 pp.

Kageyama, M., Valdes, P. J., Ramstein, G., Hewitt, C., Wypytta, U. 1998. Northern Hemisphere storm tracks in present day and last glacial maximum climate simulations: A comparison of the European PMIP models. *Journal of Climatology 12*: 742-760.

- Kaplan, M. R., Miller, G. H., Steig, E. J. 2001. Low-gradient outlet glaciers (ice streams?) drained the northeastern Laurentide Ice Sheet. *Geology* **29**: 343–346.
- Kiehl, J. T., Hack, J. J. Bonan, G. B. Boville, B. A. Williamson, D. L., Rasch P. J. 1998a. The National Center for Atmospheric Research Community Climate Model: CCM3. *Journal of Climatology* **11**: 1131-1149.
- Kiehl, J. T., Hack, J. J., Hurrell, J. W. 1998b. The energy budget of the NCAR Community Climate Model: CCM3. *Journal of Climatology* **11**: 1151-1178.
- Klassen, R. 1998. Geological factors affecting the distribution of trace metals in glacial sediments of central Newfoundland. *Environmental Geology* **33**(2-3): 154-169.
- Klassen, R. A., Paradis, S., Bolduc, A. M., Thomas, R. D. 1992. Glacial landforms and deposits, Labrador, Newfoundland and eastern Quebec. *Geological Survey of Canada, Map 1814A*, scale 1:1000000.
- Klein, J., Middleton, R., Tang, H.-Q., 1982. Modifications of an FN Tandem for Quantitative Measurements of ^{10}Be . *Nuclear Instruments and Methods* **193**: 601-616.
- Kleman, J. 1994. Preservation of landforms under ice sheets and ice caps. *Geomorphology* **9**: 19–32.

- Kohl, C. P., Nishiizumi, K. 1992. Chemical isolation of quartz for measurement of in-situ-produced cosmogenic nuclides. *Geochemica et Cosmochemica Acta* **56**: 3583-3587.
- Koons, P. O. 1989. The topographic evolution of collisional mountain belts: a numerical look at the southern Alps, New Zealand. *American Journal of Science* **289**: 1044-1069.
- Koons, P. O., Norris, R. J., Craw, D., Cooper, A. F. 2003. Influence of exhumation on the structural evolution of transpressional plate boundaries: An example from the Southern Alps, New Zealand. *Geology* **31**(1): 3–6.
- Kubik, P. W., Ivy-Ochs, S. 2004. A re-evaluation of the 0-10 ka ^{10}Be production rate for exposure dating obtained from the Köffels (Austria) landslide. *Nuclear Instruments and Methods B* **223-224**: 618-622.
- Kurz, M. D., Brook, E. J. 1994: Surface exposure dating with cosmogenic nuclides, in Beck, C., ed., *Dating in exposed and surface contexts*: Albuquerque, University of New Mexico Press, p. 139-159.
- Lal, D. 1991. Cosmic ray labelling of erosion surfaces: in situ nuclide production rates and erosion rates. *Earth and Planetary Science Letters* **104**: 424-439.

- Lal, D., and Peters B. 1967. Cosmic-ray produced radioactivity on the earth. *Handbook of Physics* **46** (2): 551–12.
- Larsen, P. 1995. In situ production rates of cosmogenic ^{10}Be and ^{26}Al over the past 21,500 years determined from the terminal moraine of the Laurentide ice sheet, north central New Jersey, M.S. thesis, Univ. of Vermont, Burlington.
- Larsen, P. L., Bierman, P. R. and Caffee, M. 1995. Preliminary in situ production rates of cosmogenic ^{10}Be and ^{26}Al over the past 21.5 ky from the terminal moraine of the Laurentide ice sheet, north-central New Jersey. *Geological Society of America Abstract with Programs* **27**: A59.
- Larsen, N. K., Piotrowski, J. A., Kronborg, C. 2004. A multiproxy study of a basal till: a time-transgressive accretion and deformation hypothesis. *Journal of Quaternary Science* **19**: 9–21.
- Larson, P. C., Moores, H. D. 2004. Glacial indicator dispersal processes: a conceptual model. *Boreas* **33**: 238-249.
- Lidmar-Bergström, K. 1995. Relief and saprolites through time on the Baltic Shield. *Geomorphology* **12**: 45-61.

- Lidmar-Bergstrom, K. 1997. A long-term perspective on glacial erosion. *Earth Surface Processes and Landforms* **22**: 297–306.
- Little, E. C., Holme, P., Hilchey, A., Young, M. 2004. Glacial Geology, Ice- Movement Chronology and Drift Prospecting in the Vicinity of Icebound Lakes (NTS 37G), Northern Baffin Island, Nunavut. Geological Survey of Canada Current Research Paper.
- Little, E. C., Young, M., Utting D. J. 2005. Preliminary bedrock geochemistry and drift prospecting results from the North Baffin Project (NTS 37F, 37G, 47E), Northern Baffin Island, Nunavut. Geological Survey of Canada Open File Report.
- Macciaroli, P., Giegengack, R., Klein, J., Middleton, R., Lawn, B. 1994. Late Quaternary glaciation of exposed rock surfaces along a ridge of the Appalachian Mountains, dated using ^{26}Al and ^{10}Be produced in situ. *Geological Society of America. Abstracts with Programs* **26**: A-125.
- MacGregor, K. R., Anderson, R. S., Anderson, S. P., Waddington, E. D. 2000. Numerical simulations of glacial-valley longitudinal profile evolution. *Geology* **28**(11): 1031–1034.
- MacLean, B., Andrews, J. T., Gray, J. T., Hall, F. R., Hardy, I., Jennings, A. E., Manley, W. F., Pfeffer, W. T., Vilks, G. 2001. Late Quaternary sediments, depositional

environments, and late glacial-deglacial history derived from marine and terrestrial studies. in *Marine geology of Hudson Strait and Ungava Bay, eastern Arctic Canada*; MacLean, B. (eds.) Bulletin of the Geological Survey of Canada, Report: **566**: 181-191.

Mäkinen, J. 2003. A mathematical model to explain the effect of comminution, re-sedimentation and outwashing on the finest fractions of till in four test areas in central Finland, in Räisänen, M.L. and Nikkarinen, M. (eds.) Complexity of glacial dispersal and hydromorphic processes in till geochemistry, *Geological Survey of Finland, Special Paper 34*: 43-69.

Marchant, D. R., Denton, G. H., Swisher, C. C. 1993. Miocene-Pleistocene glacial history of Arena Valley, Quartermain Mountains, Antarctica. *Geografiska Annaler 75A*: 269-302.

Marquette, G. C., Gray, J. T., Gosse, J. C., Courchesne, F., Stockli, L., Macpherson, G., Finkel, R. 2004. Felsenmeer persistence under non-erosive ice in the Torngat and Kaumajet mountains, Quebec and Labrador, as determined by soil weathering and cosmogenic nuclide exposure dating. *Canadian Journal of Earth Sciences 41*(1): 19-38.

- Marsella, K. A., Bierman, P. R., Davis, P. T., Caffee, M. W. 2000. Cosmogenic ^{10}Be and ^{26}Al ages for the last glacial maximum, eastern Baffin Island, Arctic Canada. *Geological Society of America Bulletin* **112**(8): 1296-1312.
- Marshall, S. J., Clark, P. U. 2002. Basal temperature evolution of North American ice sheets and implications for the 100-kyr cycle. *Geophysical Research Letters* **29**(24): 2214-2218.
- Masarik, J., Frank, M. Schäfer, J.M., Wieler, R. 2001. Correction of in situ cosmogenic nuclide production rates for geomagnetic field intensity variations during the past 800,000 years. *Geochimica et Cosmochimica Acta* **65**(17): 2995-3003.
- Mellor, M., Testa, R. 1969. Effect of temperature on the creep of ice. *Journal of Glaciology* **8**: 131–145.
- Ménières, M. A., Martinerie. P., Raynaud, D., Lliboutry, L. 1991. Glacial-interglacial mean sea level pressure change due to sea level, ice sheet and atmospheric mass changes. *Palaeogeography Palaeoclimatology Palaeoecology* **89**: 333-340.
- Mengel, F., Rivers, T., Reynolds, P. 1991. Lithotectonic elements and tectonic evolution of the Torngat Orogen, Saglek Fiord, northern Labrador. *Canadian Journal of Earth Sciences* **28**: 1407-1423.

- Middleton, R., Brown, L., Dezfouly-Arjomandy, B., Klein, J. 1993. On ^{10}Be standards and the half-life of ^{10}Be . *Nuclear Instruments and Methods in Physics Research B* **82**: 399-403.
- Miller, G. H., Wolfe, A. P., Steig, E. J., Sauer, P. E., Kaplan, M. R., Briner, J. P. 2002. The Goldilocks Dilemma: Big Ice, Little Ice, or “Just-Right” Ice in the Eastern Canadian Arctic. *Quaternary Science Reviews* **21**: 33-48.
- Molnar P., England, P. 1990. Late Cenozoic uplift of mountain ranges and global climate change: Chicken or egg? *Nature* **346**: 29-34.
- Montgomery, D. R., 2002. Valley formation by fluvial and glacial erosion, *Geology* **30**(11): 1047-1050.
- Moores, H. D. 1990. A glacial-process model: The role of spatial and temporal variation in glacier thermal regime. *Geological Society of America Bulletin* **102**(2): 243-251.
- Näslund, J. O., Rodhe, L., Fastook, J. L., Holmlund, P. 2003. New ways of studying ice sheet flow directions and glacial erosion by computer modelling – examples from Fennoscandia. *Quaternary Science Reviews* **22**: 245-258.

- Nesje, A., Whillans, I. M., 1994. Erosion of Sognefjord, Norway. *Geomorphology* **9**: 33–45.
- Nishiizumi, K., Winterer, E. L., Kohl, C. P., Klein, J., Middleton R., Lal, D., Arnold, J. R. 1989. Cosmic ray production rates of ^{10}Be and ^{26}Al in quartz from glacially polished rocks. *Journal of Geophysical Research* **94**(B12): 17,907-17,915.
- Nishiizumi, K., Finkel, R. C. Klein, J., Kohl, C. P. 1996. Cosmogenic production of ^7Be and ^{10}Be in water targets. *Journal of Geophysical Research* **101**: 22,225-22,232.
- Ochs, M., Ivy-Ochs, S., 1996. The chemical behavior of Be, Al, Fe, Ca, and Mg during AMS target preparation from terrestrial silicates modeled with chemical speciation calculations. *Radiocarbon* **38**(1): 53-54.
- Odell, N. E. 1933. The mountains of Labrador (continued), *The Geographical Journal* **82**(4): 315-325.
- Oerlemans, J. 1980. Model experiments on the 10,000 year glacial cycle. *Nature* **287**: 430–432.
- Oerlemans, J. 1985. Numerical experiments on large-scale glacial erosion. *Zeitschrift für Gletscherkunde und Glazialgeologie* **20**: 107–126.

- Partridge, T. C., Granger, D. E., Caffee, M. W., Clarke, R. J. 2003. Lower Pliocene hominid remains from Sterkfontein. *Science* **300**: 607-12.
- Paterson W. S. B. 1994. *The Physics of Glaciers*. Elsevier Science Ltd., Trowbridge.
- Peizhen Z., Molnar P., Downs, W. R. 2001. Increased sedimentation rates and grain sizes 2-4 Myr ago due to the influence of climate change on erosion rates. *Nature* **410**: 891-896.
- Piotrowski, J. A., Tulaczyk, S. 1999. Subglacial conditions under the last ice sheet in northwest Germany: ice bed separation and enhanced basal sliding. *Quaternary Science Reviews* **18**: 737–751.
- Porter, S. C. 2001. Snowline depression in the tropics during the last glaciation. *Quaternary Science Reviews* **20**: 1067-1091.
- Powell, R. D., Alley, R. B. 1997. Grounding-line systems: processes, glaciological inference and the stratigraphic record. In: *Geology and Seismic Stratigraphy of the Antarctic Margin, Part 2*, Barker, P. F., Cooper, A. K.(eds.). *Antarctic Research Series* **71**: 169–187.

- Press, W. H., Teukolsky, S. A., Vetterling, W. T., Flannery, B. P. 1992. *Numerical recipes in FORTRAN: The art of scientific computing*, 963 pp., Cambridge University Press., New York.
- Puranen, R., 1988. Modelling of glacial transport of basal tills in Finland. Report of Investigation 81, Geological Survey of Finland. 36 pp.
- Putkonen, J., Swanson, T. 2003. Accuracy of cosmogenic ages for moraines. *Quaternary Research* **59**: 1-7.
- Raymo, M. E. and Ruddiman, W. F. 1992. Tectonic forcing of late Cenozoic climate. *Nature* **359**: 117-122.
- Rightmire, V. R. A., Kohman, T. P., Hintenberger, H., 1958. Über die Halbwertszeit des langlebigen ²⁶Al. *Zeitschrift für Naturforschung* **13A**: 847-853.
- Robin, G. de Q.. 1955. Ice movement and temperature distribution in glaciers and ice sheets. *Journal of Glaciology* **2**: 523– 532.
- Rogerson, R.J., Josenhans, H.W. and Bell, T. A 1986. 3.5 Khz Acoustic Survey of Nachvak Fiord, Northern Labrador. *Geological Survey of Canada Paper* **86-1A**: 221-228.

- Röthlisberger, H. 1968. Erosive processes which are likely to accentuate or reduce the bottom relief of valley glaciers. In General assembly of Bern (25 sept. - 7. Oct. 1967), *IAHS. Publication 79*: 87-97.
- Röthlisberger, H., Iken, A. 1981. Plucking as an effect of water pressure variations at the glacier bed. *Annals of Glaciology* **2**: 23-28.
- Schetz, J., Fuhs, A., (eds.). 1996. Handbook of fluid dynamics and fluid machinery. John Wiley and Sons, Inc., New York.
- Siegert, M. J., Dowdeswell, J. A., Gorman, M. R., McIntyre, N. F. 1996. An inventory of Antarctic sub-glacial lakes. *Antarctic Science* **8**(3): 281–286.
- Shackleton, N. 1987. Oxygen isotopes, ice volume and sea level. *Quaternary Science Reviews* **6**: 183–190.
- Shilts, W. W. 1976. Glacial till and mineral exploration. in Legget, R. F. ed. Glacial Till: *Royal Society of Canada Special Publication* **12**: 205-224.
- Shilts, W. W. 1978. Nature and genesis of mudboils, central Keewatin, Canada. *Canadian Journal of Earth Science* **15**: 1053-1068.

- Shreve, R. L. 1984. Glacier sliding at subfreezing temperatures. *Journal of Glaciology* **30**: 341-347.
- Small, E. E., Anderson, R. S. 1998. Pleistocene relief production in Laramide Mountain ranges, western United States. *Geology* **26**: 123-126.
- Spotila, J. A., Buscher, J. T., Meigs, A. J., Reiners, P. W. 2004. Long-term glacial erosion of active mountain belts: Example of the Chugach–St. Elias Range, Alaska. *Geology* **32**(6): 501-504.
- Steig, E. J., Wolfe, A. P., Miller, G. H. 1998: Wisconsinan refugia and the glacial history of eastern Baffin Island, Arctic Canada: coupled evidence from cosmogenic isotopes and lake sediments. *Geology* **26**: 835-838.
- Stokes C. R., Clark C. D. 2001. Palaeo-ice streams. *Quaternary Science Reviews* **20**(13): 1437-1457.
- Stone, J. O. 2000. Air pressure and cosmogenic isotope production. *Journal of Geophysical Research* **105**(B10): 23,753-23,759.
- Stone J. O., Ballantyne, C. K., Fifield, L. K. 1998. Exposure dating and validation of periglacial weathering limits, NW Scotland. *Geology* **26**: 587-590.

- Stone, J. O., Todd, C., Balco, G. 2003. Extraction of Al and Be from quartz for isotopic analysis. (<http://depts.washington.edu/cosmolab/chem.html>).
- Stone J. O., Balco, G. A., Sugden D. E., Caffee M. W., Sass L.C. III, Cowdery S. G., Siddoway, C. 2003. Holocene deglaciation of Marie Byrd Land, West Antarctica. *Science* **299**(5603): 99-102.
- Sugden. D. E. 1976. A case against deep erosion of shields by ice sheets. *Geology* **4**: 580–582.
- Sugden D. E. 1978. Glacial erosion by the Laurentide ice sheet. *Journal of Glaciology* **20**: 367-391.
- Sugden. D. E. 1989. Modification of old land surfaces by ice sheets. *Zeitschrift für Geomorphologie* **72**: 163–172.
- Sugden, D. E., Balco, G., Cowdery, S. G., Stone, J. O., Sass, L.C. III. 2005. Selective glacial erosion and weathering zones in the coastal mountains of Marie Byrd Land, Antarctica. *Geomorphology* **67**(3-4): 317-334.
- Summerfield, M. A., Hulton, N. J. 1994. Natural controls of fluvial denudation rates in major world drainage basins. *Journal of Geophysical Research, B, Solid Earth and Planets* **99**(7): 13 871-13 883.

- Summerfield, M. A., Stuart, F. M., Cockburn, H. A. P., Sugden, D. E., Denton, G. H., Dunai, T., Marchant, D. R. 1999. Long-term rates of denudation in the Dry Valleys, Transantarctic Mountains, southern Victoria Land, Antarctica based on in-situ-produced cosmogenic ^{21}Ne . *Geomorphology* **27**(1-2): 113-129.
- Syvitski, J. P. M., 1989, On the deposition of sediment within glacier-influenced fjords: Oceanographic controls. *Marine Geology* **85**: 301–329.
- Taylor, F. C. 1979. Reconnaissance geology of a part of the Precambrian shield, northeastern Quebec, northern Labrador and Northwest Territories. *Geological Survey of Canada Memoir* **393**: 1-99.
- Tomkin, J. H., Braun, J. 2002. The influence of alpine glaciation on the relief of tectonically active mountain belts. *American Journal of Science* **302**(3): 169-190.
- Toracinta, E. R., Oglesby, R. J., Bromwich, D. H. 2004. Atmospheric response to modified CLIMAP ocean boundary conditions during the Last Glacial Maximum. *Journal of Climatology* **17**: 504-522.
- Tucker, G. E. and Slingerland, R. 1997. Drainage basin responses to climate change. *Water Resources Research* **33**(8): 2031-2047.

- Twidale, C. R. 1976. On the survival of paleoforms. *American Journal of Science* **276**: 77-95.
- Whipple, K. X., Kirby, E., Brocklehurst, S. H. 1999. Geomorphic limits to climate-induced increases in topographic relief. *Nature* **401**: 39-43.
- Whipple, K. X., Tucker, G. E. 1999. Dynamics of the stream-power river incision model; implications for height limits of mountain ranges, landscape response timescales, and research needs. *Journal of Geophysical Research, B, Solid Earth and Planets* **104**(8): 17,661-17,674.
- White, W. 1972. Deep erosion by continental ice sheets. *Geological Society of America Bulletin* **83**: 1037–1056.
- Willett, S. D., 1999. Orogeny and orography: The effects of erosion on the structure of mountain belts, *Journal of Geophysical Research*. **104**: 28 957- 28 981.
- Willgoose, G., Bras, R. L., Rodriguez-Iturbe, I. 1991a. A coupled channel network growth and hillslope evolution model; 1, Theory. *Water Resource Research* **27**: 1671-1684.

- Willgoose, G., Bras, R. L., Rodriguez-Iturbe, I. 1991b. A coupled channel network growth and hillslope evolution model; 2, Nondimensionalization and applications. *Water Resource Research* **27**: 1685-1696.
- Wright, J.D., 2001. Paleo-oceanography: Cenozoic Climate - Oxygen Isotope Evidence, in *Encyclopedia of Ocean Sciences*, J.Steele, S.Thorpe, K.Turekian (eds.) Academic Press.
- Yiou, F., Raisbeck, G. M. 1972. Half-life of ^{10}Be . *Physical Review Letters* **29** (6): 372-375.